Error estimation and adaptivity for finite element structural dynamics models under parameter uncertainty

Cardiff School of Engineering

A thesis submitted to the graduate school

in fulfilment of the requirements for the degree of

Doctor of Philosophy

Pedro Bonilla-Villalba

November 2018

Summary

The optimisation of discretisation and stochastic errors under a single criterion is not a simple task. The nature of the errors derived from both phenomena is totally different and so are the measures needed to assess them. Nonetheless, they are related and if either of the errors dominates a problem, any obtained solution is suboptimal.

Error estimation research is focused on optimising and bounding the discretisation error only. On the other hand, stochastic research treats error estimation as a black box that ensures enough accuracy to avoid interference with the stochastic process and/or the surrogate of the numerical model, with the only exception of stochastic finite element method. This dissertation presents an adaptive approach to optimise locally the relation between the aforementioned numerical approximations in any stochastic framework.

The main novel contribution of this thesis is the development of an algorithm that ensures that all errors are of the same scale after an adaptive process. The numerical problem posed is a structure vibrating steadily under parametric uncertainty, although any partial differential equation could have been selected modifying the refinement strategy. Steady dynamic problems were chosen because they tend to need less intuitive concentration of refinements, the lack of time dependency allows non-conforming meshes and yet, natural frequencies highly influence the solution. The definitions of all measures of error are linked to the relative discretisation error, and are therefore controlled by the algorithm under this single criterion.

Another novelty is a new family of residual error estimators based on the Saint-Venant principle rather than on limiting the support of the test function. This new approach allows to unlink the definition of the patch sub-domain from the split of the residual. In addition to the resulting freedom of patch choice, it is proven than the new approach provides enhanced stability to some element centered patch estimators proposed in the past.

Finally, two minor new contributions are a discrete way to obtain an indicator of refinement for quantities of interest not involving gradients (simpler than the choices already present in literature), and the testing of analogy between error estimators and preconditioners.

Acknowledgements

I would like to express my deep gratitude to the Engineering Research Network Wales Grant (Rhwydwaith Ymchwil Peirianneg Cymru). Without its support and funding for project NRN071, this thesis would not have been possible.

I am particularly grateful to Dr. Pierre Kerfriden and Dr. Abhishek Kundu, my research supervisors, for their wisdom and guidance. I also want to thank them for their patience, unconditional encouragement and friendly but extremely useful critiques.

I wish to extend my thanks to Dr. Susanne Claus, for her help and contribution with the localisation of the influence field. I hope we find the time to extend our collaboration in the future as we initially planned.

I am indebted to the Cardiff University School of Engineering team for their support and for providing a propitious environment for my research. Especially to Sandra Chelmis, Loredana Ionescu, Chris Lee, Aderyn Reid and Jeanette White from Research Office.

I would also like to thank my colleagues in research rooms W2.14 and W1.32 for a friendly and pleasant working atmosphere. Special thanks to Dr. Daniel Paladim for our often inspirational discussions and of course, for the deductive reasoning we did together.

Thanks to my parents for their support and encouragement, and to my family for their understanding in the difficult moments when I have not been there.

I am grateful to my friends for always raising my morale.

Finally, I want to thank Dr. Esther Dorado-Ladera for her assistance and proof-reading of this work. But more importantly, for her love, encouragement, example and patience, which made me pursue this path out of my comfort zone in the first place.

Pedro Bonilla-Villalba

Cardiff, November 2018

List of symbols and acronyms

Acronyms

BC	Boundary conditions
CI	Confidence interval
CL	Confidence level
CRE	Constitutive relation estimate
DOF	Degree of freedom
EC	Element centred (patch)
EC_AN	Element centred patch including adjacent neighbours
EC_FN	Element centred patch including the full neighbourhood
eq.	Equation
FE(M)	Finite element (method)
FFNI	Full factor numerical integration method
(F)GMRES	(Flexible) Generalised minimal residual method
GMRES(R)	Generalised minimal residual (recursive) method
KA	Kinematically admissible
KDE	Kernel density estimation
l.h.s.	Left hand side
MC	Monte Carlo
NC	Node centred (patch)
OA	Alternative orthogonal (patch)
OE	Orthogonal elemental (patch)
PC(E)	Polynomial chaos (expansion)
PDF	Probability density function

QoI	Quantity of interest
r.h.s.	Right hand side
SA	Statically admissible
SFEM	Stochastic finite element method
SoE	System of Equations
SPR	Super patch recovery method

Sets

$\mathbb{N}$	Set of all natural numbers
$\mathbb{Z}$	Set of all integer numbers
$\mathbb{R}$	Set of all real numbers
$\cup$	Set union
$\cap$	Set intersection
$\emptyset$	Empty set
$\in$	Is a member of; belongs to
$\ni$	Is not a member of; does not belongs to
$\subset$	Is a subset of
$\not\subseteq$	Is not a subset of
$\forall$	For all; for each

General symbols

$\boldsymbol{a}$	Generic vector $\boldsymbol{a} = \{a_1, \ ... \ , a_n\}$
$\|\| \bullet \|\|_n$	n norm of $\bullet$, where n stands for the Lebesque functional space (eq. 1.2.5) or the weight (If n=E, E stands for energy and the weight is the matrix of the system 1.2.4). For the definition of the norm of a matrix see eq. 3.3.10
∇ ; ∇_s	Gradient and strain gradient
$\triangle$	Laplace operator or divergence of the gradient
p	Polynomial
$\mathbb{I}$	Identity matrix

Boundary valued problems

Ω	Domain
$\partial\Omega$	Boundary
Γ_d ; Γ_n	Subset of the boundary where Dirichlet and Neumann prescribed values are applied
u	Continuous solution field (concentration for convection-diffusion problems, displacement for vibrating structure)
v	Continuous test field used in the weak formulation
e	Error in the solution of a boundary value problem (eq. 1.1.1)
ϵ	Error in a quantity of interest. Specific errors in quantities of errors are : $\epsilon_/$ relative, ϵ_σ normalised by the standard deviation, ϵ_{NM} of the numerical model, ϵ_{PC} due to polynomial chaos
ε	Estimation of an error or tolerance for an error
$a^{\odot}(\cdot,\cdot)$	General bilinear form of a boundary value problem
$a^{D}(\cdot,\cdot)$	Bilinear form of the diffusion equation (eq. 1.2.3)
$a^{C}(\cdot,\cdot)$	Bilinear form of the convection-diffusion equation (eq. 4.5.3)
$a^{\omega}(\cdot,\cdot)$	Bilinear form of the vibrating structure problem under a harmonic load (eq. 5.2.4)
$l(\cdot)$	Right hand side of the weak boundary valued problem including source/forcing function & prescribed BC terms (eq. 1.2.3)
$f(\cdot)$; $F(\cdot)$	Source or forcing function. Capital for time dependent functions
$u_d(\cdot)$; $U_d(\cdot)$	Prescribed Dirichlet boundary data
$g_n(\cdot)$; $G_n(\cdot)$	Prescribed Neumann boundary data
$\mathcal{R}$	Residual of a boundary valued problem
$\mathcal{R}^D$	Residual of the diffusion equation (eq. 1.3.13)
$\mathcal{R}^\omega$	Residual of the vibrating structure problem under an harmonic load (eq. 5.2.11)
A	Matrix of the system to solve (eq. 1.2.11, 3.3.6, 5.2.7)
M	Mass matrix (eq. 5.2.5)
K	Stiffness matrix (eq. 5.2.6)

Finite element method

$\mathcal{L}^p$	Lesbesgue functional space with finite p-norms
$\mathcal{H}^o$	Sobolev space which contains $\mathcal{L}^2$ functions whose weak derivatives up to order o are also $\mathcal{L}^2$
$\mathcal{U}$	Space of continuous solutions to the problem posed
$\mathcal{V}$	Space of trial solutions equalling zero at the Dirichlet boundary
$\mathcal{V}^{\mathbb{h}}$; $\widehat{\mathcal{V}}$; $\widetilde{\mathcal{V}}$	Coarse, refined (rich) and pseudo-analytical piece-wise discrete spaces of trial functions. Notation extended to solution spaces, meshes, shape functions, solution and error fields, estimators and indicators related with the corresponding discretisation
$\mathcal{M}$	Mesh defining a discretisation
$\mathbb{h}$	Characteristic radius of the circumcircle or circumsphere of the elements of a finite element mesh
$\mathbb{e}$	Element of the mesh
$\mathbb{k}$	Index identifying an element of the mesh
np	Nodal points in a mesh or element (*e.g.* triangular linear elements have 3 nodal points, triangular quadratic ones 6)
ψ	Shape functions
$[u^{\mathbb{h}}]$	Vector of coefficients of a field that multiplies the shape functions. Field $u^{\mathbb{h}}$ can be reproduced as $[u^{\mathbb{h}}] \cdot \psi^{\mathbb{h}}$
R	Number of refinements applied to an element in a regular mesh to obtain a rich space
$\mathbb{P}$	Patch
$\mathbb{p}$	Index identifying a patch. If not specified it equals the index of an element's vertex in the mesh
$\mathbb{Q}$	Alternative patches
$\mathbb{q}$	Index identifying an alternative patch
$\mathbb{i}$	Index identifying an arbitrary patch
$\underset{\mathcal{V}^{\mathbb{h}}}{\overset{\widehat{\mathcal{V}}}{I}}$	Interpolation operator from a coarse to a rich field (eq. 4.2.1)
$\underset{\widehat{\mathcal{V}}}{\overset{\mathcal{V}^{\mathbb{h}}}{\pi}}$	Projector operator from a rich to a coarse field (eq. 1.4.6)

	Convection-diffusion problems
$\boldsymbol{j}(\cdot)$	Flux vector valued field in convection-diffusion problems
C	Diffusion coefficient
α	Convective velocity
b	Parameter for the reaction term
	Vibrating structure problem
C	Fourth order Hooke tensor
$E(\boldsymbol{\mu})$	Parametric Young modulus (see stochastic symbols)
ν	Poisson ratio
ρ	Mass density
ω	Circular frequency
	Error control
η	Global or local estimation of the norm of the error. In its local version, it also denotes an indicator of refinement
z	Influence field (eq. 1.4.2 and 1.4.4)
$q(\cdot)$	Function mapping from the solution to a quantity of interest
Q	Scalar magnitude representing a quantity of interest
	Iterative methods for solving systems of equations
$\mathfrak{P}$	Preconditioner. $\mathfrak{P}_L$, $\mathfrak{P}_R$ left and right preconditioners
$\mathcal{K}_m$	m-dimensional Krylov subspace (eq. 3.3.12)
n	Index to identify the iteration in a GMRES algorithm
$\mathfrak{r}$	Residual of the system of equations (eq. 3.3.14)
$\mathscr{Q}_n = \{\mathfrak{q}_1, ..., \mathfrak{q}_n\}$	Orthonormal basis of a Krylov space after Arnaldi algorithm
$\mathcal{Q}_n$	Orthonormal basis $\mathscr{Q}_n$ in matrix form
$\bar{H} = [..., \mathfrak{h}_{j,\mathfrak{k}-1}]$	Hessenberg superior matrix and its last component, where j and $\mathfrak{k}$ are indexes in the FGMRES and Arnoldi algorithms
$\mathfrak{E}$	Error estimator used as preconditioner (eq. 3.3.18)

	Stochastic process
$\mathfrak{M}()$	Numerical FEM model. It maps from the primary known random variable(s) to the unknown stochastic process function of it(them)
Θ ; Θ_Q	Sampling spaces of the primary and response stochastic processes
$\mathscr{F}$	Smallest σ-algebra consisting of a set of all measurable subsets
$\mathcal{P}$	Probability measure
X ; $\boldsymbol{\mu}$	Primary random variable. X is generic, $\boldsymbol{\mu}$ is a r-dimensional vector of real parameters characterising the field of Young's modulus
Y ; Q	Response random variable. Y is generic, Q a quantity of interest
θ ; Q	Outcomes of the random variables $\boldsymbol{\mu}$ and Q respectively
$f_X^{\mathcal{P}}$; $f_{\boldsymbol{\mu}}^{\mathcal{P}}$; $f_Y^{\mathcal{P}}$; $f_Q^{\mathcal{P}}$	Probability density function of the subindexed random variable
s	Index identifying a sample point
$\mathcal{U}(1,2)$	Uniform distribution in the interval [1,2]
$\mathcal{N}(1,2)$	Normal distribution with mean 1 and variance 2
$\mathrm{g}(\cdot)$	Explicit equation for the Gaussian PDF (eq. 2.2.2)
$var(\bullet)$; σ^2	Variance of $\bullet$ (eq. 2.2.4)
$std(\bullet)$; σ	Standard deviation of $\bullet$
$\mathcal{E}[\bullet]$	Expectation of $\bullet$ (eq. 2.2.3)
$\overline{\mathcal{E}}[\bullet]$	Monte Carlo approximation of the expectation of $\bullet$ (eq. 2.3.1)
$\mathcal{C}_\bullet$	Centile $\bullet$, percentile $\bullet$
CI	Confidence interval
CL	Confidence level
$\mathscr{Z} = \{Z_0, ..., Z_\mathfrak{o}\}$	Polynomial basis up to order $\mathfrak{o}$ in a polynomial chaos expansion
$He_\mathfrak{o}^{[\sigma, \mathcal{E}[\theta]]}(\theta)$	Hermite polynomial of order $\mathfrak{o}$ (eq. 2.4.10)
$\mathfrak{c} = \{\mathbb{C}_0, ..., \mathbb{C}_\mathfrak{o}\}$	Coefficients minimising the distance between PCE and the response surface of the original numerical model (eq. 2.4.12)
$\mathfrak{p}$	Perturbation (used in perturbation methods)

List of figures

List of algorithms

Contents

Introduction

Motivation

The Finite Element Method (FEM) is a well established procedure for computing deterministic engineering problems described by partial differential equations. The method consists of diverse numerical techniques that enable computers to solve these differential equations used currently in modern science to mathematically model any physical phenomena. FEM produces discrete approximations of the solution with a discretisation error that can be controlled by means of various intricate techniques, some of which are explored in this dissertation.

Additionally, probability theory provides mathematical tools to assess uncertainty quantification. In particular, stochastic processes allow the characterisation and measurement of random events that can significantly influence the simulation of any physical problem posed. When paired with FEM models to determine their parametric uncertainty, the result is a function output or response surface instead of a unique deterministic solution. The description of this surface needs sampling because the FEM only produces an outcome of the surface due to its deterministic nature. Consequently, on top of the discretisation error, an uncertainty level is introduced as well as other numerical errors due to the finite sampling and non-analytical description of the stochastic process.

In this context, the challenge is to understand and improve computational versions of mathematical models where both FEM and stochastic processes are involved. Independent control of each of the errors has its own difficulties, as can be deduced from the prolificacy of both fields of research. Therefore, further complications are

to be expected for simultaneous control of all the approximations. This interaction is scarcely studied at the moment, being the general approach to ensure that discretisation error is unduly small so that it does not interfere with the stochastic process. This over-discretisation is a computationally suboptimal approach.

The main purpose of this thesis is the understanding and discussion of the different errors that play a role in this sort of problems, as well as the optimisation of the computations where they are involved. The framework chosen to test the findings is that of steady state structural dynamics, where a given parametric uncertainty in the Young's modulus generates forward uncertainty propagation in the general response of the structure. Several of the discussions included in this thesis could be extended to other problems where FEM and stochastic processes are involved, such as any adjustable or unknown physical quantity in the constitutive equations or boundary conditions (boundary data, mass densities, excitation frequency, etc.), other physical laws (*e.g.* elasticity, heat transfer, even time dependent structural dynamics if the refinement strategy is changed to conforming meshes with hanging nodes) or inverse uncertainty quantification (where the sampling method should change from MC to one based on Markov Chain Monte Carlo).

Prior to enumerating the specific contributions of this work, a brief history of the methods forming the backbone of the computational problem to optimise are summarised.

Regarding the discretisation of the mathematical models posed in the continuum, adaptive refinement [29] is one of the first tools developed to optimise meshes (and consequently computational resources while using FE). This process is naturally driven by a-posteriori error estimations based on the residual [18, 20], gradient recovery [190] (and all its later evolutions) or the constitutive relation error [106] based on the Prager-Synge hypercircle [138]. Afterwards, goal-oriented duality techniques are introduced in the works of Becker and Rannacher [25], Cirak and Ramm [44] and Oden and Prudhomme [129]. Their purpose is to shift the objective of the estimators from the energy norm towards any quantity of interest.

As for uncertainty quantification, worst-case scenario [16] and fuzzy arithmetic

methods [42] allow to bound the uncertainty, while probabilistic methods allow full characterisation of the parameter domain. Within the latter category, the simplest methods rely in properly sampling the parameter space. Apart from brute force Monte Carlo [147, 72, 151], different methods to optimise the sampling have been proposed (for instance, importance sampling [121], adaptive sampling [36] or collocation [126, 17]). In parallel, several techniques to create surrogate models have been presented. Surrogates produce outcomes with negligible computational cost in relation to the cost of evaluating the usually complex original numerical models. Some of these techniques are based on functional expansion [73, 186] or numerical integration [63, 160]. Later on, weak formulation of the functions defining the surrogates and even estimation and local adaptivity of surrogates are proposed in [96, 127].

For the aforementioned possible extension of this work to inverse uncertainty characterisation, Kalman filters [94, 65] and Bayesian inversion [46, 168] are by far the favoured techniques at the moment. Nevertheless, both methods (and most of their alternatives) rely on Monte Carlo or Markov Chain Monte Carlo [74] sampling techniques, so they would also benefit from an optimal relation between the discretisation and stochastic error.

Error estimation research usually focuses on how to ensure bounds for spatial discretisation error only [41, 6]. On the other hand, stochastic research is more interested in the reduction of the sampling error [93, 36, 126, 17, 142], the cost of the sample evaluations of the model [28, 118, 189, 73, 186] or the number of relevant parameters [79, 21, 104]. As stated, probabilistic approaches consider error estimation as a tool to ensure that the discrete error is small enough compared to the error of characterising the response surface. Lately, some of this stochastic research [119] defines adaptivity as the local enrichment of the surrogate model and uses error estimation to bound this error, with no mention of spatial discretisation or the adaptivity on the spatial domain.

Returning to the specified problem of interest, its resolution requires a large number of computations. This is due not only to the complexity of the resulting

numerical models for structures, but also to the often vast number of evaluations of this model required to sample the response surface. This surface is the assembly of outcomes of an unknown stochastic process function of the primary random variable defining the parametric uncertainty (known in this work).

In order to achieve the optimisation of all errors generated by the combination of FEM and forward uncertainty propagation, a-posteriori error estimation is explored as a starting point. Two antagonistic approaches are pursued to that effect. The first one aims to achieve an estimation of the error in a target rich space on an algebraic level without the need of globally refining the mesh ever. The second one follows the classical adaptive mesh refinement strategy, trying to improve the predictions by means of new error estimators. Lastly, the objective is shifted to the optimisation of the interaction between the discretisation and the stochastic errors.

In summary, the novel contributions of this thesis are listed next in sequential order. The last one in the list is the most relevant and the original motive for the present work.

- A variety of residual error estimators enforcing Dirichlet boundary conditions to the local patches are compared. The selected methods are reformulated in a common framework in order to allow efficiency comparison besides effectivity rating. Moreover, the reformulation allows the addition of an hybrid estimator to the analysed collection.

- A new perspective about error estimators is presented, which are studied as preconditioners. An error estimator based on the residual is integrated in an iterative solver of linear equations. The aim is to recover the exact reference solution in a rich space from multiple iterations of the error estimator defined in the coarse space. This unique approach helps to iteratively improve the quality of the error estimation in a target discrete space on demand. Ultimately, convergence of the estimation and the target solution or truth might be achieved. For this purpose, the computational benefits are equivalent to the benefits of iterative solvers with respect to direct methods.

- A new family of error estimators is propounded based on the residual and local Dirichlet boundary conditions. It was detected that patch size profoundly influences the estimators accuracy. However, existing methods to increase the patch size proved unstable. To address instability, the new developed estimators rely on the Saint-Venant Principle rather than on limiting the test functions support to delimit the local patch subdomain. This allows reliably decoupling the patch definition from its correspondent local residual partition of unity, and shows equivalent performance. Furthermore, it leads to additive contributions to the global error field avoiding the need of an average rule if this global field is to be assembled.

- A simple discrete way is suggested to localise the influence field in a dual-weighted goal-oriented error estimator to properly lead a refinement strategy. This idea is not genuinely new, [129] proposes to achieve this goal by using a product of indicators, [75] incorporates a gradient in the quantity of interest (uses stresses), and [150] employs equilibration of the residual and integration by parts and redistribution of the normal derivative. This thesis achieves the same goal than including a gradient in the quantity of interest, by taking advantage of Galerkin orthogonality and using p-refinement in addition to removing all the coarse component from the influence field.

- An algorithm is devised aiming to jointly control the level of refinement for each of the building-blocks forming the chain of approximations that typically make finite element methods with a sub-domain level stochastic component tractable: (i) finite element approximation of the spatial fields (ii) meta-modelling to interpolate quantities of interest(s) in the parameter domain and (iii) Monte-Carlo sampling of the probability distribution of the quantity of interest (QoI). This algorithm ensures that computational efforts are devoted to reduce the larger error at each step in an adaptive iterative process. Once all errors are at the same scale as the one derived from the uncertainty introduced by the probability distribution of some parameters in a vibrating structure, the algorithm stops. From this point on, it is not possible

to be certain that any reduction in the error is consistent if the computation is repeated with different sampling points to assess the random parameters. Unpropitious results for the stochastic approximation can be predicted from lack of discretisation. However, excess of discretisation has heightened repercussions on stochastic programming computational cost, despite being ignored in the general approach. The algorithm avoids this undue cost due to the multiple evaluations of an over-discretised FEM model required to produce outcomes.

Structure of the thesis

This thesis is structured in six chapters. The relevant literature is reviewed in the first two and part of the third one. Chapters three to five proffer the novel contributions proposed in this thesis regarding the improvement or reduction of computational cost of discretisation errors. The fifth chapter incorporates stochastic errors. The last chapter summarises the conclusions and lists possible future directions of research based on this work.

- Chapter 1 includes the state of the art of error estimation. After introducing the basic concepts of a-priori error estimation, the most popular approaches to a-posteriori error estimation are summarised and formulated. Goal-oriented error estimation is also examined. Finally, the adaptivity of mesh refinement is explored.

- Chapter 2 reviews how uncertainty is faced in literature. Since the interest lies in the optimisation of stochastic processes, non-probabilistic methods are only mentioned in the introduction. The stochastic review starts with sampling methods using the original numerical model with Monte Carlo formulation as an example. Then, an example of building surrogate models using local expansion, functional expansion and numerical integration are portrayed. Finally, the integration of stochastic characterisation at the finite element level is included, leading to the formulation of the stochastic finite element method

using Monte Carlo and also a Taylor expansion based surrogate.

- In chapter 4, error estimators based on the residual and Dirichlet boundary conditions are discussed in more depth. Several of the available methods are assessed under a common framework. This framework allows the hybridisation of the methods. A novel approach based on the Saint-Venant principle leading to more alternatives to be assessed, is presented. The assessment is performed by means of a diffusion numerical example, and its results are extended to a steady convection-diffusion numerical example.

- Chapter 3 proposes to look at error estimators as preconditioners, which would mean the possibility to improve error estimation in an algebraic scope. Iterative solvers and preconditioners are briefly described. The soundness of the analogy is tested by integrating an error estimator in a FGMRES algorithm and testing a convection numerical example.

- In chapter 5, parametric uncertainty is introduced into vibrating structure problems. The different sources of error are identified and the measures to control them presented or recalled from previous chapters. Then, the relation between the different sources of error of this problem and the uncertainty is studied. Lastly, a newly devised algorithm to optimise the adaptive process is tested with a numerical example.

- The conclusions and plans for future research are included in chapter 6.

Papers and presentations

This section includes the author's papers presented, submitted or in preparation. Some journal paper passages and figures have been quoted verbatim from this dissertation. Their submission processes to journals will be concurrent with the submission process of this dissertation, so their publication might precede this thesis publication.

Journal articles

- Bonilla-Villalba, P.; Claus, S.; Kundu, A.; and Kerfriden, P.; "Goal-oriented model adaptivity in stochastic elastodynamics: simultaneous control of discretisation, meta-modelling and sampling errors". *Accepted, under review.*

- Bonilla-Villalba, P.; Kundu, A.; and Kerfriden, P.; "Comparison and hybridisation of implicit residual error estimates based on reduction to local Dirichlet patch problems through a unified framework". *In Preparation.*

Conference papers and presentations

- Bonilla-Villalba, P.; Kundu, A.; and Kerfriden, P.; [2016] "Comparison and improvement of implicit residual error estimates based on reduction to local Dirichlet patch problems through an unified framework". *Presented in 24th UKACM Conference*

- Bonilla-Villalba, P.; Kundu, A.; and Kerfriden, P.; [2017] "Efficiency analysis of patch size and type for error estimates based on implicit residual and local Dirichlet patch problems". *In "Proceedings of the 25th UKACM Conference on Computational Mechanics"*

- Bonilla-Villalba, P.; Kundu, A.; and Kerfriden, P.; [2017] "Efficiency analysis of patch size and type for error estimates based on implicit residual and local Dirichlet patch problems". *Presented in ADMOS Conference (Advanced Modelling and Simulation)*

- Bonilla-Villalba, P.; Claus, S.; Kundu, A.; and Kerfriden, P.; [2018] "Finite element adaptivity in probabilistic model updating". *Presented in ECCM – ECFD, (European Conference on Computational Mechanics)*

Chapter 1

Error control review

1.1 Introduction

The spatial discretisation introduced by the Finite Element Method (FEM) originates a numerical error in the solution of the mathematical model of any posed problem. Immediately after the presentation of FEM, research about how to estimate or bound this error started. The error is defined as

$$e := u - u^{\mathbb{h}}, \tag{1.1.1}$$

where u is the continuous analytical solution of the model problem, $u^{\mathbb{h}}$ is a discrete approximation computable through numerical methods, and $\mathbb{h}$ stands for the maximum size of the elements in the mesh. FEM is a well known method with its origins in the works of Hrennikoff [86] and Courant [47]. The key features of the sort of solutions $u^{\mathbb{h}}$ produced by FEM are summarised in section 1.2.1. A vast number of books and reviews about FEM have been published, for instance [89, 34].

Error control comprises three different aspects:

- To rate the decay of the error as the discretisation is refined. This is known as convergence, and since FEM is usually an iterative process, it indicates which of the FEM variants for the posed problem would advance faster to a solution within the acceptance tolerances.

- To predict or bound its magnitude. Knowing the magnitude of the error is the main criterion to validate a solution. Ultimately, this validated solution is the base to engineering decisions, for instance a design viability or if a structure needs reinforcement.

- The optimisation of the distribution of the error along the mesh. It is fundamental to FEM that the smaller the element or the larger the number of Degrees Of Freedom (DOF), the smaller the error and the higher the computational cost. However, the local magnitude of the error in any numerical model is not distributed uniformly. Knowing how the error is distributed allows to devote computational efforts where the error is more significant (*i.e.* using smaller elements in the areas with large local error and larger elements in areas with small local error). The process to guide this mesh refinement is known as adaptivity, and is driven by error estimation. Some examples of mesh refinement can be found at figure 1.2.

A-priori error estimators predict the general accuracy of a FE problem as a function of some parameters describing the mesh (usually $\mathbb{h}$, which is the characteristic radius of the circumcircle or circumsphere of the elements of the mesh), the level of continuity of the Hilbert space, the problem, and the solution u itself. Since u is not solvable, this estimators serve only to know the rate of convergence of the problem and type of solution enforced. Their derivation leads to solutions of the form

$$||e||_{\mathcal{L}^2} = ||u - u^{\mathbb{h}}||_{\mathcal{L}^2} \leq \alpha_M \mathbb{h}^{\alpha_C} |u|_{\mathcal{H}^2}, \tag{1.1.2}$$

where $\mathcal{L}^p$ is the Lebesgue functional space of p-norms; $\mathcal{H}^o$ is a Sobolev space which contains $\mathcal{L}^2$ functions whose weak derivatives up to order o are also $\mathcal{L}^2$; α_C is the order of convergence; α_M is a constant generally unknown and depending on the geometry of the mesh; u is the unsolvable solution of the continuous problem (strong form); and $u^{\mathbb{h}}$ is the unsolved solution to the discrete problem (weak form in the coarse space).

A-priori error estimators are derived for optimal control problems governed by partial differential equations. A number of estimators have been published for dif-

ferent variety of problems as linear elliptic control problems [66], non-linear elliptic control problems [57, 81], the Stokes equation [50] or the Discontinuous Galerkin Method [140]. Later estimators include parameter identification [146, 67, 170, 95]. Recently, an a-priori error estimator for an inverse problem solving the Poisson equation was presented [90].

In contrast, a-posteriori error estimators are fully computabile from precomputed discrete solutions $u^{\mathbb{h}}$. Their objective is to compute approximations or bounds of the real error. They usually take the form

$$||u - u^{\mathbb{h}}||_n \approx \eta \qquad or \qquad ||u - u^{\mathbb{h}}||_n \leq \eta, \tag{1.1.3}$$

where η is a representative scalar norm or measure. Furthermore, the measure η can be localised in order to determine which areas of the mesh concentrate more error. This local information is crucial to lead the adaptivity process mentioned as third aspect of error control.

A-posteriori error estimation is a vastly treated topic in the literature. There are several reviews for elliptic problems, for instance the ones written by Ainsworth, Oden and Tinsley [5, 6], Stein, Rüter and Ohnimus [167], Chamoin and Díez [41] or Gratsch and Bathe [77]. For transient dynamics the reader is referred to Verdugo, Parés and Díez [179].

1.2 Generic model problem and notation

A simple model problem is introduced next for the sake of illustration and notation. It consists of a bounded domain $\Omega \subset \mathbb{R}^d$, of $d = 2$ or $d = 3$ governed by the diffusion equation. The boundary $\partial\Omega$ with outward unit normal $\overrightarrow{n}$ is divided into the complementary subsets Γ_n and Γ_d, where Neumann and Dirichlet conditions are prescribed respectively. Furthermore, Γ_d is defined such that it is not empty and excludes all zero energy possible solutions. $f(\boldsymbol{x}) : \Omega \to \mathbb{R}$ is a given scalar function representing the source term of inflow or outflow material generated inside the domain. $u_d(\boldsymbol{x}) : \Gamma_d \to \mathbb{R}$ is a prescribed boundary concentration of material.

$g_n(\boldsymbol{x}) : \Gamma_n \to \mathbb{R}^d$ is a prescribed boundary flux. Finally, C is a constant diffusion coefficient.

In this framework the strong form of the problem reads

$$\nabla \cdot \boldsymbol{j}(\boldsymbol{x}) = f(\boldsymbol{x}) \qquad \text{in}\,\Omega, \qquad \text{continuity equation,} \tag{1.2.1a}$$

$$u(\boldsymbol{x}) = u_d(\boldsymbol{x}) \qquad \text{on}\,\Gamma_d, \qquad \text{prescribed concentration,} \tag{1.2.1b}$$

$$\boldsymbol{j}(\boldsymbol{x}) \cdot \overrightarrow{n} = g_n(\boldsymbol{x}) \qquad \text{on}\,\Gamma_n \qquad \text{prescribed fluxes,} \tag{1.2.1c}$$

$$\boldsymbol{j}(\boldsymbol{x}) = -C\nabla u(\boldsymbol{x}) \qquad \text{in}\,\Omega, \qquad \text{constitutive relation,} \tag{1.2.1d}$$

where the unknowns are the concentration scalar field $u(\boldsymbol{x}) : \Omega \to \mathbb{R}$ belonging to the space of functions with at least 2 continuous derivatives; and the flux vector-valued field $\boldsymbol{j}(\boldsymbol{x}) : \Omega \to \mathbb{R}^d$ belonging to the space of functions with at least 1 continuous derivative.

In order to formulate the equivalent variational problem known as weak form, the definition of the test and trial Sobolev Spaces are needed ($\mathcal{V} = \{v \in \mathcal{H}^1(\Omega) \,|\, v = 0 \; on \; \Gamma_d\}$ and $\mathcal{U} = \{u \in \mathcal{H}^1(\Omega) \,|\, u = u_d \,\text{on}\, \Gamma_d\}$, respectively). Both are spaces of functions with square integrable derivatives. In particular, this thesis uses piecewise linear, quadratic or cubic space functions for the convection diffusion problems and piecewise bi-linear or bi-quadratic for the steady state dynamics problem. Then, after multiplication by a test function and integrating by parts, the problem posed in equation 1.2.1.a becomes: find $u \in \mathcal{U}$ such that

$$\int_\Omega \nabla v(\boldsymbol{x}) C \nabla u(\boldsymbol{x}) d\Omega = \int_\Omega v(\boldsymbol{x}) f(\boldsymbol{x})\, d\Omega + \int_{\Gamma_n} v(\boldsymbol{x}) g_n(\boldsymbol{x})\, d\Gamma_n, \qquad \forall\, v(\boldsymbol{x}) \in \mathcal{V}. \tag{1.2.2}$$

For the sake of simplicity the bilinear and linear functional operators $a^D(\cdot,\cdot)$ and $l(\cdot)$ are introduced to match both sides of equation 1.2.2, which now simply reads

$$a^D(u, v) = l(v), \qquad \forall\, v \in \mathcal{V}. \tag{1.2.3}$$

The most common norm of the defined spaces is the energy norm $||\cdot||_E$. This norm is based on the bilinear operator of the variational problem which is problem dependent.

$$||e||_E := \sqrt{a^{\odot}(e(\boldsymbol{x}), e(\boldsymbol{x}))} \tag{1.2.4}$$

In the present case $a^{\odot} \equiv a^{D}(\cdot,\cdot)$

However, the $\mathcal{L}^2$ norm is sometimes of interest since it is proportional to the mass norm.

$$||e||_{\mathcal{L}^2} := \sqrt{\int_{\Omega} e(\boldsymbol{x}) e(\boldsymbol{x})} \tag{1.2.5}$$

1.2.1 Discretisation of the model problem through finite elements

The discrete test $\mathcal{V}^{\mathbb{h}} \subset \mathcal{V}$ and trial $\mathcal{U}^{\mathbb{h}} \subset \mathcal{U}$ vector spaces used in the FEM are projections of the already defined function spaces. These subdomains are defined through a given mesh and each piece of the domain is called an element of the mesh.

A mesh consist in the tessellation of the domain $\Omega \subset \mathbb{R}^d$ in a set of $n_{\mathbb{e}}$ elements $\mathscr{E} = \{\mathbb{e}^1, ..., \mathbb{e}^{\mathbb{k}}, ..., \mathbb{e}^{n_{\mathbb{e}}}\}$ satisfying

$$\begin{aligned}
\Omega_{\mathbb{k}} - \partial\Omega_{\mathbb{k}} &\neq \emptyset && \forall \mathbb{k} && \text{elements are non-empty,} \\
\bigcup_{k\,=\,1}^{n_{\mathbb{e}}} \Omega_{\mathbb{k}} &= \Omega && && \text{elements form the whole domain,} \\
\bigcup_{\mathbb{k}\,=\,1,\,\mathbb{k}'\,=\,1}^{n_{\mathbb{e}},\,n_{\mathbb{e}}} \left(\Omega_{\mathbb{k}} \bigcap_{\mathbb{k} \neq \mathbb{k}'} \Omega_{\mathbb{k}'} \right) \cup \partial\Omega &= \bigcup_{\mathbb{k}\,=\,1}^{n_{\mathbb{e}}} \partial\Omega_{\mathbb{k}} && && \text{elements do not overlap.}
\end{aligned} \tag{1.2.6}$$

In the case of curved domains, the second condition cannot be fulfilled unless the shape functions of the mesh elements can reproduce the curve exactly. The general approach is to neglect the difference between $\bigcup_{\mathbb{k}\,=\,1}^{n_{\mathbb{e}}} \Omega_{\mathbb{k}}$ and Ω, since it is small and decreases as the mesh is refined.

The type of elements in a mesh defines a set of n_{np} nodal points $\mathscr{N}_{\mathscr{P}} = \{np_1, np_2, ..., np_{n_{np}}\}$ (*e.g.* the vertexes of $\Omega_{\mathbb{k}}$ in the case of elements with linear shape functions).

For any field $u^{\mathbb{h}} \in \mathcal{U}^{\mathbb{h}}$ there exist coefficients c_i, where $i = 1, 2, ..., n_{np}$ such that

$$u^{\mathbb{h}}(\boldsymbol{x}) = \sum_{i=1}^{n_{np}} c_i \psi_i^{\mathbb{h}}(\boldsymbol{x}). \tag{1.2.7}$$

The coefficients c_i coincide with the field value at the correspondent nodal points $np_i \in \mathscr{N}_{\mathscr{P}}$. The field value in the rest of the domain Ω can be interpolated through

the shape functions $\psi^{\mathbb{h}}(\boldsymbol{x})$, which satisfy the following conditions.

$$\begin{aligned} \psi_i^{\mathbb{h}}(\boldsymbol{x}_i = np_i) &= 1 \\ \psi_i^{\mathbb{h}}(\boldsymbol{x}_j = np_{j\neq i}) &= 0 \\ \sum_{i|np_i\in\Omega_{\mathbb{k}}} \psi_i^{\mathbb{h}}(\boldsymbol{x}_l) &= 1 \qquad \forall \boldsymbol{x}_l \in \Omega_{\mathbb{k}} \\ \psi_i^{\mathbb{h}}(\boldsymbol{x}_l) &= 0 \qquad \forall \boldsymbol{x}_l \in \{\Omega_{\mathbb{k}'} \in \Omega \mid np_i \notin \Omega_{\mathbb{k}'}\} \quad . \end{aligned} \tag{1.2.8}$$

Because the coefficients coincide with the field value at the nodal point, the notation

$$[u^{\mathbb{h}}]\psi^{\mathbb{h}}(\boldsymbol{x}) := u^{\mathbb{h}}(\boldsymbol{x}) \tag{1.2.9}$$

is introduced. In the notation, the components of the vector $[u^{\mathbb{h}}]$ are the coefficients $c_1, c_2, ..., c_{n_{np}}$ corresponding to the field $u^{\mathbb{h}}(\boldsymbol{x})$.

After discretisation and approximation of the fields $u^{\mathbb{h}} \approx u$ and $v^{\mathbb{h}} \approx v$, the problem 1.2.3 becomes the following discrete linear system of equations (SoE)

$$a^D(\psi_u^{\mathbb{h}}(\boldsymbol{x}), \psi_v^{\mathbb{h}}(\boldsymbol{x})) \cdot [u^{\mathbb{h}}] = l(\psi_v^{\mathbb{h}}(\boldsymbol{x})). \tag{1.2.10}$$

This SoE is usually expressed in terms of the global matrix of the system A^D as

$$A^D[u^{\mathbb{h}}] = [l^{\mathbb{h}}], \tag{1.2.11}$$

where $A^D = a^D(\psi_u^{\mathbb{h}}(\boldsymbol{x}), \psi_v^{\mathbb{h}}(\boldsymbol{x}))$ and $[l^{\mathbb{h}}] = l(\psi_v^{\mathbb{h}}(\boldsymbol{x}))$. The matrix of the system is usually expressed in terms of the mass matrix M relating to convection or inertial forces and the stiffness matrix K relating to the diffusion or elastic forces. In the present only diffusion case $A^D = K$.

Apart of the benefits of having a discrete well posed problem, both sides of the system can be systematically computed at the element level. For instance, the global stiffness matrix can be computed as

$$K = \sum_{\mathbb{k}=1}^{n_{\mathbb{e}}} K^{\mathbb{e}^{\mathbb{k}}} = \sum_{\mathbb{k}=1}^{n_{\mathbb{e}}} a^D_{\Omega_{\mathbb{k}}}(\psi_u^{\mathbb{h}}(\boldsymbol{x}), \psi_v^{\mathbb{h}}(\boldsymbol{x})), \tag{1.2.12}$$

where $K^{\mathbb{e}^{\mathbb{k}}}$ is known as the elemental stiffness matrix, and $a^D_{\Omega_{\mathbb{k}}}$ is defined as the restriction of a^D to the domain $\Omega_{\mathbb{k}}$ belonging to element $\mathbb{e}^{\mathbb{k}}$.

The present work employs only polynomials of order 1 (p1) and order 2 (p2) as shape functions. A space $\widehat{\mathcal{V}} \subset \mathcal{V}$ is richer than another space $\mathcal{V}^{\mathbb{h}} \subset \mathcal{V}$ if it contains

more nodal points. This can be achieved either by increasing the order of the polynomial shape functions or by reducing the characteristic length $\mathbb{h}$, which stands for the diameter of the circumcircle (or circumsphere if $d = 3$) of a finite element in a mesh (typically *characteristic length* means the larger or the average). The first case is known as p-refinement and the second one as h-refinement (see figure 1.2 for some choices of h-refinement). Note that not necessarily $\mathcal{V}^{\mathbb{h}} \subset \widehat{\mathcal{V}}$, which in the present work is enforced for reference spaces, any p-refinement and h-refinement of quadrilateral meshes. On the contrary, it is not enforced for the case of h-refinement of triangular meshes.

Although r-refinement techniques exist they are not considered in the present dissertation. In r-refinement, the nodes are redistributed to form a new mesh which is not richer than the former one. Nevertheless, the new mesh improves the solution accuracy by reducing the distance between the nodes in the regions where the error was higher in the previous mesh. The reader is referred to [9] for details in the framework of arbitrary Lagrangian-Eulerian methods [55].

1.3 Classification of a-posteriori estimators

A-posteriori error estimators can be classified in four main families depending on the methodology followed to derive the estimate of the error. A brief summary is included in this chapter as literature review of the alternatives considered for the present work. Section 1.6 states the reasons why a-posteriori error estimators based on the residual were selected and chapter 4 explores in detail this kind of estimators and some original proposed contributions to their improvement.

1.3.1 Explicit estimates

The explicit a-posteriori error estimates are similar to the a-priori ones, since a constant α_M multiplies the approximation η which depends on $\mathbb{h}$ in the form

$$||e||_{\mathcal{L}^2} \leq \alpha_M \eta(\mathbb{h})^2, \tag{1.3.1}$$

resembling equation 1.1.2.

Both η and α_M are computable based on the information extracted from $u^{\mathbb{h}}$ and the mesh. However, the estimation of α_M is difficult and provides in general less accuracy than other options. Quoting [19], the included results are "extremely pessimistic and have mainly theoretical value. The main corollary from these results is that the effectivity of the explicit estimator cannot be improved by multiplying it by an 'optimal' scaling constant, especially for meshes with high aspect ratios." Initial formulations can be found at [18, 99, 15]. See [6, 41] for further reviews of error estimators that contain chapters devoted to this.

An example of explicit estimator based on least squares extracted from [6] reads

$$\eta^2 = \sum_{\mathbb{k}=1}^{n_{\mathbb{e}}} \eta_{\mathbb{k}}^2 = \sum_{\mathbb{k}=1}^{n_{\mathbb{e}}} \mathbb{h}_{\mathbb{k}}^2 ||\mathcal{R}_I||^2_{\mathcal{L}^2(\Omega_{\mathbb{k}})} + \mathbb{h}_{\mathbb{k}} ||\mathcal{R}_B||^2_{\mathcal{L}^2(\partial\Omega_{\mathbb{k}})}, \tag{1.3.2}$$

being $\mathbb{k}$ the index identifying an element, $\Omega_{\mathbb{k}}$ and $\partial\Omega_{\mathbb{k}}$ the interior and boundary of element $\mathbb{e}^{\mathbb{k}}$ respectively, $\mathcal{R}_I$ the interior residual ($f(\boldsymbol{x}) + \boldsymbol{j}(\boldsymbol{x})$ in problem 1.2.1) and $\mathcal{R}_B$ the boundary residual (for interior edges equals the jump between elements and for external ones equals $g_n(\boldsymbol{x}) - \boldsymbol{j}(\boldsymbol{x}) \cdot \overrightarrow{n}$).

1.3.2 Implicit recovery based estimates

The gradient recovery family of estimates was first presented by Zienkiewich and Zhu [190]. Its main idea consists in the approximation of a better recovered gradient post-processing the data computed for the coarse solution (making the stress continuous in an elasticity problem or the flux in a diffusion problem, for instance).

The scalar norm of the estimate is defined as the one produced by the bilinear form of the corresponding weak equation. It is also known as the energy norm due to its direct relation with the energy of the physical problem represented (*e.g.* heat energy or potential elastic energy). The global error estimation is the difference between this norm computed from the coarse solution and the one resulting from the post-process, which is considered close enough to the continuous model.

The usual post-process involves the estimation of a continuous stress or flux field $\boldsymbol{j}^*(\boldsymbol{x})$. Then the global error estimator η_R is the error in the energy norm, which reads

$$||e||_E \approx \eta_R := \sqrt{\int_\Omega (\boldsymbol{j^*}(\boldsymbol{x}) - \nabla u^{\mathbb{h}}(\boldsymbol{x}))C(\boldsymbol{j^*}(\boldsymbol{x}) - \nabla u^{\mathbb{h}}(\boldsymbol{x}))d\Omega}. \tag{1.3.3}$$

This global estimator can be localised by restricting the area of integration to the desired scale (usually the elements in the mesh).

In order to recover a continuous stress field $\boldsymbol{j^*}(\boldsymbol{x})$, the initial proposition [190] was to solve a global problem involving all Degrees Of Freedom (DOF) of the mesh. The same Zienkiewich [191, 192] proposed the Super Patch Recovery (SPR) method, where the reconstruction of the global stress field is undertaken through the computation of local patches and interpolation. The type of patch $\mathbb{P}$ used consists of all elements $\mathbb{e}^{\mathbb{k}}$ that contain a vertex $np_{\mathbb{p}}$, which is also a nodal point. Unless otherwise noted, index $\mathbb{p}$ identifies each node centred patch $\mathbb{P}_{\mathbb{p}}$ and also the nodal point in its centre (*i.e.* $np_{\mathbb{p}} \equiv \mathbb{p}$). See figures 4.1.a,e for 2D examples of this kind of patch.

The post-processed field $\boldsymbol{j^*}(\boldsymbol{x})$ is obtained from a polynomial expansion of the same order as the shape functions $\boldsymbol{\psi}$ in the patches $\mathbb{P}_{\mathbb{p}}$. Its local version reads

$$\boldsymbol{j^*}_{\mathbb{p}} = \boldsymbol{p}(\boldsymbol{x})\boldsymbol{c_p}, \tag{1.3.4}$$

where $\boldsymbol{c_p}$ is a vector of scalar coefficients weighting the terms of the polynomials contained in $\boldsymbol{p}(\boldsymbol{x})$ (i.e $\boldsymbol{p}(\boldsymbol{x}) = \{1, x, y, xy, x^2, y^2\}$ for 2 dimensions and order 2 shape functions).

The coefficients $\boldsymbol{c_p}$ for each component of the stress or flux can then be found using least squares method. Using the super-convergent points of integration as points to be fitted in the least squares method, the size of the local linear system of equations is kept at minimum size.

Yet, another improvement was presented by Ródenas et al. [149] by enforcing the local satisfaction of the equilibrium equation in the local patches.

$$\nabla \cdot \boldsymbol{j^*}_{\mathbb{p}}(\boldsymbol{x}_j) = f(\boldsymbol{x}_j) \qquad \forall \boldsymbol{x}_j \in \mathbb{P}_{\mathbb{p}}, \qquad \text{internal equilibrium,} \tag{1.3.5a}$$

$$\boldsymbol{j^*}_{\mathbb{p}}(\boldsymbol{x}_j) \cdot \overrightarrow{n} = g_n(\boldsymbol{x}_j) \qquad \forall \boldsymbol{x}_j \in \Gamma_n \cap \mathbb{P}_{\mathbb{p}}, \qquad \text{boundary equilibrium.} \tag{1.3.5b}$$

In some cases, such as elasticity problems, the compatibility equation or the Beltrami equation must also be enforced [175].

By applying the concepts of kinematic admissible solutions introduced in section 1.3.3, SPR can be modified to recover lower bounds of the error [54].

A specific review of variations of the SPR method was presented by Wiberg [184] including estimators for dynamic problems which are out of the scope of the present work.

Robustness of the recovery based estimates

Even though recovery based estimators are widely exploited and have many desirable features, it is known that they fail to predict any arbitrary large error under certain circumstances.

As an example extracted from [6], let the problem to be solved be a 1D variation of 1.2.1 such that

$$\frac{\partial}{\partial x} j(x) = f(x) := \alpha_R \cdot \sin(2^{\alpha_M} \pi x) \qquad \text{in } \Omega = [0,1], \tag{1.3.6a}$$

$$u(x) = u_d(x) := 0 \qquad \text{on } \Gamma_d = \{0,1\}, \tag{1.3.6b}$$

$$\Gamma_n = \emptyset, \tag{1.3.6c}$$

$$j(x) = -\frac{\partial}{\partial x} u(x) \qquad \text{in } \Omega, \tag{1.3.6d}$$

where $\alpha_M \in \mathbb{N}$ and $\alpha_R \in \mathbb{R}$ are constants.

If only uniform meshes of 2^{α_N} elements are considered (where $\alpha_M \neq \alpha_N \in \mathbb{N}$), it is known that any FE approximation $u^{\mathbb{h}}$ is an element linear interpolant of the exact solution

$$u(x) = \frac{\alpha_R \cdot \sin(2^{\alpha_M} \pi x)}{4^{\alpha_R} \pi^2}. \tag{1.3.7}$$

Then, as long as $\alpha_M > \alpha_N$ and there are 2^{α_N} uniform elements, the solution at all the nodal points is zero. Consequently, the predicted error between any of these discrete solutions is also zero.

1.3.3 Implicit constitutive relation based estimates

Ladevèze and Leguillon were pioneers of the Constitutive Relation Estimate (CRE) [106]. They made use of the Prager-Synge hypercircle [138] (figure 1.1). The idea

behind it is the computation of two different discrete solutions of the posed problem and the measurement of the distance between them. Both solutions are related to the same mesh.

The first solution is the most extended weak form of the problem. In this solution, the displacement (heat or concentration) $u^{\mathbb{h}}$ is kinetically admissible (KA) such that

$$\begin{array}{lll} u^{\mathbb{h}}(\boldsymbol{x}) = u_d(\boldsymbol{x}) & \text{on}\,\Gamma_d, & u^{\mathbb{h}}(\boldsymbol{x}) \text{ is prescribed at Dirichlet Boundary,} \\ \lim\limits_{\boldsymbol{x}\longrightarrow\boldsymbol{x}_i} u^{\mathbb{h}}(\boldsymbol{x}) = u^{\mathbb{h}}(\boldsymbol{x}_i) & \forall \boldsymbol{x}_i \in \Omega, & u^{\mathbb{h}}(\boldsymbol{x}) \text{ is continuous.} \end{array} \tag{1.3.8}$$

The second choice of weak problems is not as popular. It produces a statically admissible (SA) solution such that

$$\begin{array}{lll} \nabla \cdot \boldsymbol{j}^{\mathbb{h}}(\boldsymbol{x}) = f(\boldsymbol{x}) & \forall \boldsymbol{x} \in \Omega, & \boldsymbol{j}^{\mathbb{h}}(\boldsymbol{x}) \text{ fulfils the equilibrium/momentum,} \\ \boldsymbol{j}^{\mathbb{h}}(\boldsymbol{x}) \cdot \overrightarrow{n} = g_n(\boldsymbol{x}) & \forall \boldsymbol{x} \in \Gamma_n, & \boldsymbol{j}^{\mathbb{h}}(\boldsymbol{x}) \text{ is prescribed at Neumann Boundary.} \end{array} \tag{1.3.9}$$

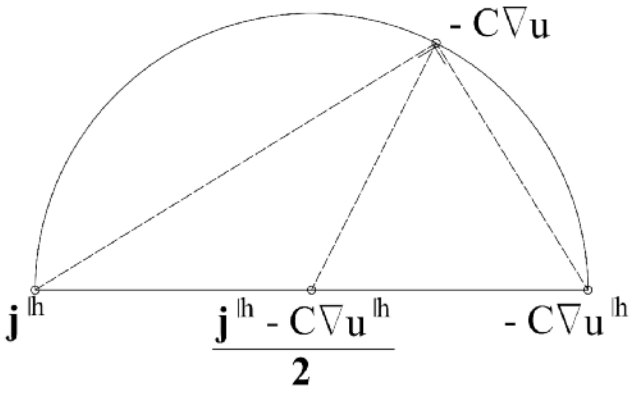

Figure 1.1: Prager-Synge hypercircle

The difference between the discrete stress fields obtained through both methods is equivalent to the error produced due to the non-verification of the constitutive relation. Then, by the Prager-Synge hypercircle theorem it is known that

$$||u-u^{\mathbb{h}}||_E^2+\int_\Omega C^{-1}(-C\nabla u-\boldsymbol{j}^{\mathbb{h}})(-C\nabla u-\boldsymbol{j}^{\mathbb{h}})d\Omega = \int_\Omega C^{-1}(C\nabla u^{\mathbb{h}}+\boldsymbol{j}^{\mathbb{h}})(C\nabla u^{\mathbb{h}}+\boldsymbol{j}^{\mathbb{h}})d\Omega. \tag{1.3.10}$$

Therefore, since $\int_\Omega C^{-1}(-C\nabla u - \boldsymbol{j}^{\mathbb{h}})(-C\nabla u - \boldsymbol{j}^{\mathbb{h}})d\Omega$ is strictly positive

$$||u - u^{\mathbb{h}}||_E^2 \leq \eta_{CRE} := \int_\Omega C^{-1}(C\nabla u^{\mathbb{h}} + \boldsymbol{j}^{\mathbb{h}})(C\nabla u^{\mathbb{h}} + \boldsymbol{j}^{\mathbb{h}})d\Omega. \tag{1.3.11}$$

Two different reviews on how to construct statically admissible problems were presented by Pled, Chamoin and Ladevèze [137] and de Almeida and Munder [48]. Of special interest is the work by Parés et al. [135], where both upper and lower bounds for the error are presented.

1.3.4 Implicit residual based estimates

The last category of estimators was presented by Babuŝka [18, 20]. They are based on the residual of the weak equation. The discretisation error $e(\boldsymbol{x}) = u(\boldsymbol{x}) - u^{\mathbb{h}}(\boldsymbol{x})$ belongs to the space $\mathcal{V}$ of continuous functions, and it is defined by the following expression

$$a^D(e(\boldsymbol{x}), v(\boldsymbol{x})) = l(v(\boldsymbol{x})) - a^D(u^{\mathbb{h}}(\boldsymbol{x}), v(\boldsymbol{x})), \qquad \forall\, v(\boldsymbol{x}) \in \mathcal{V}, \tag{1.3.12}$$

where the energy of the discrete solution is subtracted from both sides of the global problem. Therefore the residual can be defined as

$$\mathcal{R}^D(v(\boldsymbol{x})) := l(v(\boldsymbol{x})) - a^D(u^{\mathbb{h}}(\boldsymbol{x}), v(\boldsymbol{x})). \tag{1.3.13}$$

A partition of unity is used in the residual equation or in the test function to define patches where a local problem in a richer reference discrete space is solved. The global solution on the reference space can be reconstructed through the addition of all the local solutions. In contrast, the global norm can only be reconstructed through addition of local estimators if the patches are orthogonal with respect to each other. The most common way to partition the residual is to employ the Lagrange basis function $\lambda_{\mathbb{p}}$ (see equations 4.3.4 and 4.3.5 for details). Leading to the following local problems defined at patches $\mathbb{P}_{\mathbb{p}}$,

$$a^D_{\mathbb{p}}(e(\boldsymbol{x}), \lambda_{\mathbb{p}} v(\boldsymbol{x})) = \mathcal{R}^D_{\mathbb{p}}(\lambda_{\mathbb{p}} v(\boldsymbol{x})), \qquad \forall\, v(\boldsymbol{x}) \in \mathcal{V}, \qquad v(\boldsymbol{x}) = 0,\ on\ \Omega \backslash \Omega_{\mathbb{p}} \tag{1.3.14}$$

or alternatively

$$a^D_{\mathbb{p}}(e(\boldsymbol{x}), v(\boldsymbol{x})) = \mathcal{R}^D_{\mathbb{p}}(\lambda_{\mathbb{p}} v(\boldsymbol{x})), \qquad \forall\, v(\boldsymbol{x}) \in \mathcal{V}, \qquad v(\boldsymbol{x}) = 0,\ on\ \Omega \backslash \Omega_{\mathbb{p}} \tag{1.3.15}$$

where $a^D_{\mathbb{P}}(\cdot,\cdot)$ is the restriction to the patch $\mathbb{P}_{\mathbb{P}}$ of the bilinear form and $\Omega_{\mathbb{P}}$ is the local domain of the same patch.

If the local patches are solved applying zero Neumann Boundary Conditions (BC), implementation difficulties are to be expected. In general, it originates unsolvable problems due to the existence of zero energy modes. There are two ingredients to overcome this problem. The first one is restricting the subspace of solutions so that it excludes this modes [3]. The second one is to equilibrate the residual on patches of neighbours [106] so that the problem is well-posed. The latter adds the desired property of providing guaranteed upper bounds for the error when solving linear elliptic problems [4].

In the particular case of Neumann BC, the second option to define the patches (equation 1.3.15) and equilibration of the residual in the patch is called flux-free in literature, which is by far the most popular of the residual methods. An improved way of equilibrating the residual can be found in [134], which leads not only to a smaller computational cost, but also to an improved accuracy.

The residual reduction to local Dirichlet Problems retains most of the good properties of the residual family such as problem independence, access to the reference solution or the suitability for non-linear and non-smooth solutions [109, 88]. Furthermore its ease of implementation is unmatched because the FEM data structures can be reused for the local problems. On the other hand, it lacks the property of guaranteed upper bounds provided by the equilibrated residual approaches.

One of the novel contributions of the present work is the presentation of a technique that enables decoupling the definition of the patch from the partition of unity of the residual, allowing a higher accuracy in the estimates. Residual based estimates and other type of patches is discussed in more depth in chapter 4.

1.4 Goal-oriented error estimation

All of the aforementioned error estimators are defined for the energy norm. Even though the energy in a system is a very relevant quantity to characterise a problem,

it is not always the most relevant physical magnitude in the design or the solution of an engineering problem. Goal-oriented error estimation is a technique that allows to change the scalar measure assessing the error and the local estimates from the energy norm to any functional of the solution. This functional is known as the Quantity of Interest (QoI).

The first goal-oriented estimators were aimed to elliptic problems [25, 44, 133, 139]. Despite it is possible to compute the error in the QoI from a coarse field and an estimated improved field obtained through any error estimation technique, this approach cannot be localised. In order to localise the computed QoI, the adjoint problem of the QoI must be introduced. The exact solution for the error in the adjoint problem must be replaced by a suitable numerical approximation [26].

The goal is to find the error ϵ^Q in a QoI and to formulate its adjoint problem. Let q be the linear functional $q(u(\boldsymbol{x}))$ that extracts the desired QoI from the solution $u(\boldsymbol{x})$. Then ϵ^Q reads

$$\epsilon^Q = q(u(\boldsymbol{x})) - q(u^{\mathbb{h}}(\boldsymbol{x})) = q(e(\boldsymbol{x})). \tag{1.4.1}$$

The starting point is trying to find a functional z that relates the residual and $q(e(\boldsymbol{x}))$

$$q(e(\boldsymbol{x})) = z(\mathcal{R}^D(\boldsymbol{x})). \tag{1.4.2}$$

As stated in [129] "z is an element of the bidual of $\mathcal{V}$, and since $\mathcal{V}$ was assumed a Hilbert space, and *a fortiori* a reflexive space, 1.4.2 becomes

$$q(e(\boldsymbol{x})) = \mathcal{R}^D(z(\boldsymbol{x})), \tag{1.4.3}$$

where $z(\boldsymbol{x})$ is now identified with an element of $\mathcal{V}$".

The field z is known as the *influence field* or *influence function*, since it reflects how the residual influences the QoI. From equation 1.4.3 and using the definition of the residual (equation 1.3.13), it is immediate to derive the dual-weighted form of the adjoint problem.

$$\mathcal{R}^D(z(\boldsymbol{x})) = q(e(\boldsymbol{x})) = a^D(e(\boldsymbol{x}), z(\boldsymbol{x})). \tag{1.4.4}$$

This adjoint leads to the computation of any discrete version of z, and due to Galerkin orthogonality

$$\mathcal{R}^D(z(\boldsymbol{x})) \approx \mathcal{R}^D(\hat{z}(\boldsymbol{x}))) = \mathcal{R}^D(\hat{z}(\boldsymbol{x}) - z^{\mathbb{h}}(\boldsymbol{x})) = \mathcal{R}^D((\hat{z}(\boldsymbol{x}) - \overset{\nu^{\mathbb{h}}}{\underset{\widehat{\nu}}{\pi}}(\hat{z}(\boldsymbol{x}))), \tag{1.4.5}$$

where $\overset{\nu^{\mathbb{h}}}{\underset{\widehat{\nu}}{\pi}}$ is a projector of any field $\hat{v} \in \widehat{\mathcal{V}}$ to a coarse space $\mathcal{V}^{\mathbb{h}} \subset \widehat{\mathcal{V}}$ defined below.

$$\overset{\nu^{\mathbb{h}}}{\underset{\widehat{\nu}}{\pi}}(\widehat{v}) = \overset{\nu^{\mathbb{h}}}{\underset{\widehat{\nu}}{\pi}}([\widehat{v}]\widehat{\psi}) = v^{\mathbb{h}*} = [v^{\mathbb{h}*}]\psi^{\mathbb{h}} \begin{cases} [v^{\mathbb{h}*}{}_{i_{\mathrm{DOF}}}] = [\widehat{v}_{i_{\mathrm{DOF}}}] & \text{if } i_{\mathrm{DOF}} \in \mathcal{V}^{\mathbb{h}}; \\ [v^{\mathbb{h}*}{}_{i_{\mathrm{DOF}}}] = \varnothing & \text{if } i_{\mathrm{DOF}} \notin \mathcal{V}^{\mathbb{h}}. \end{cases} \tag{1.4.6}$$

Note that if $\mathcal{V}^{\mathbb{h}} \nsubseteq \widehat{\mathcal{V}}$, some nodal points must be interpolated using equation 1.2.7, but it is not be the case of the present work.

Most importantly, the same partition of unity used in residual estimators can be applied to estimate the local contribution of the residual and the influence field to a given QoI.

Goal-oriented error estimation can be utilised with any other family of estimators apart from the residual based.

Multiple goal-oriented estimators have been proposed for different kind of problems. A non-exhaustive list includes ordinary differential equations [61], gradient elasticity theory of Aifantis [39], non-linear elasticity [109], reduced order modelling [100], plasticity [145], non-linear reaction diffusion [62], wave propagation [22], hyperbolic system [108], compressible flows [157] and incompressible Navier-Stokes equation [85].

1.4.1 Bounds for goal-oriented error estimation

Notwithstanding bounds for the norm including the QoI are in general not available, it is possible to obtain bounds by expressing this norm as a combination of different energy norms.

The use of the Cauchy-Schwarz inequality leads to

$$|a^D(e(\boldsymbol{x}), z(\boldsymbol{x}) - z(\boldsymbol{x})^{\mathbb{h}})| \leq ||e(\boldsymbol{x})||_E ||z(\boldsymbol{x}) - z(\boldsymbol{x})^{\mathbb{h}}||_E. \tag{1.4.7}$$

Another possibility is to exploit polarisation identity

$$a^D(e(\boldsymbol{x}), z(\boldsymbol{x}) - z(\boldsymbol{x})^{\mathbb{h}}) = \frac{||(z(\boldsymbol{x}) - z(\boldsymbol{x})^{\mathbb{h}}) + e(\boldsymbol{x})||_E^2 - ||(z(\boldsymbol{x}) - z(\boldsymbol{x})^{\mathbb{h}}) - e(\boldsymbol{x})||_E^2}{4}, \tag{1.4.8}$$

which does not involve an inequality.

1.5 Mesh adaptivity

The purpose of mesh adaptivity is to minimise the number of DOF needed to reach the desired accuracy in the solution. To achieve this goal the adaptive iterative process consists of four phases repeated at each step of mesh refinement. The phases are: (1) computing the solution for the mesh corresponding to the current mesh, (2) checking the desired global error, (3) estimating the local error and (4) refining the mesh in the areas where the local error is higher according to the estimation. The process is stopped at the second step if the desired global accuracy has been reached.

The process ensures that the density of DOF is larger on the parts of the domain where it is more difficult to characterise the solution. Ideally, at the end of the process all local contributions of the error are of the same magnitude, whatever the size of the element. Of course, since the process is iterative and not deterministic, the absolute minimum is never reached, but with each local refinement the distance to the ideal mesh is reduced.

Once determined where the local refinement of the mesh must be enforced, there exist 3 options to proceed.

- The mesh remains unchanged except for the elements marked for refinement. This approach leads to a non-conforming mesh. The new smaller elements have hanging nodes which belong also to the interior of edges of adjacent unrefined elements (these hanging nodes are illustrated as red dots in figure 1.2.a). Therefore, constrains must be applied to the shape functions of the refined elements to ensure continuity with the solution of the adjacent coarse element. If there is just one level of hanging nodes only direct constrains to

some shape functions of that refined elements must be imposed. In particular, they must be compatible with the shape functions of the adjacent coarse elements which are not zero in an edge shared with the refined elements. In contrast, if there is more than one level of hanging nodes, indirect constrains arise. For details about the involved procedure of imposing more than one level of constrains, the reader is referred to [165, 105, 53].

- If the mesh consists of triangular elements, new edges can be produced from each hanging node to the node not belonging to the edge in the coarse element. This option removes the non-conformity of the mesh, but leads to cumulative badly shaped elements. Skewed elements (as the one marked in red in figure 1.2.b) make the condition number of the resulting stiffness matrix to increase. In practice, irregularity rules are implemented to entirely re-mesh adjacent elements in a way that the level of hanging nodes is minimised for the next mesh, and at the same time the shape of the elements remains within acceptable skewness margins.

- A completely different way to perform adaptivity is to re-mesh the whole mesh at each refinement step. In order to do so, a map of the required characteristic length $\mathbb{h}$ for the elements is used when drawing each mesh. If an element is marked for refinement, the required characteristic length is reduced locally in the map, allowing a transitional region to match adjacent magnitudes of required characteristic lengths. This approach completely removes any hanging node and maintains a good shape for all the elements. However, the need of transition zones slightly increase the number of DOF required in a mesh. Furthermore, since each mesh is completely different, it makes the transfer of information between meshes cumbersome (interpolation is needed), so it is not recommended for time dependent problems. Figure 1.2.c includes an example of a refined mesh with grey shapes where the miss-matched elements of previous meshes laid prior to be marked for refinement.

Convergence of adaptive meshes with hanging nodes was mathematically proved

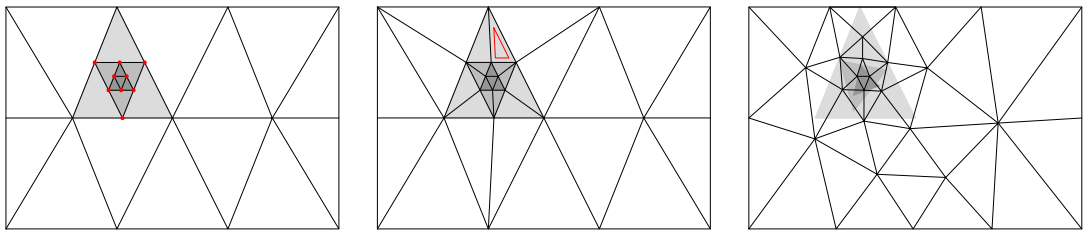

(a) Unchanged mesh allowing hanging nodes

(b) Unchanged mesh suppressing hanging nodes by adding edges

(c) Re-meshing by density of characteristic length map

Figure 1.2: Resulting meshes depending on the approach after 4 levels of adaptive local refinement

in [56, 123]. Later, rates of convergences where incorporated to this proof [30]. More recently [40] investigates the axioms that determine if the adaptive process driven by a particular error estimator leads to quasi optimal convergence.

1.6 Conclusion

This chapter summarises the type of error estimators for discretisation of boundary valued problems. A-priori and explicit a-posteriori error estimators allow to estimate the error as a function of mesh parameters, problems parameters and a constant. Even though this estimation is known to be pessimistic, it suffices to predict the convergence of a method. On the contrary, the rest of a-posteriori estimators use an already computed discrete solution to estimate or to bound the distance between it and the non-discrete one.

Among the latter, SPR methods are based on reconstructing the stress or flux fields so that it is smooth and optionally fulfils some equilibrium or compatibility requirements. These methods are in general of easy implementation but they are known to occasionally fail to estimate arbitrary large errors (see section 1.3.2).

CRE methods are based on the constitutive relation and a pair of discrete solutions, one of them statically admissible and the other one kinematically admissible. The methods produce guaranteed bounds but their implementation is not easy. The

difficulty lies in the requirement of two different finite solutions in complementary spaces and thus two programs to compute them.

Finally, the residual family requires the computation of local problems in a reference space generated through a partition of unity of the residual equation. If zero Neumann BC are imposed in the local problems, equilibration and the exclusion of the zero energy modes are needed, but they guarantee upper and lower bounds. On the contrary, if Dirichlet BC are applied, its implementation is the easiest of all methods. However, bounds are not guaranteed even though the accuracy of the approximation is usually sharp.

In this work, only a-posteriori error estimators based on the residual and local Dirichlet BC are employed and explored in detail. One reason is that published literature offers the larger range of patch size choice and this dissertation delves into the effect of local patch size in the estimations. Furthermore, the fact that they are based on the residual, allows the integration into an iterative solver algorithm to decrease the error of the approximations at an algebraic level (see chapter 3). Lastly, on a more practical view, the easiness of implementation, first class accuracy and ability to capture non smooth stresses fit perfectly the scope of the dissertation regarding the characterisation and optimisation of the discretisation error.

Goal-oriented estimation is a necessary inclusion because the unknown of the problem to solve in chapter 5 is a QoI response surface. This technique allows to change the measure of any error estimation method from the energy norm to any linear functional of the solution defined by the user. The localisation of the QoI for residual estimators can be achieved easily through the same partition of unity employed to compute the estimated reference solution.

Chapter 2

Uncertainty propagation and random processes in the finite element method

2.1 Introduction

The previous chapter reviews error estimation for computational mechanics problems specifically from the perspective of controlling the discretisation error within a deterministic framework. However, uncertainty can make the estimation of this error unreliable and introduces new errors associated with the finite description of the probabilistic measures used to characterise the solution stochastic process. Assessing this uncertainty is an essential ingredient in engineering computations. A non-exhaustive list of possible sources of uncertainty is:

- Problems based on data which may contain noise, be incomplete, conflicting or too complex (*e.g.* earthquake or wind loads or physical quantities defined through measurements).
- Manufacturing tolerances (*e.g.* geometrical imperfections, heterogeneity of aggregates or distribution of reinforcement fibres).
- Problems involving predictions (*e.g.* probability of failure problems or inverse

problems where a physical quantity must be predicted from the stored data history of another quantity, which may have multiple solutions).

There are two possibilities to study the effects of uncertainty in structures. The non-probabilistic approach (see examples at the end of this introduction) assesses the uncertainty or risk completely apart from the numerical model and without using probability theory. Once this analysis is done, some characteristic values are attained and applied to the deterministic numerical model. Then, the model produces solutions for these characteristic values obtained from the uncertain magnitudes in the first step. The typical values tested are the mean, minimum and maximum effects considered after the uncertainty assessment. The goal is to test the normal behaviour of the structure and its resistance to all extreme cases considered. While this approach is unable to represent the range on uncertainty, it can be more efficient when the purpose of the engineering problem is to verify the integrity of a structure, which is very common. The reason is that the amount of data required to establish conservative limit values is smaller than the amount needed to characterise completely a random event as an stochastic process.

In contrast, the aim of probabilistic approaches is to describe in detail the uncertainty and its outcomes by introducing probabilistic descriptors for modelling uncertainty in the parameters of the numerical model. Each uncertain parameter considered becomes a new dimension in the numerical model describing the variation of the solution in that particular dimension. Including these additional parametric dimensions leads to a solution response surface (if the number of parameters is larger than 2, the response is a volume or hyper-volume, even if it is still known as response surface). This surface contains all possible outcomes for the structure and is linked to a probability measure which describes the likelihood of each outcome.

Regarding uncertainty, the aim of this thesis is to control the stochastic error (sampling and surrogate model) of an unknown stochastic function process where the aleatory input parameters are given and assumed to be well characterised. The unknown stochastic function produces a response, dependent or ultimate random variable, which is function of the input parameters described by known primary or

explanatory random variables. In particular, the input parameters are Young's moduli of some parts of a vibrating structure defined through a primary random variable ruled by Gaussian probability distribution and the FEM model is the function mapping to the dependent variable which is the QoI. Section 2.3 presents a more detailed review for probabilistic approaches, and only a brief summary of non-probabilistic or hybrid approaches is listed next.

A first example of non-probabilistic approach is worst case scenario [16, 27]. The method poses the uncertainty as an addition of a nominal value and a perturbation series [28], and then determines the combination of perturbations that leads to the most unfavourable solution.

A second example is Fuzzy logic [42, 58]. In contrast with classical set theory, in fuzzy theory the belonging of an element to a set is not binary ($\{0, 1\}$). Instead, the degree of belonging is determined by a characteristic function that maps to the closed interval $[0, 1]$. The fuzzy number is the set of elements that are above a given threshold in the interval. Consequently, the lower and upper bounds of admissible perturbations are the minimum and maximum elements belonging to the set defined by this fuzzy number.

Methods based on the most probable point [82] use stochastic processes to compute the probability of failure. However, they do not describe the ultimate stochastic process. The most known practices in this category are first and second order reliability methods.

In addition, other hybrid approaches have been presented attempting to combine the best aspects of probabilistic and non-probabilistic methods. Some hybrid examples are the lack of knowledge technique [107] or the work presented in [185] which combines modal analysis [83], second-order perturbation [28] and the number theoretical method [114, 111].

2.2 Probability space definition

Before reviewing any probabilistic approach to uncertainty propagation, it is essential to define a problem and a probabilistic framework. Let $\mathfrak{M}$ be a numerical model based on FE that produces a QoI $q(u(\boldsymbol{\mu}))$, given a vector of parameters $\boldsymbol{\mu}(\boldsymbol{\theta})$ and a spatial mesh $\mathcal{M}_{i_\mathcal{M}}$ used to discretise the problem. An example would be a problem based on the weak form 1.2.2 with the boundary conditions defined at equation 1.2.1, considering that the diffusion coefficient $C(\boldsymbol{x}, \boldsymbol{\mu}(\boldsymbol{\theta}))$ has a known statistical variation. In the posed example, the domain $\Omega(\boldsymbol{x})$ is split into r non-overlapping subdomains and the components of the random variable $\boldsymbol{\mu}(\boldsymbol{\theta}) = \{\mu_1, ..., \mu_r\}$ define the stochastic process describing the variation of the diffusion coefficient at each subdomain. Consequently, μ_j are called the parameters and r the number of parametric dimensions. The QoI is any functional $q(\cdot)$ that produces a scalar quantity from the response surface solution $u(\boldsymbol{x}, \boldsymbol{\mu}; \mathcal{M}_{i_\mathcal{M}})$ to the problem 1.2.2.

In order to characterise the primary known stochastic process describing $C(\boldsymbol{x}, \boldsymbol{\mu}(\boldsymbol{\theta}))$ (and the one resulting of applying the FEM model $\mathfrak{M}$), a probability space must be defined. A continuous probability space comply with the following conditions:

- A sampling space that is a non-empty set $\Theta \subseteq \mathbb{R}^r$ containing all possible outcomes $\boldsymbol{\theta}$.

- The smallest σ-algebra $\mathscr{F}$ consisting of a set of all measurable subsets $\mathscr{S}_{i_\mathcal{S}}$, including the empty set and Θ. In order to be a σ-algebra, a set of events or subsets $\mathscr{S}_{i_\mathcal{S}}$ must be closed under complements, countable unions and countable intersections. The first closure condition means that if $\mathscr{S}_{i_\mathcal{S}} \in \mathscr{F}$, then also $(\Theta \backslash \mathscr{S}_{i_\mathcal{S}}) \in \mathscr{F}$. From the second closure condition, if $\mathscr{S}_{i_\mathcal{S}} \in \mathscr{F}$ for $i_\mathcal{S} = 1, ..., \infty$ then also $\left(\bigcup_{i_\mathcal{S}=1}^{\infty} \mathscr{S}_{i_\mathcal{S}} \right) \in \mathscr{F}$. Furthermore, $\left(\bigcap_{i_\mathcal{S}=1}^{\infty} \mathscr{S}_{i_\mathcal{S}} \right) \in \mathscr{F}$ must also be satisfied from the third condition. The smallest σ-algebra that includes all measurable subsets is also known as Borel algebra.

- The probability that an outcome $\boldsymbol{\theta}$ of $\boldsymbol{\mu}$ is included in a measurable subset of $\mathscr{F}$ reads $\mathcal{P}(\boldsymbol{\mu} \in \mathscr{S}_{i_\mathcal{S}}) = \int_{\mathscr{S}_{i_\mathcal{S}}} f_{\boldsymbol{\mu}}^{\mathcal{P}}(\boldsymbol{\theta}) d\boldsymbol{\theta}$, where $\mathcal{P}$ is the probability measure, and the probability density function (PDF) $f_{\boldsymbol{\mu}}^{\mathcal{P}}$ is known. The PDF must fulfil the

following requirements: $\mathcal{P}(\boldsymbol{\mu} \in \Theta) = \int_\Theta f_{\boldsymbol{\mu}}^{\mathcal{P}}(\boldsymbol{\theta}) d\boldsymbol{\theta} = 1$; $f_{\boldsymbol{\mu}}^{\mathcal{P}}(\boldsymbol{\theta}) \geq 0 \quad \forall \boldsymbol{\theta}$; and if a countable set $\{\mathscr{S}_{i_\mathcal{S}}\}_{i_\mathcal{S}=1}^{\infty} \subseteq \mathscr{F}$ such that $\mathscr{S}_{i_\mathcal{S}} \cap \mathscr{S}_{i'_\mathcal{S}} = \emptyset, \ \forall i_\mathcal{S} \neq i'_\mathcal{S}$, then, $\mathcal{P}\Big(\bigcup_{i_\mathcal{S}=1}^{\infty} \mathscr{S}_{i_\mathcal{S}}\Big) = \sum_{i_\mathcal{S}=1}^{\infty} \mathcal{P}\Big(\mathscr{S}_{i_\mathcal{S}}\Big)$.

Subsequently, a probability space is formed by the triple $(\Theta, \mathscr{F}, \mathcal{P})$. And the primary random variable can be expressed as $\boldsymbol{\mu}(\boldsymbol{\theta}) : \Theta \mapsto \mathbb{R}^r$.

Applying the numerical model $\mathfrak{M}(\boldsymbol{\mu})$ with a given mesh $\mathcal{M}_{i_\mathcal{M}}$ results in an unknown stochastic process. The response QoI random variable $Q_{i_\mathcal{M}}(\theta_Q) : \Theta_Q \mapsto \mathbb{R}$ is ruled by an unknown PDF $f_Q^{\mathcal{P}}$, yet it is function of the primary random variable $(Q_{i_\mathcal{M}}(\theta_Q) \equiv Q_{i_\mathcal{M}}(\boldsymbol{\mu}, \mathcal{M}_{i_\mathcal{M}}))$. Due to this dependence there exists a surjective non-injective map between both sampling spaces allowing to pose the problem as

$$\mathfrak{M}(\boldsymbol{\mu}(\boldsymbol{\theta})) : \Theta \longmapsto Q_{i_\mathcal{M}}(\theta_Q), \tag{2.2.1}$$

where $\boldsymbol{\theta} \in \Theta \subseteq \mathbb{R}^r$ and $\theta_Q = q(u(\boldsymbol{\mu}(\boldsymbol{\theta}))) \in \Theta_Q \subseteq \mathbb{R}$. In other words, the numerical FEM model maps a random variable $\boldsymbol{\mu}$ belonging to $\mathbb{R}^r$ to another random variable $Q_{i_\mathcal{M}}$ belonging to $\mathbb{R}$. Since the samples are always drawn from the primary stochastic space Θ, this dissertation drops the notation θ_Q, and $Q_{i_\mathcal{M}}$ henceforth denotes both the dependent random variable and its outcomes.

2.2.1 Probabilistic representation of random fields

The focus of the present work is to optimise the discretisation and stochastic errors as well as to scale them until reducing them is unreliable due to the uncertainty. This can be done through a very simple representation of the probabilistic fields. Therefore random variables are used to model the random fields. However, this section presents a few alternatives present in literature.

Collection of random variables (normal distribution example)

The simplest way to describe a probabilistic field $u(\boldsymbol{x}, \boldsymbol{\theta})$ is to make use of the triplet $(\Theta, \mathscr{F}, \mathcal{P})$ forming a probability space. In this approach, a collection of random variables $\mu^j(\theta_j)$ must be defined associated to n_j different spatial subdomains $\Omega_j \subset \Omega \subset \mathbb{R}^d$ of d dimensions. Then, the components of the resulting multivariate random

variable $\boldsymbol{\mu(\theta)} = \{\mu^j(\theta_j)\}_{j=1}^{j=n_j} \in \Theta \subset \mathbb{R}^{n_j}$ are indexed by the coordinate vector $\boldsymbol{x} \in \Omega$. Each of them is ruled by a unidimensional PDF, or alternatively, a multidimensional PDF can be employed if the correlation between all components is known.

An example of unidimensional PDF is the normal distribution reading

$$\mathrm{g}(\mu) = \frac{1}{\sqrt{2\pi\sigma^2}} e^{\frac{-(\mu-\mathcal{E}[\mu])^2}{2\sigma^2}}, \tag{2.2.2}$$

where $\mathcal{E}[\mu]$ stands for the expectation of μ and σ^2 for the variance, namely

$$\mathcal{E}[\mu(\theta)] = \int_{-\infty}^{\infty} \theta f_{\mu}^{p}(\theta) d\theta \tag{2.2.3}$$

$$\sigma^2 = var(\mu) := \mathcal{E}[(\mu - \mathcal{E}[\mu])^2]. \tag{2.2.4}$$

For future reference, the standard deviation σ equals the square root of the variance.

The r-dimensional version of $\mathrm{g}(\boldsymbol{\mu})$ reads

$$\mathrm{g}(\boldsymbol{\mu}) = \frac{1}{\sqrt{(2\pi)^r |\boldsymbol{\Sigma}|}} e^{\frac{-(\boldsymbol{\mu}-\mathcal{E}[\boldsymbol{\mu}])\boldsymbol{\Sigma}^{-1}(\boldsymbol{\mu}-\mathcal{E}[\boldsymbol{\mu}])}{2}}, \tag{2.2.5}$$

where $\boldsymbol{\mu}$ is a random variable of r dimensions and $\boldsymbol{\Sigma}$ is the covariance matrix. The covariance operator in general form for two random variables X and Y reads

$$cov(X, Y) = \mathcal{E}[(X - \mathcal{E}[X])(Y - \mathcal{E}[Y])], \tag{2.2.6}$$

which allows to obtain $\boldsymbol{\Sigma} = cov(\boldsymbol{\mu}, \boldsymbol{\mu})$ or equivalently $\boldsymbol{\Sigma}_{ij} = \mathcal{E}[(\mu_i - \mathcal{E}[\mu_i])(\mu_j - \mathcal{E}[\mu_j])]$.

Karhunen-Loève expansion

The Karhunen-Loève expansion [117, 189] represents a probabilistic field $u(\boldsymbol{x}, \boldsymbol{\theta})$ as the following infinite series

$$u(\boldsymbol{x}, \boldsymbol{\theta}) = \mathcal{E}[u(\boldsymbol{x})] + \sum_{k=1}^{k=\infty} \sqrt{\lambda_k} \Phi_k(\boldsymbol{x}) \xi_k(\boldsymbol{\theta}), \tag{2.2.7}$$

where $\xi_k(\boldsymbol{\theta})$ are uncorrelated random variables fulfilling $\mathcal{E}[\xi_k] = 0$, $var(\xi_k) = 1$; and λ_k and Φ_k are the eigenvalues and eigenfunctions of the covariance function $C_u(\boldsymbol{x_1}, \boldsymbol{x_2}) = cov(u(\boldsymbol{x_1}), u(\boldsymbol{x_2}))$. Then, the covariance has the following spectral decomposition

$$C_u(\boldsymbol{x_1}, \boldsymbol{x_2}) = \sum_{k=0}^{k=\infty} \lambda_k \Phi_k(\boldsymbol{x_1}) \Phi_k(\boldsymbol{x_2}). \tag{2.2.8}$$

Furthermore, each pair of λ_k and Φ_k is the solution to

$$\int_{\Omega} C_u(\boldsymbol{x_1}, \boldsymbol{x_2})\Phi_k(\boldsymbol{x})d\boldsymbol{x_1} = \lambda_k \Phi_k(\boldsymbol{x_2}). \tag{2.2.9}$$

In practice, the series is truncated taking advantage of eigenvalue value decay. The PDF of ξ_k must be known or enough data must be available to fit the variables. Since the covariance is needed in this polynomial expansion, it is usually used in literature to define input or primal variables.

Polynomial chaos expansion representation of random quantities

One of the applications of Polynomial Chaos Expansion (Wiener chaos or PCE) [73, 186] is to represent a multivariate random field $u(\boldsymbol{x}, \boldsymbol{\theta})$ when the covariance function $C_u(\boldsymbol{x_1}, \boldsymbol{x_2})$ is unknown. The expansion takes the form

$$u(\boldsymbol{x}, \boldsymbol{\theta}) := \sum_{i_Z=1}^{\infty} \mathbb{c}_{i_Z} Z_{i_Z}, \tag{2.2.10}$$

where $\{Z_{i_Z}\}_{i_Z=0}^{\infty}$ is an orthogonal polynomial basis and $\{\mathbb{c}_{i_Z}\}_{i_Z=0}^{\infty}$ are coefficients that need to be fit. Because PCE does not need information about the covariance, it is mostly used to represent dependent variables when the orthogonality of the polynomial expansion contributes to the speed or accuracy of the computations.

This thesis does not uses PCE to represent random quantities. However, it uses PCE as a reduced model to avoid multiple evaluations of the FEM model. More details about this use and PCE can be found in section 2.4.2, where the coefficients are fit to match the response variable field or QoI.

2.3 Stochastic approaches to forward uncertainty propagation based on sampling

As in the case of probabilistic representation of random variables, the simplest sampling technique to evaluate forward uncertainty propagation was selected. That are Monte Carlo methods. However for the sake of completeness on the literature review section of the present dissertation some other sampling approaches are commented.

2.3.1 Monte Carlo methods

Monte Carlo (MC) methods [147, 72, 151] were developed as a way to evaluate integrals in the probability space. Even in the case that a perfect random number generator matching exactly the primary PDF can be exploited, MC's convergence is very slow ($\mathcal{O}(\sqrt{n_s})$ being n_s the number of samples). On the positive side, this convergence is independent of the number of dimensions in any stochastic space. In the case of study, the exact primary cumulative distribution function is known and is continuous; hence almost-perfect sampling generation can be considered thanks to the inverse random sampling, also known as inverse probability integral transform (see [52] for a review on random sampling generation).

MC methods can be applied to approximate response random variables function of primary variables, which is particular useful for this thesis. Provided that a random variable X is ruled by the known PDF $f_X^{\mathcal{P}}$, the unknown PDF $f_Y^{\mathcal{P}}$ ruling the random variable $Y = F(X)$ function of X can be approximated by extracting samples X_s of X following the PDF $f_X^{\mathcal{P}}$ and evaluating them to produce outcomes $Y_s = F(X_s)$ of Y.

The accuracy of this approximations and the significance of sampling according to $f_X^{\mathcal{P}}$ can be seen in figure 2.1. In both cases $F(X) := X^2$, so the only difference in the MC method to estimate $Y_{\mathcal{U}} = (X_{\mathcal{U}(0,2)})^2$ and $Y_{\mathcal{N}} = (X_{\mathcal{N}(2,1,1)})^2$ is the generation of samples according to the correspondent PDF. Here, $\mathcal{U}(0, 2)$ denotes a uniform PDF in the interval [0 , 2] and $\mathcal{N}(2.1, 1)$ a normal distribution with mean 2.1 and variance 1. The analytical solutions can be obtained performing a change of variable. This leads to $f_{Y_{\mathcal{U}}}^{\mathcal{P}} = \frac{1}{4}Y^{-1/2}$ as analytical solution for the former and $f_{Y_{\mathcal{N}}}^{\mathcal{P}}$ equal to the *Chi-squared* PDF with 1 Degree Of Freedom (DOF) and 2.1^2 as non-centrality parameter for the latter.

MC methods also allow to approximate any statistical moment of the ultimate variable from the outcomes attained after evaluating the samples drawn from the primary variable. Going back to the case of interest defined in section 2.2, the MC

approximation of the expectation $\mathcal{E}[Q]$ of the dependent variable $Q(\boldsymbol{\mu})$ reads

$$\mathcal{E}[Q] = \int_{-\infty}^{\infty} Q f_Q^{\mathcal{P}} dQ \approx \overline{\mathcal{E}}[Q] := \frac{1}{n_s} \cdot \sum_{s=1}^{n_s} \mathfrak{M}(\boldsymbol{\mu_s}) = \frac{1}{n_s} \cdot \sum_{s=1}^{n_s} Q_s, \qquad \boldsymbol{\mu_s} \sim f_{\boldsymbol{\mu}}^{\mathcal{P}}(\boldsymbol{\theta}), \quad (2.3.1)$$

where $\boldsymbol{\mu_s}$ are the samples equivalent to X_s, $\mathfrak{M}(\boldsymbol{\mu_s})$ is the functional equivalent to $F(X)$, and Q_s are the outcomes of the response variable equivalent to Y_s.

2.3.2 Other sampling methods

Pure MC methods have two major drawbacks. Firstly, its convergence rate ($\mathcal{O}(\sqrt{n_s})$ assuming perfect sampling generation) is small compared to other methods. Secondly, the PDF of the initial stochastic process must be known in order to correctly draw the samples.

Three initial approaches to address the first drawback and optimise the sampling of a known stochastic process can already be found at [93]. To begin with, if the stochastic process is a linear combination of several initial processes, correlation can be exploited to reduce the samples. Next, importance sampling (which is the most prolific approach *e.g.* [121, 148]) replaces the PDF $f_{\boldsymbol{\mu}}^{\mathcal{P}}$ for another one $f_{\boldsymbol{\mu}}^{*}$ such that $\mathcal{E}[\mathfrak{M}(\boldsymbol{\mu})] = \int \mathfrak{M}(\boldsymbol{\mu}) f_{\boldsymbol{\mu}}^{\mathcal{P}}(\boldsymbol{\mu}) = \int \frac{\mathfrak{M}(\boldsymbol{\mu}) f_{\boldsymbol{\mu}}^{\mathcal{P}}(\boldsymbol{\mu})}{f_{\boldsymbol{\mu}}^{*}(\boldsymbol{\mu})} f_{\boldsymbol{\mu}}^{*}(\boldsymbol{\mu}) = \int \mathfrak{M}^{*}(\boldsymbol{\mu}) f_{\boldsymbol{\mu}}^{*}(\boldsymbol{\mu})$ and $\mathfrak{M}^{*}(\boldsymbol{\mu})$ has the minimum variance possible. Finally, statistical-estimation methods take advantage of the relations that the posed problem imposes between the problem's conditions and the stochastic processes.

Apart from these initial principles, there exists a vast variety of strategies that, under certain conditions (*e.g.* in a Markov Chain Monte Carlo process [74]) and based on the known previous samples, drive the subsequent samplings towards the regions of the PDF where the probability is larger. Consequently, they do not require PDF knowledge. They are useful in Gaussian regression or inverse problems (out of the scope of the present work). Some of these alternatives are adaptive sampling [36], collocation [172, 126, 17], Latin hypercube sampling [120, 84, 91] or sparse grid sampling [23, 183, 158]. More recently, some of these alternatives (along with some surrogates relying on these sampling schemes to fit them) have been classified under the "improved Monte Carlo" category, *e.g.* in paper [87].

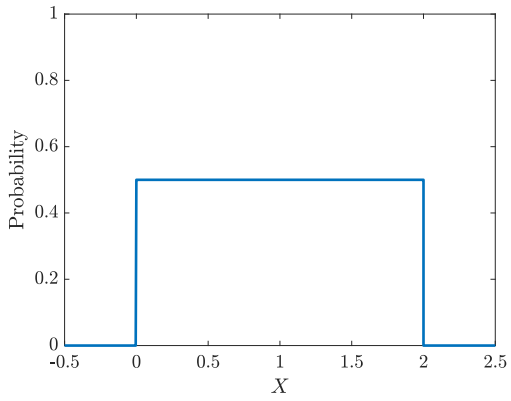

(a) PDF of $X_{\mathcal{U}(0,2)}$

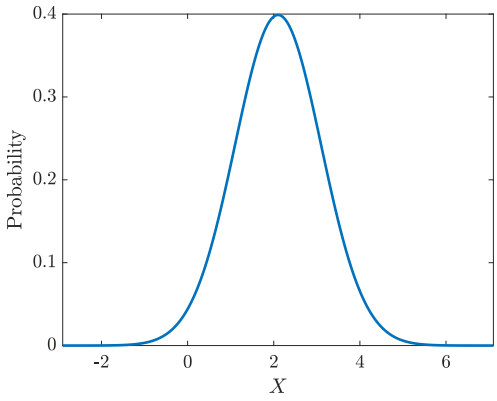

(b) PDF of $X_{\mathcal{N}(2.1,1)}$

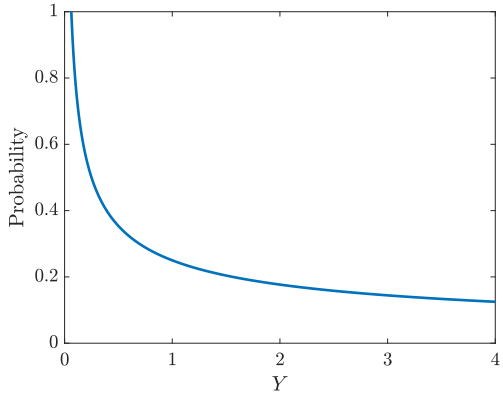

(c) Analytical PDF of $Y_U = (X_{\mathcal{U}(0,2)})^2$

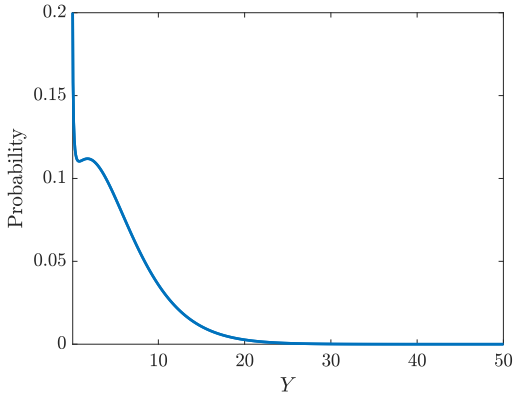

(d) Analytical PDF of $Y_N = (X_{\mathcal{N}(2.1,1)})^2$

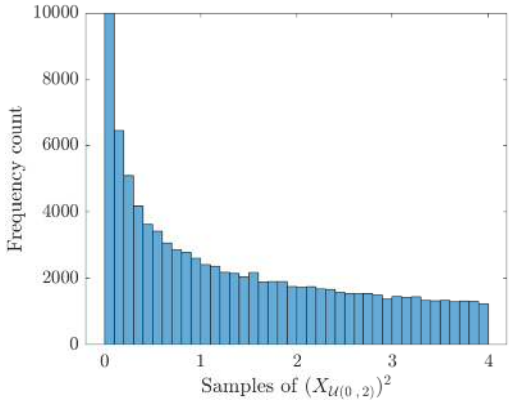

(e) MC approx. of PDF of $Y_{\mathcal{U}} = (X_{\mathcal{U}(0,2)})^2$

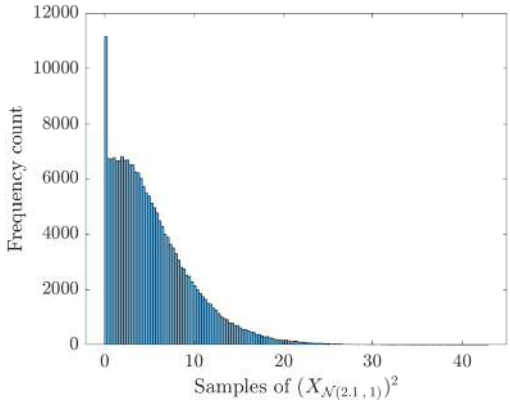

(f) MC approx. of PDF of $Y_{\mathcal{N}} = (X_{\mathcal{N}(2.1,1)})^2$

Figure 2.1: Monte Carlo approximation of the response random variable $Y(X) = X^2$ with different initial PDFs of X

2.4 Stochastic approaches to forward uncertainty propagation based on reduced surrogate models

In parallel to sampling methods, several techniques to create surrogate models have been published. Surrogates produce response surfaces with reduced or even negligible computational cost in comparison with the cost of evaluating the usually complex original numerical models. On the other hand, the cost of building this surrogate model must be taken into consideration. Since the surrogate stochastic models are simpler, statistical moments can be computed analytically in some cases. Nevertheless, MC or any other type of sampling method can still be employed in the surrogate model at a much smaller cost.

This section reviews some common techniques to derive surrogates within a FEM framework. However, methods based in regressions of available data are not considered (*e.g.* Kriging methods [102, 176] or neural networks [171, 144]) since the uncertainty propagation model assumed does not depend on available data. Furthermore, due to the dissertation focus on the interaction between discretisation and stochastic errors rather than reduction of the latter, more advanced approaches allowing estimation and local adaptivity of surrogates are also omitted (*e.g.* [96, 127]).

2.4.1 Local expansion methods

Local expansion methods reformulate an unknown propagated random field $u(\boldsymbol{x}, \boldsymbol{\mu}(\boldsymbol{\theta}))$ (solution of a weak form *e.g.* problem 1.2.2) as a sum of a nominal deterministic solution u_0 and a stochastic expansion series of additive local terms. The nominal response u_0 can be determined from the mean of the primary process. For example, if the parametric uncertainty comes from the diffusion coefficient $C(\boldsymbol{x}, \boldsymbol{\mu}(\boldsymbol{\theta}))$, u_0 is obtained deterministically using $C_0 = \mathcal{E}[C(\boldsymbol{x}, \boldsymbol{\mu}(\boldsymbol{\theta}))]$ in the FEM problem.

The rest of terms account for the randomness and their mean equals zero. Most of the alternatives utilise random variables as weights for the series terms. For

instance, perturbation method [28], Taylor series [118, 174] or Neumann expansion [187, 182]. Another possibility is to employ a combination of trigonometric functions with different phases in a particular use of the spectral representation method [136, 162, 79]. The spectral representation combines a series of solutions with high degree polynomials or trigonometric functions as basis.

In all the approaches, the final solution is forced to be a linear combination of u_0 and several PDFs through different error minimisation approaches (*e.g.* [156, 141]). The result is a stochastic solution field centered around the nominal solution and the adapted covariance.

For the sake of illustration, let $A(C(\boldsymbol{x},\boldsymbol{\theta}))[u^{\mathbb{h}}(\boldsymbol{x},\boldsymbol{\theta})] = [l^{\mathbb{h}}(\boldsymbol{x})]$ be the SoE to solve after discretising the weak form of the problem. Making use of C_0 and $A_0 = A(C_0)$, u_0 is obtained. For the stochastic part $C(\boldsymbol{x},\boldsymbol{\theta})$, the Karhunen-Loève expansion is selected (see section 2.2.1). Then, using n_k terms for the truncation the approximation

$$C(\boldsymbol{x},\boldsymbol{\theta}) = C_0 + \sum_{k=1}^{n_k} \sqrt{\lambda_k}\Phi_k(\boldsymbol{x})\xi_k(\boldsymbol{\theta}) \tag{2.4.1}$$

is obtained. This leads to a SoE of the form

$$\left(A_0 + \sum_{k=1}^{n_k} \xi_k A_k\right)[u^{\mathbb{h}}] = [l^{\mathbb{h}}]. \tag{2.4.2}$$

If perturbation local expansion is applied the SoE 2.4.2 becomes

$$\left(A_0 + \sum_{k=1}^{n_k} \xi_k A_k\right)\left([u^{\mathbb{h}}]_0 + \sum_{k=1}^{n_k} \xi_k [u^{\mathbb{h}}]_k + \sum_{k=1}^{n_k}\sum_{j=1}^{n_k} \xi_k\xi_j [u^{\mathbb{h}}]kj + ...\right)[u^{\mathbb{h}}] = [l^{\mathbb{h}}]. \tag{2.4.3}$$

Then, the perturbed solution terms can computed following the scheme

$$\begin{aligned} [u^{\mathbb{h}}]_0 &= A_0^{-1}[l]_0, \\ [u^{\mathbb{h}}]_k &= -A_0^{-1}A_k[u^{\mathbb{h}}]_0, \\ [u^{\mathbb{h}}]_{kj} &= A_0^{-1}A_kA_0^{-1}A_l[u^{\mathbb{h}}]_0. \end{aligned} \tag{2.4.4}$$

Alternatively, the SoE 2.4.2 can be reformulated as

$$[u^{\mathbb{h}}] = \Big(\mathbb{I} + B\Big)^{-1} A_0^{-1}[l^{\mathbb{h}}], \tag{2.4.5}$$

where $B = (A_0^{-1}\sum_{k=1}^{n_k}\xi_k A_k)$ and $\mathbb{I}$ is the identity matrix. And after applying a Neumann expansion the solution can be simplified as

$$[u^{\mathbb{h}}] = [u^{\mathbb{h}}]_0 - B[u^{\mathbb{h}}]_0 + B^2[u^{\mathbb{h}}]_0 - B^3[u^{\mathbb{h}}]_0 + ... \tag{2.4.6}$$

2.4.2 Functional expansion methods (polynomial chaos expansion)

The most representative functional expansion method is PCE [73, 186]. In section 2.2.1 PCE was briefly introduced as a way to reproduce a probabilistic field. Another of its applications is the creation of a sample-based surrogate. To build this surrogate, the coefficients of the expansion (see equations 2.2.10 or 2.4.7) are obtained by fitting the global functional expansion in such a way that minimises the distance with respect to the original response surface. This is the approach followed in chapter 5 to build the surrogate model.

PCE assumes that a random variable Q can be approximated through the product of a denumerable set of polynomials $\mathscr{Z} = \{Z_1, ..., Z_{i_Z}, ..., Z_{n_Z}\}$ as basis, and undetermined coefficients $\mathscr{C}^Z = \{\mathbb{c}_1, ..., \mathbb{c}_{i_Z}, ..., \mathbb{c}_{n_Z}\}$. It can be proven that, for the particular case where the associated non-deterministic QoI has a finite variance, this approximation is exact if an infinite number of polynomials is considered in the series (*i.e.* $n_Z = \infty$) [164]. This implies that the higher the number of polynomials used in the expansion, the better its accuracy. Subsequently, for a maximum number of polynomials n_Z (fixed by choosing a maximum polynomial order considered in the truncation), it can be assumed that

$$Q \approx Q_{PC} := \sum_{i_Z=1}^{n_Z} \mathbb{c}_{i_Z} Z_{i_Z}. \tag{2.4.7}$$

For the one-dimensional case, the first polynomial Z_1 is the polynomial of order 0, and the last one Z_{n_Z} is the polynomial of maximum order $\mathbb{o}_{Max}$ after the truncation. Then, equation 2.4.7 becomes

$$Q \approx Q_{PC} := \sum_{\mathbb{o}=0}^{\mathbb{o}=\mathbb{o}_{Max}} \mathbb{c}_{\mathbb{o}} Z_{\mathbb{o}}, \tag{2.4.8}$$

where $\mathbb{o}$ is an index denoting the order of the polynomial in the expansion.

Xiu and Karniadakis [186] obtained the families of orthonormal polynomials associated to the most common distributions. The present work assumes that the distribution is well approximated by a Gaussian, hence the family of multidimensional Hermite polynomials must be employed as orthonormal basis $\mathscr{Z}$.

The probabilistic version of the 1D Hermite polynomials are orthogonal with respect to the weight function, namely the standard normal probability function with $\sigma = 1$ and $\mathcal{E}[\mu] = 0$ (equation 2.2.2). The Hermite polynomial $He_{\mathfrak{O}}$ of order $\mathfrak{O}$ is described by the following equation

$$He_{\mathfrak{O}}(\theta) = (-1)^{\mathfrak{O}} e^{\frac{\theta^2}{2}} \frac{d^{\mathfrak{O}}}{d\theta^{\mathfrak{O}}} e^{-\frac{\theta^2}{2}} = \left(\theta - \frac{d}{d\theta}\right)^{\mathfrak{O}} \cdot 1, \tag{2.4.9}$$

where the last expression is a non-commutative power; e is the mathematical constant base of the natural logarithm; and the derivatives must be performed after all the products in the power of order $\mathfrak{O}$ have been calculated.

This orthogonality can be generalised for any variance and expectation by scaling the polynomials through the following expression

$$He_{\mathfrak{O}}^{[\sigma,\mathcal{E}[\theta]]}(\theta) = \sigma^{\mathfrak{O}/2} He_{\mathfrak{O}}\left(\frac{\theta - \mathcal{E}[\theta]}{\sqrt{\sigma}}\right) \tag{2.4.10}$$

		Order dim 1				
		0	1	2	3	4
Order dim 2	0	o	o	o	o	o
	1	o	o	o	o	x
	2	o	o	o	x	x
	3	o	o	x	x	x
	4	o	x	x	x	x

Table 2.1: Standard truncation table for 2 dimensional order 4 polynomials

For multidimensional parameter spaces, Hermite (or any other) polynomials can be extended through tensor product. Since the number of dimensions used in the present work is low, standard truncation is preferred due to its simplicity. For high-dimensional spaces the curse of dimensionality arises. Hyperbolic or sparse truncation schemes reduce the number of cross order polynomials that are meaningful, but they are out of the purpose of the present work. The reader is referred to [31, 32] for an insight into hyperbolic truncation schemes.

Regarding sparse grid sampling [23, 183, 158], the tensor product is modified by the introduction of Smolyak isotropic formulas [163]. These formulas reduce the number of products taken into account by selecting them in such a way that loss of interpolation properties is negligible. Afterwards, Clenshaw-Curtis [45] formulas or Filippi formulas [71, 24] are usually employed instead of Gauss quadratures to reduce the sampling even further. The reader is referred to [23, 126] for implementation details in partial differential equations.

Using tensor product and the standard order truncation scheme T_{Sch} displayed in table 2.1, the i_Z-th component of the multidimensional PCE basis $\mathscr{Z}$ reads

$$Z_{i_Z}(\boldsymbol{\theta}) := He_{\mathbb{o}_{i_1}}^{[\sigma_1,\mathbb{E}[\theta_1]]}(\theta_1)\times ...\times He_{\mathbb{o}_{i_r}}^{[\sigma_r,\mathbb{E}[\theta_r]]}(\theta_r) \qquad \text{if} \qquad \mathbb{o}_{i_1}\times ...\times \mathbb{o}_{i_r} \in T_{Sch}, \tag{2.4.11}$$

where $\{i_1, ..., i_r\}$ are indexes representing the 1D Hermite polynomial order in each of the parametric dimensions $\{1, ..., j, ..., r\}$. The i-th particular mixture of unidimensional orders is combined in the tensor product to obtain the i_Z-th multidimensional polynomial. The range of all orders $\mathbb{o}_{i_j}$ (j standing for the parametric dimension) is $\{0, ..., \mathbb{o}_{Max}\}$ and the truncation scheme dictates if the i_Z-th combination of orders makes Z_{i_Z} a valid member of $\mathscr{Z}$.

After the selection of a maximum unidimensional order $\mathbb{o}_{Max}$ for any parametric dimension and a truncation scheme, a least squares fitting process can be exploited with a set of control points to find the coefficients $\mathfrak{c} = \{\mathbb{c}_1, ..., \mathbb{c}_{i_Z}, ..., \mathbb{c}_{n_Z}\}$ weighting the polynomials basis $\mathscr{Z}$. Note that if general truncation scheme is selected, the maximum multidimensional order $\mathbb{o}^{\#} := \max_{i=1}^{i=n_{i_Z}}((\sum_{j=1}^{j=r}\mathbb{o}_{i_j}) \in T_{Sch})$ of any polynomial $Z_{i_Z} \in \mathscr{Z}$ equals $\mathbb{o}_{Max}$.

The fitting consists in finding the vector $\mathfrak{c}$ that minimises the distance between Q and the approximated Q_{PC} weighted by the primary PDF.

$$\mathfrak{c} = \underset{\mathfrak{c}\,\in\,\mathbb{R}^{\mathbb{o}+1}}{\operatorname{argmin}}\left(\int_\Theta \left(Q - Q_{PC}\right)^2 \mathrm{g}(\boldsymbol{\mu}(\boldsymbol{\theta}))d\boldsymbol{\theta}\right). \tag{2.4.12}$$

The error in this norm (equivalent to the variance) decreases as the maximum multidimensional order $\mathbb{o}^{\#}$ employed in the PCE estimating Q_{PC} increases.

The vector of coefficients $\mathfrak{c}$ is easily computable because of the polynomial se-

quence orthogonality. Namely,

$$\int_{\Theta} Z_{i_Z}(\boldsymbol{\theta}) Z_{j_Z}(\boldsymbol{\theta}) \mathrm{g}(\boldsymbol{\mu}(\boldsymbol{\theta})) d\boldsymbol{\theta} = 0 \qquad \forall\, i_Z \neq j_Z. \tag{2.4.13}$$

This leads to the direct computation of the i_Z-th component of $\mathbb{c}$ as

$$\mathbb{c}_{i_Z} = \frac{\int_{\Theta} Z_{i_Z}(\boldsymbol{\theta}) Q(\boldsymbol{\mu}(\boldsymbol{\theta})) \mathrm{g}(\boldsymbol{\mu}(\boldsymbol{\theta})) d\boldsymbol{\theta}}{\int_{\Theta} Z_{i_Z}^2(\boldsymbol{\theta}) \mathrm{g}(\boldsymbol{\mu}(\boldsymbol{\theta})) d\boldsymbol{\theta}}. \tag{2.4.14}$$

Hermite polynomials can be integrated exactly using a Gauss-Hermite quadrature (the zeros of Hermite polynomials with respect to the weighting function). For m^r quadrature points (being r the number of parametric dimensions), the corresponding numerical integration covering the whole parameter domain $\Theta \in \mathbb{R}^r$ is exact up to order $\mathfrak{o} = 2m - 1$ in any parametric direction. Then, for a low number of parametric dimensions, the number of evaluations needed to fit PCE is lower than the number of sample evaluations needed to reach convergence in the expectation through brute force MC. Note that PCE is powered by the dimensions considered while MC is unaffected by this. Therefore, the computational benefits of using a PCE surrogate model vanish as the number of parameters increases. It may even be counter-productive for a very large number of dimensions.

In addition to the m^r evaluations needed to fit a PCE surrogate with r parameters, some evaluations at control points are needed to verify the required accuracy. The formulas to compute the exact values and weights for the quadrature points can be found at [2]. On the other hand, the set of control points is randomly drawn from the primary PDF and must not coincide with set of samples even if they are drawn from the same PDF. Section 5.3.1 justifies the number of control points used in the algorithm.

2.4.3 Numerical integration methods

Numerical integration methods [63, 160] estimate the uncertainty propagation in two steps. First, statistical moments are computed by direct numerical integration. Second, the PDF or the tail region probability is approximated empirically based on the computed moments [92].

As an example, the Full Factor Numerical Integration method (FFNI) computes the first 4 moments of the QoI random variable $Q = q(\boldsymbol{\mu}(\boldsymbol{\theta}))$ by using a $\mathfrak{m}$-mode Gaussian integration rule and the following product quadrature rule [64]

$$\begin{aligned}\mathcal{E}[Q^{\mathfrak{o}}] = \int_{\Omega}\{q(\boldsymbol{\mu}(\boldsymbol{\theta}))\}^{\mathfrak{o}} f^{\mathcal{P}}_{\boldsymbol{\mu}} d\boldsymbol{\theta} \approx \\ \sum_{i_{\mathfrak{m},1}=1}^{n_{\mathfrak{m}}} \dots \sum_{i_{\mathfrak{m},r}=1}^{n_{\mathfrak{m}}} \mathfrak{w}_{i_{\mathfrak{m},j}} (q(\mathcal{E}[\boldsymbol{\mu}(\boldsymbol{\theta})] + \{\alpha_{i_{\mathfrak{m},1}}\sigma_{\theta_1} \ , \ \dots \ , \ \alpha_{i_{\mathfrak{m},r}}\sigma_{\theta_r}\}))^{\mathfrak{o}},\end{aligned} \tag{2.4.15}$$

where $\alpha_{i_{\mathfrak{m},j}}$ are the location parameters at the $i_{\mathfrak{m}}$-th quadrature point in the j-th of r parametric dimensions, $\mathfrak{w}_{i_{\mathfrak{m},j}}$ their correspondent weight, σ_j the standard deviation of μ_j, and the integer $\mathfrak{o}$ denotes the order of the moments.

Calling $M_{\mathfrak{o}}$ the $\mathfrak{o}$-th central moment of $\boldsymbol{\mu}(\boldsymbol{\theta})$, the moment-matching equation to obtain $\alpha_{i_{\mathfrak{m}}}$ and $\mathfrak{w}_{i_{\mathfrak{m}}}$ reads

$$M_{\mathfrak{o}} = \int_{\Omega} (\boldsymbol{\mu}(\boldsymbol{\theta}) - \mathcal{E}[\boldsymbol{\mu}(\boldsymbol{\theta})])^{\mathfrak{o}} f^{\mathcal{P}}_{\boldsymbol{\mu}} d\boldsymbol{\theta} = \sum_{i_{\mathfrak{m},1}=1}^{n_{\mathfrak{m}}} \dots \sum_{i_{\mathfrak{m},r}=1}^{n_{\mathfrak{m}}} \mathfrak{w}_{i_{\mathfrak{m},j}} (\{\alpha_{i_{\mathfrak{m},1}}\sigma_{\theta_1} \ , \ \dots \ , \ \alpha_{i_{\mathfrak{m},r}}\sigma_{\theta_r}\})^{\mathfrak{o}}$$
$$\mathfrak{o} = 0, ..., 2\mathfrak{m} - 1 \ . \tag{2.4.16}$$

This leads to a non-linear SoE increasingly difficult to solve.

Some choices for the empirical approximation of the PDF once the first four moments are known are the Pearson system, the Johnson system or the Gram-Chalier series (see [92] for the specifics of empirical choices).

2.5 Stochastic finite element method

Stochastic Finite Element Method (SFEM) incorporates the stochastic definition of the random variables into the weak FE formulation. That is to say, there is a unique FE model whose elements have probabilistic properties opposed to a separated global deterministic numerical model that produces different outcomes depending on some input parameters. Due to this integration, the SoE derived from the model is scaled with the parametric dimensions considered. Even though the resultant SoE can be forced to be block diagonal, the exponential size increase is one of the issues of SFEM approach.

The most pursued approaches to formulate SFEM are the perturbation [101, 115, 116] and the spectral [73] versions. On top of that, an orthogonal basis with

respect to the joint PDF of the parameters is generally preferred in order to enforce Galerkin orthogonality and obtain block diagonal SoE. This means that, starting from a bilinear form analogous to 1.2.3 but dependent on the random parameters

$$a^D(u(\boldsymbol{x},\boldsymbol{\theta}), v(\boldsymbol{x},\boldsymbol{\theta})) = l(v(\boldsymbol{x},\boldsymbol{\theta})), \qquad \forall\, v(\boldsymbol{x},\boldsymbol{\theta}) \in \mathcal{V} \times \Theta. \tag{2.5.1}$$

The test and trial functions can be expressed in an orthogonal stochastic basis and follow the same process described in section 1.2.1. Trigonometric, Karhunen-Loève expansion or PCE are suitable orthogonal basis to represent stochastic processes. Using the last one as illustrative example leads to the problem: find $u_{\mathfrak{O}}(\boldsymbol{x})Z^u_{\mathfrak{O}}(\boldsymbol{\theta}) \in \mathcal{U} \times \Theta^{PC}$ such that

$$a^D\left(\sum_{\mathfrak{O}=0}^{\mathfrak{O}=\mathfrak{O}_{Max}} u_{\mathfrak{O}} Z^u_{\mathfrak{O}}, \sum_{\mathfrak{O}=0}^{\mathfrak{O}=\mathfrak{O}_{Max}} v_{\mathfrak{O}} Z^v_{\mathfrak{O}}\right) = l\left(\sum_{\mathfrak{O}=0}^{\mathfrak{O}=\mathfrak{O}_{Max}} v_{\mathfrak{O}} Z^v_{\mathfrak{O}}\right), \qquad \forall\, v_{\mathfrak{O}}(\boldsymbol{x}) Z^v_{\mathfrak{O}}(\boldsymbol{\theta}) \in \mathcal{V} \times \Theta^{PC}, \tag{2.5.2}$$

where the orthogonal basis acts as shape functions in the stochastic dimensions and Θ^{PC} is the "discretisation" of the probabilistic space Θ.

This discrete approximation produces a stochastic error. The relation between this error and the spatial discretisation error is crucial for the reliability and the computational cost of the joined model. In fact, it is the same problem investigated in this dissertation for the framework of stochastic processes non-integrated into the FE. However and contrary to the case studied in this thesis, unless two different meshes are used as proposed by [51], in SFEM the errors can not be assessed separately. This makes SFEM highly intrusive with regards to the constitutive and equilibrium equations.

Through empirical analysis, most works about the subject [110, 51, 188] agree on determining the adequate size for the stochastic mesh as belonging to the approximate interval $\frac{\alpha_{CR}}{2} \lessapprox \mathbb{h}_{RF} \lessapprox \frac{\alpha_{CR}}{4}$. The parameters defining the interval are α_{CR}, which denotes the correlation length, and $\mathbb{h}_{RF}$, which is the characteristic length defining the elements size in the mesh linked to the random field.

2.5.1 Formulation of the stochastic finite element

This section formulates some of the SFEM options based on the general common formulation introduced in [166]. For an analysis of about how to extend this general formulation of the stiffness matrix to specific cases the reader is referred to [132, 76, 7] for beams, plates and shells.

In SFEM, the introduction of the stochastic fields is done at element level. Then, the elemental stiffness matrix (defined at equation 1.2.12) is expanded as

$$K^{\mathbb{e}^{\mathbb{k}}} = K_0^{\mathbb{e}^{\mathbb{k}}} + \Delta K^{\mathbb{e}^{\mathbb{k}}}, \tag{2.5.3}$$

where $K_0^{\mathbb{e}^{\mathbb{k}}}$ is the mean value and $\Delta K^{\mathbb{e}^{\mathbb{k}}}$ is the stochastic part of the FE. Let $f_{\boldsymbol{\mu}}^{\mathbb{e}^{\mathbb{k}}}(\boldsymbol{x},\boldsymbol{\theta})$ be an homogeneous stochastic field with 0 mean propagating to the whole domain, and C_0 the mean constitutive parameter. Then, the random variation in $C(\boldsymbol{x},\boldsymbol{\theta})$ can be expressed as $C(\boldsymbol{x},\boldsymbol{\theta}) = (1 + f_{\boldsymbol{\mu}}^{\mathbb{e}^{\mathbb{k}}}(\boldsymbol{x},\boldsymbol{\theta}))C_0$. Furthermore, following the application of the weak formulation the elemental stiffness terms become

$$K_0^{\mathbb{e}^{\mathbb{k}}} := \int_{\Omega_{\mathbb{k}}} \nabla\psi_v^{\mathbb{h}} C_0 \nabla\psi_u^{\mathbb{h}} d\Omega_{\mathbb{k}} \tag{2.5.4}$$

and

$$\Delta K^{\mathbb{e}^{\mathbb{k}}} := \int_{\Omega_{\mathbb{k}}} \nabla\psi_v^{\mathbb{h}} C_0 \nabla\psi_u^{\mathbb{h}} f_{\boldsymbol{\mu}}^{\mathbb{e}^{\mathbb{k}}}(\boldsymbol{x},\boldsymbol{\theta}) d\Omega_{\mathbb{k}} \tag{2.5.5}$$

respectively. Alternatively, the random variation can be accounted by means of a series of random variables. In that case $C(\boldsymbol{x},\boldsymbol{\theta}) = C_0 + \sum_i C_i(\boldsymbol{x})\xi_i^{\mathbb{e}^{\mathbb{k}}}(\boldsymbol{\theta})$ leads to

$$\Delta K^{\mathbb{e}^{\mathbb{k}}} := \sum_i \int_{\Omega_{\mathbb{k}}} \nabla\psi_v^{\mathbb{h}} C_i(\boldsymbol{x}) \nabla\psi_u^{\mathbb{h}} \xi_i^{\mathbb{e}^{\mathbb{k}}}(\boldsymbol{\theta}) d\Omega_{\mathbb{k}}. \tag{2.5.6}$$

If MC is adopted to assess the stochastic component of SFEM, the SoE 1.2.11 is solved n_s times with n_s sampling points $\boldsymbol{\mu_s}$. In an analogous way as equation 2.3.1, the expectation for the solution $u^{\mathbb{h}}$ at the i_{DOF}-th DOF can be approximated as

$$\mathcal{E}[u_{i_{\text{DOF}}}^{\mathbb{h}}] \approx \overline{\mathcal{E}}[u_{i_{\text{DOF}}}^{\mathbb{h}}] := \frac{1}{n_s} \cdot \sum_{s=1}^{n_s} u_{i_{\text{DOF}}}^{\mathbb{h}}(\boldsymbol{\mu_s}). \tag{2.5.7}$$

As another example, if perturbation method is appointed instead, the global stiffness matrix becomes

$$K = K^0 + \sum_{i_{\mathfrak{p}}=1}^{n_{\mathfrak{p}}} K^I_{i_{\mathfrak{p}}} \mathfrak{p}_{i_{\mathfrak{p}}} + \sum_{i_{\mathfrak{p}}=1}^{n_{\mathfrak{p}}} \sum_{j_{\mathfrak{p}}=1}^{n_{\mathfrak{p}}} K^{II}_{i_{\mathfrak{p}}\, j_{\mathfrak{p}}} \mathfrak{p}_{i_{\mathfrak{p}}} \mathfrak{p}_{j_{\mathfrak{p}}} + \dots, \tag{2.5.8}$$

where

$$K^I_{i_\mathfrak{p}} = \left.\frac{\partial K}{\partial \mathfrak{p}_{i_\mathfrak{p}}}\right|_{\mathfrak{p}=0} \quad , \quad K^{II}_{i_\mathfrak{p}\, j_\mathfrak{p}} = \left.\frac{\partial^2 K}{\partial \mathfrak{p}_{i_\mathfrak{p}} \partial \mathfrak{p}_{j_\mathfrak{p}}}\right|_{\mathfrak{p}=0}, \tag{2.5.9}$$

and the perturbations $\{\mathfrak{p}_{i_\mathfrak{p}}\}_{i_\mathfrak{p}=1}^{n_\mathfrak{p}}$ are random variables than can be grouped in a vector $\mathfrak{p} = \{\mathfrak{p}_1, \mathfrak{p}_2, ..., \mathfrak{p}_{n_\mathfrak{p}}\}$.

The same Taylor expansion must be applied to the left hand side of the equation and to the solution $u^{\mathbb{h}}$ leading to the following iterative process to find the mean solution and the fluctuations

$$\begin{aligned} [u^{\mathbb{h}}]_0 &= K_0^{-1}[l]_0, \\ [u^{\mathbb{h}}]^I_{i_\mathfrak{p}} &= K_0^{-1}([l]^I_{i_\mathfrak{p}} - K^I_{i_\mathfrak{p}}[u^{\mathbb{h}}]_0), \\ [u^{\mathbb{h}}]^{II}_{i_\mathfrak{p}\, j_\mathfrak{p}} &= K_0^{-1}([l]^{II}_{i_\mathfrak{p}\, j_\mathfrak{p}} - K^I_{i_\mathfrak{p}}[u^{\mathbb{h}}]^I_{j_\mathfrak{p}} - K^I_{j_\mathfrak{p}}[u^{\mathbb{h}}]^I_{i_\mathfrak{p}} - K^{II}_{i_\mathfrak{p}\, j_\mathfrak{p}}[u^{\mathbb{h}}]_0). \end{aligned} \tag{2.5.10}$$

2.6 Conclusion

This chapter reviews the modelling of uncertainty within a FEM framework. The general idea of MC and estimating the parameter surface from a set of samples is the base of all stochastic approaches to characterise the uncertainty.

Then, several options to generate a surrogate model that reduces the cost of producing an outcome in comparison with the original numerical model are presented. Firstly, local expansion methods build the surrogate as a sum of a mean solution and a series of random variables. Secondly, functional expansion techniques replace the random variables with a sum of functions approximating them. Thirdly, numerical integration methods exploit integration rules to compute statistical moments that are later employed to select the approximated empirical distribution.

PCE and numerical integration method allow direct estimation of the QoI response surface and adaptive accuracy of the surrogate, which serves the purpose of this work. Since the number of stochastic dimensions considered in the present work is low, the exponential cost of evaluating quadrature points in PCE fitting process is preferred to (1) the complexity of the non-linear SoE needed in numerical integration surrogates, (2) the low convergence/cost ratio of pure sampling methods, and (3) the limited adaptivity of local expansion methods.

Lastly, SFEM is reviewed, which allows to introduce stochastic parametrisation at the element level. Despite the increase of flexibility introduced by this approach, it is not considered in this work because of the exponential growth of the SoE to solve and the intrusiveness of the formulation.

Several authors [110, 51, 188] have studied an optimal empiric relation between the mesh size and the stochastic characterisation within the SFEM framework. This approach has not been pursued out of SFEM, since the stochastic error is not directly linked to the mesh discretisation, and the discretisation error can be forced to be small enough to avoid interference. However, the present thesis delves into the unexplored issue to adaptively optimise the mesh and the sampling. In that way, the discretisation error does not interfere with the stochastic error, and on top of that, computational time is not wasted due to excess of discretisation or unnecessary sampling.

Chapter 3

Residual error estimators seen as preconditioners

3.1 Introduction

Boundary value problems posed through the finite element method (*e.g.* equations 1.2.2, 3.4.1, 4.5.3 or 5.2.3 in this work) are ultimately reduced to the resolution of a non-singular System of Equations (SoE). Chapter 1 illustrates how an equivalent problem can be posed for the error instead of the displacements. Then, error estimation approximates the solution of the SoE in the reference space by a collection of local systems where the degrees of freedom are reduced. Error estimation is commonly used to bound the error and guide the mesh refinement process. Each step of the process produces better approximations but also increases the computational cost of the estimation.

This self-contained chapter pursues an antagonistic approach than the rest of the thesis. The goal is to iteratively improve the estimations avoiding any refinement process. The improvement on the estimation of the error is sought as analogy of the iterative solvers of linear equations. The efficient resolution of linear SoE is a very complex and prolific field of linear algebra and only the basics will be reviewed in this chapter. If the analogy could be proven, would mean that in order to converge to the exact error in any target rich space, there would be no need to refine the

mesh. Instead, the local problems would be reused to improve the estimation at an algebraic level as iterative solvers for SoE do.

Regarding the resolution of SoE, the traditional way to solve them before the computer era was Gaussian elimination. However, computers allowed to pose increasingly complex problems leading to increasingly large systems. Even with the enhancements that address lack of stability due to machine rounding precision, the order of operations of any Gaussian elimination method based algorithm is $\mathcal{O}(DOF^3)$. DOF stands for the degrees of freedom in the FE mesh and therefore, the unknowns in the resulting SoE.

Several methods to optimise the performance of linear and non-linear systems have been proposed. Saad's work [155] tried to compile all relevant approaches. For a non-exhaustive list of reviews, less extensive but including the mathematical formulations, the reader is referred to [10, 11, 33, 35, 78, 97, 153, 181]. Simplifying, the principles behind these methods can be summarised into two.

Firstly, the constitutive equations and finite elements usually lead to matrices where most of the values are equal to zero. By properly rearranging the rows and columns it is possible to reshape the matrix into a block diagonal one. Then, different algebraic techniques are applied to exploit this fact and avoid most of the computations that would involve a product by zero. Furthermore, this allows to avoid the storage and memory access to those ignored zero values. The partially stored matrices are known as sparse matrices.

Secondly, the original SoE can be substituted for another system whose computational and storage cost is almost negligible in comparison. The solution of this new system is a vector solution which is not necessarily a good approximation, but the distance to the real solution is guaranteed to be smaller. Then, several algebraic operations are implemented to repeat this step in an iterative process, maintaining the guaranteed reduction of the distance of each new solution. Eventually, the new solution will be accurate enough to stop the iterative process. Some of these methods even guarantee that the exact solution is obtained after a known number of iterations.

Often, both approaches are combined to enhance the efficiency of the methods. Preconditioners are one of the several techniques presented within the scope of iterative methods in order to approximate a SoE to a less expensive one. It is not within the scope of the present work to delve into the different algebraic propositions. Consequently, no literature review about the different methods is included in this thesis.

Note that error estimators have the same goal as preconditioners, but it is yet to be explored if they are truly equivalent. This is exactly the aim of the present chapter. Error estimators are implemented as preconditioners into one of the iterative algorithms presented in the linear algebra scope. Then the convergence towards the reference solution is studied.

3.2 Selection of an iterative solver and an error estimator

In a similar way than preconditioners, error estimators approximate the solution of the SoE to be solved (see equation 3.3.10 for details). In particular, residual error estimators seen in section 4 do so by approximating the residual equation 1.3.13. However, the global matrix of the system is never assembled. Instead, the estimators directly produce an approximation to the system residual as if it was already preconditioned.

All presented error estimators produce an approximation to the error $\widehat{e} = \widehat{u} - u^{\mathbb{h}}$ in the reference space, but they use information from a precomputed $u^{\mathbb{h}}$ solution belonging to the coarse space. In order to implement the error estimator as a preconditioner, all fine approximations must be projected back to the coarse space. In this step, the symmetry of the modified SoE is lost.

Some options for iterative solvers of non-symmetric SoE based on the residual are listed next. The Generalised Minimal Residual method (GMRES) [154] has received more attention than other iterative techniques. The two main alternatives to include preconditioners based on GMRES are FGMRES [152] (where the F stands

for Flexible) and GMRESR [178] (where the R stands for Recursive). The former is of much easier implementation that the latter. However, it has been proved that GMRESR is more robust [180]. There are other alternatives not based on GMRES (*e.g.* [12]). Nevertheless, because of its ease of implementation, FGMRES is selected as the iterative algorithm where the error estimator is assimilated as a left preconditioner.

On the other hand, an eligible error estimator must be able to update the coarse solution in all DOF. Furthermore, the complete field must always be recovered to perform the following step in the iterative process. Consequently, the selected error estimator is the node centered patch in its additive version (see section 4.4.1 for the formulation of the estimator). This estimator has the capacity to update all DOF, and does not require an averaging rule to recover the complete field.

3.3 Notation and incorporation of error estimation into an iterative solver

3.3.1 System of equations to solve

The first thing to specify is what SoE is going to be solved. This section uses the diffusion problem 3.4.1 posed in chapter 4 as a benchmark. In order to obtain the system, the starting point is the weak form 1.2.2 with $C = 1$, or in short notation, the bilinear equation 1.2.3.

The solution to the problem in a coarse discrete space is $u^{\mathbb{h}} \in \mathcal{U}^{\mathbb{h}}$ and in a discrete reference space is $\widehat{u} \in \widehat{\mathcal{U}}$. Using the definition of shape functions in 1.2.8 those fields can be expressed as $\widehat{u} = [\widehat{u}] \cdot \widehat{\psi_u}$ and $u^{\mathbb{h}} = [u^{\mathbb{h}}] \cdot \psi_u^{\mathbb{h}}$, where $[\cdot]$ stands for the scalar nodal coefficients grouped in vector form. The same can be done for the test functions $\widehat{v} = [\widehat{v}] \cdot \widehat{\psi_v}$ and $v^{\mathbb{h}} = [v^{\mathbb{h}}] \cdot \psi_v^{\mathbb{h}}$ belonging to the test spaces $\widehat{\mathcal{V}}$ and $\mathcal{V}^{\mathbb{h}}$.

Considering the discrete reference space, the shape functions and $[\cdot]^T$ as the transpose vector of $[\cdot]$, the left hand side of equation 1.2.3 becomes

$$a^D(\widehat{u}, \widehat{v}) = \int_\Omega [v]^T \nabla \widehat{\psi_v} \cdot \nabla [u] \widehat{\psi_u} d\Omega \tag{3.3.1}$$

and the right hand side reads

$$l(\widehat{v}) = \int_{\Omega} [v]^T \widehat{\psi_v} f(\boldsymbol{x})\, d\Omega + \int_{\Gamma_n} [v]^T \widehat{\psi_v} g_n(\boldsymbol{x})\, d\Gamma_n. \tag{3.3.2}$$

Since the weak form is fulfilled for all $\widehat{v} \in \widehat{\mathcal{V}}$, the vectors of coefficients corresponding to the test field can be removed from both sides of the equation. Then, introducing the notations

$$A_D := a^D(\psi_u, \psi_v) \tag{3.3.3}$$

and

$$[l] := l(\psi_v), \tag{3.3.4}$$

leads to the SoE to be solved

$$\widehat{A_D}[\widehat{u}] = [\widehat{l}], \tag{3.3.5}$$

or equivalently

$$\begin{bmatrix} \widehat{A_D}_{(1,1)} & \widehat{A_D}_{(1,2)} & \widehat{A_D}_{(1,3)} & \dots & \widehat{A_D}_{(1,DOF)} \\ \widehat{A_D}_{(2,1)} & \widehat{A_D}_{(2,2)} & \widehat{A_D}_{(2,3)} & \dots & \widehat{A_D}_{(2,DOF)} \\ \vdots & \vdots & \vdots & \ddots & \vdots \\ \widehat{A_D}_{(DOF,1)} & \widehat{A_D}_{(DOF,2)} & \widehat{A_D}_{(DOF,3)} & \dots & \widehat{A_D}_{(DOF,DOF)} \end{bmatrix} \cdot \begin{bmatrix} \widehat{u}_1 \\ \widehat{u}_2 \\ \vdots \\ \widehat{u}_{DOF} \end{bmatrix} = \begin{bmatrix} \widehat{l}_1 \\ \widehat{l}_2 \\ \vdots \\ \widehat{l}_{DOF} \end{bmatrix} \tag{3.3.6}$$

3.3.2 Preconditioners

Preconditioning means to transform a SoE (*e.g.* $\widehat{A_D}[\widehat{u}] = [\widehat{l}]$) into an equivalent one that fulfils the following conditions. The new system must have a much lower computational cost and produce an approximation of $[\widehat{u}]$. Even if the accuracy of the approximation is small, it helps the iterative algorithm as long as it points to the right direction.

Defining a left preconditioner as $\mathfrak{P}_L$, the equivalent system reads

$$\mathfrak{P}_L{}^{-1} \cdot \widehat{A_D}[\widehat{u}] = \mathfrak{P}_L{}^{-1} \cdot [\widehat{l}]. \tag{3.3.7}$$

Note that the closer the inverses $\mathfrak{P}_L{}^{-1}$ and $\widehat{A_D}^{-1}$ are, the better the approximation of $[\widehat{u}]$ is. On the limit, when $\mathfrak{P}_L^{*\,-1} = \widehat{A_D}^{-1}$ the exact solution would be recovered, since $\mathfrak{P}_L^{*\,-1} \cdot \widehat{A_D}[\widehat{u}] = \widehat{A_D}^{-1} \cdot \widehat{A_D}[\widehat{u}] = [\widehat{u}]$. But obviously, the cost of exactly inverting the matrix $\widehat{A_D}$ is equivalent to Gaussian elimination.

Preconditioners can also be defined on the right, but they require the substitution of the original vector of unknowns $[\widehat{u}]$ by another one $[\widehat{u_{\mathfrak{P}}}]$

$$\widehat{A_D} \cdot \mathfrak{P}_R{}^{-1}[\widehat{u_{\mathfrak{P}}}] = [\widehat{l}], \qquad [\widehat{u}] = \mathfrak{P}_R{}^{-1}[\widehat{u_{\mathfrak{P}}}]. \tag{3.3.8}$$

The combination of both approaches is called split preconditioning.

The requirement for left preconditioners to make the approximated solution advance in the right direction can be expressed as

$$||\mathbb{I} - \mathfrak{P}_L{}^{-1} \cdot \widehat{A_D}||_{\mathcal{L}^2} < 1, \tag{3.3.9}$$

where $\mathbb{I}$ is the identity matrix and the norm $||\cdot||_{\mathcal{L}^2}$ of a matrix is defined as

$$||\widehat{A_D}||_{\mathcal{L}^2} := \max_{|||[x]|||_{\mathcal{L}^2}=1} ||\widehat{A_D}[x]||_{\mathcal{L}^2}. \tag{3.3.10}$$

Recall that the $\mathcal{L}^p$ norm of a vector is

$$|||[x]|||_{\mathcal{L}^p} = \left(\sum_{i_{DOF}=1}^{n_{DOF}} |[x_{i_{DOF}}]|^p \right)^{1/p}, \tag{3.3.11}$$

being $[x_{i_{DOF}}]$ the $i_{DOF} - th$ component of the vector $[x]$, and n_{DOF} the number of components.

3.3.3 Generalised minimal residual method

The Generalised Minimal Residual method GMRES is an iterative method to solve linear SoE. It is based on the iterative minimisation of the residual of a series of approximate solutions belonging to a Krylov subspace. The $m - th$ Krylov subspace $\mathcal{K}_m$ takes the form

$$\mathcal{K}_m = \mathcal{K}_m(\widehat{A_D}, [l]) = span\{[l], \widehat{A_D}[l], \widehat{A_D}^2[l], ..., \widehat{A_D}^{m-1}[l]\}. \tag{3.3.12}$$

Then, each iteration n is characterised by the following minimisation problem

$$[u]_n \in \mathcal{K}_n; \qquad |||[l] - \widehat{A_D} \cdot [u]_n||_{\mathcal{L}^2} = \min_{\mathfrak{z} \in \mathcal{K}_n} |||[l] - \widehat{A_D} \cdot \mathfrak{z}||_{\mathcal{L}^2}, \tag{3.3.13}$$

where $\mathfrak{z}$ is any arbitrary member of $\mathcal{K}_n$ and $[u]_n$ the one that minimises the norm.

Note that in the last expression the minimised vector is the residual of the SoE, which for this section is defined as

$$\mathfrak{r}_n = [l] - \widehat{A_D} \cdot [u]_n. \tag{3.3.14}$$

At each iteration, the Krylov subspace increases and the vectors in the span eventually can become linearly dependent. To overcome this issue, GMRES adopts an stabilised Grand-Schmidt orthonormalisation process. In particular, it uses the Arnoldi algorithm [8] (algorithm num. 1) to build the orthonormal basis $\mathscr{Q}_n = \{\mathfrak{q}_1, \mathfrak{q}_2, ..., \mathfrak{q}_n\}$ of the subspace $\mathcal{K}_m$.

Algorithm 1 Arnoldi algorithm

```
1: q_1 = q_1/||q_1||_{L^2}                 # Initial q_1 is any arbitrary vector
2: for k = 2 to n do
3:     q_k = Â_D · q_{k-1}
4:     for j = 1 to k − 1 do               # Ensures orthogonality by projecting out q_k in the directions of q_1...q_{k-1}
5:         h_{j,k-1} = q_j^T q_k
6:         q_k = q_k − h_{j,k-1} q_j
7:     end for
8:     h_{k,k-1} = ||q_k||_{L^2}
9:     q_k = q_k/h_{k,k-1}
10: end for
```

Since $[u]_n \in \mathcal{K}_m$, and $\mathscr{Q}_n$ is a basis of $\mathcal{K}_m$; $[u]_n$ can be expressed in the coordinates $\mathfrak{c}_n \in \mathbb{R}^n$ of that basis $\mathscr{Q}_n$. In other words, defining $\mathcal{Q}_n$ as the $n \times m$ orthogonal matrix whose columns are $[\mathfrak{q}_1, \mathfrak{q}_2, ..., \mathfrak{q}_n]$, the vector $[u]_n$ can be expressed as $\mathcal{Q}_n \cdot \mathfrak{c}_n$.

In order to compute $\mathfrak{q}_{n+1}$, the following condition must be satisfied

$$\widehat{A_D} \cdot \mathfrak{q}_n - \sum_{j=1}^{n} (\mathfrak{q}_j^T \cdot \widehat{A_D} \cdot \mathfrak{q}_n) \cdot \mathfrak{q}_j \neq \mathbf{0}. \tag{3.3.15}$$

If it is not satisfied for $n = n*$, then in can be proven that $[u]_{n*} = [u] = \widehat{A_D}^{-1} \cdot [l] \in \mathcal{K}_{n*}$.

Note that Arnoldi algorithm builds a Hessenberg superior matrix $\bar{H}_n$ of order $n + 1 \times n$. This matrix has the property $\widehat{A_D} \cdot \mathfrak{q}_n = \mathfrak{h}_{1,n}\mathfrak{q}_a + ... + \mathfrak{h}_{n,n}\mathfrak{q}_n + \mathfrak{h}_{n+1,n}\mathfrak{q}_{n+1}$. Consequently,

$$\widehat{A_D} \cdot \mathcal{Q}_n = \mathcal{Q}_{n+1} \cdot \bar{H}_{n+1}. \tag{3.3.16}$$

Now, let $[u]_0$ be an arbitrary vector of m components, $\mathfrak{e}_1 = (1, 0, ..., 0)^T$ be the first vector in the standard basis of $\mathbb{R}^{n+1}$, and $\beta := ||\mathfrak{r}_0||_{\mathcal{L}^2} := |||[l] - \widehat{A_D} \cdot [u]_0||_{\mathcal{L}^2}$. Due to the orthogonality of the columns of any $\mathcal{Q}_n$, equation 3.3.13 can be transformed into

$$\begin{aligned} ||[l] - \widehat{A_D} \cdot [u]_n||_{\mathcal{L}^2} &= \min_{\mathfrak{z} \in \mathcal{K}_n} |||[l] - \widehat{A_D} \cdot \mathfrak{z}||_{\mathcal{L}^2} \\ &= \min_{\mathfrak{c} \in \mathbb{R}^n} ||\mathcal{Q}_{n+1}^T \cdot [l] - \bar{H}_n \cdot \mathfrak{c}||_{\mathcal{L}^2} \\ &= ||\beta \mathfrak{e}_1 - \bar{H}_n \cdot \mathfrak{c}_n||_{\mathcal{L}^2}, \end{aligned} \tag{3.3.17}$$

where the minimisation problem has been transformed so that it has a Hessenberg structure. Finally, this leads to the GMRES algorithm 2.

Algorithm 2 GMRES algorithm

1: $\mathfrak{q}_1 = [l]/|||[l]||_{\mathcal{L}^2}$
2: **for** $k = 1$ to m **do**
3: compute $\mathfrak{q}_n$ # Step n in the Arnoldi iteration (see algorithm 1)
4: compute $\mathfrak{c}_n$ # Least squares minimisation of $||\mathfrak{r}_n||_{\mathcal{L}^2}$ (see equation 3.3.17)
5: $[u]_k = \mathcal{Q}_k \cdot \mathfrak{c}_n$
6: Check if the norm of the residual is small enough
7: **end for**

3.3.4 Incorporation of residual error estimators as left preconditioner into FGMRES

As already stated, error estimators do not assemble the global matrix for test and trial vectors in the fine spaces $\widehat{\mathcal{V}}$ and $\widehat{\mathcal{U}}$. Furthermore, they construct the residual from a solution in the coarse space $\mathcal{U}^{\mathbb{h}}$. Then, prior to incorporating the error estimator as a left preconditioner, the solution field must be projected to the coarse space using the projector $\underset{\widehat{\mathcal{V}}}{\overset{\mathcal{V}^{\mathbb{h}}}{\pi}}$ defined in equation (1.4.6).

Another issue to resolve is that error estimators are always defined in relation to the residual. However, in FGMRES the left preconditioner is not always applied to the residual, but also to the computation of the next $\mathfrak{q}_k$ (see line 6 of algorithm 3). To overcome this issue, the definition of the error estimator is transformed. So, starting from equations 1.3.12 and 1.3.13, an error estimator function depending on

Algorithm 3 FGMRES with Error estimation as left preconditioner

1: $[u]_0 := [u^{\mathbb{h}}]$ # Original FGMRES: unexisting line
2: $\mathfrak{r}_0 = \mathfrak{E}([l], [u]_0)$ # Original FGMRES: $\mathfrak{r}_0 = \mathfrak{P}_L{}^{-1}([l] - \widehat{A_D} \cdot [u]_0)$
3: $\beta = ||\mathfrak{r}_0||_{\mathcal{L}^2}$
4: $\mathfrak{q}_1 = \mathfrak{r}_0/\beta$
5: **for** k = 2 to m **do**
6: $\quad \mathfrak{q}_\mathcal{k} = -\mathfrak{E}(\mathbf{0}, \mathfrak{q}_{\mathcal{k}-1})$ # Original FGMRES: $\mathfrak{q}_\mathcal{k} = \mathfrak{P}_L{}^{-1} \cdot \widehat{A_D} \cdot \mathfrak{q}_{\mathcal{k}-1}$
7: $\quad$ **for** $j = 1$ to $\mathcal{k} - 1$ **do**
8: $\quad\quad \mathfrak{h}_{j,\mathcal{k}-1} = \mathfrak{q}_j^T \mathfrak{q}_\mathcal{k}$
9: $\quad\quad \mathfrak{q}_\mathcal{k} = \mathfrak{q}_\mathcal{k} - \mathfrak{h}_{j,\mathcal{k}-1}\mathfrak{q}_j$
10: $\quad$ **end for**
11: $\quad \mathfrak{h}_{\mathcal{k},\mathcal{k}-1} = ||\mathfrak{q}_\mathcal{k}||_{\mathcal{L}^2}$
12: $\quad \mathfrak{q}_\mathcal{k} = \mathfrak{q}_\mathcal{k}/\mathfrak{h}_{\mathcal{k},\mathcal{k}-1}$
13: **end for**
14: $\mathfrak{Q}_m := [\mathfrak{q}_1, ...\mathfrak{q}_m]$
15: $\bar{H}_m = \{\mathfrak{h}_{j,\mathcal{k}-1}\}_{1 \leq j \leq \mathcal{k}; 1 \leq \mathcal{k}-1 \leq m}$
16: $\mathfrak{c}_m = \text{argmin}_\mathfrak{c} ||\beta \mathfrak{e}_1 - \bar{H}_n \cdot \mathfrak{c}_n||_{\mathcal{L}^2}$
17: $[u]_m = [u]_0 + \mathfrak{Q}_m \cdot \mathfrak{c}_m$
18: **if** satisfied **then** Stop
19: **else** $[u]_0 \psi^{\mathbb{h}} := \overset{\mathcal{V}^{\mathbb{h}}}{\underset{\widehat{\mathcal{V}}}{\prod}}([u]_m \widehat{\psi})$ & Go to 2 # Original FGMRES: $[u]_0 := [u]_m$ & Go to 2
20: **end if**

the loading vector is introduced. Then,

$$\mathfrak{E}(l(\widehat{v}(\boldsymbol{x})), u^{\mathbb{h}}(\boldsymbol{x})) := \mathcal{R}^D(\widehat{v}(\boldsymbol{x})) = l(\widehat{v}(\boldsymbol{x})) - a^D(u^{\mathbb{h}}(\boldsymbol{x}), \widehat{v}(\boldsymbol{x})), \tag{3.3.18}$$

which has exactly the same structure as $\mathfrak{r}_0 = \mathfrak{P}_L{}^{-1}([l] - \widehat{A_D} \cdot [u]_0)$ in the original FGMRES line 2 of algorithm 3.

However, it allows to modify the input parameters to match an equivalent expression to the one in line 6 of the original algorithm. The modification leads to

$$\mathfrak{q}_\mathcal{k} = \mathfrak{P}_L{}^{-1} \cdot \widehat{A_D} \cdot \mathfrak{q}_{\mathcal{k}-1} = -\mathfrak{P}_L{}^{-1} \cdot (\mathbf{0} - \widehat{A_D} \cdot \mathfrak{q}_{\mathcal{k}-1}), \tag{3.3.19}$$

which has the same structure as $-\mathfrak{E}(\mathbf{0}, \mathfrak{q}_{\mathcal{k}-1})$.

3.4 Posed problem

In order to test the equivalence between error estimation and left preconditioners, a diffusion problem taken from [5] was used. Its solution is smooth, but can not be solved exactly by any polynomial shape function because of the exponential term.

Due to the BC asymmetry, the FEM solution is asymmetric although the stiffness matrix and analytical solution are not. The strong form of the problem reads

$$-\triangle u(\boldsymbol{x}) = f(\boldsymbol{x}) \qquad in\,\Omega = \{(x,y):\, 0 \leq x \leq 1\,,\, 0 \leq y \leq 1\}, \tag{3.4.1}$$

where $\triangle$ is the Laplace operator. Two different sets of BC where used, namely

$$\begin{aligned} u(\boldsymbol{x}) = 0 \qquad on \quad & \Gamma_d = \partial\Omega \\ & \Gamma_n = \emptyset \end{aligned} \tag{3.4.2}$$

and

$$\begin{aligned} u(\boldsymbol{x}) &= 0 \qquad && on\,\Gamma_d = \{(x,y) : 0 < x < 1,\, y = 0\}, \\ \tfrac{\delta u(\boldsymbol{x})}{\delta \overrightarrow{n}} &= 0 \qquad && on\,\Gamma_n = \{\partial\Omega \setminus \Gamma_d\}. \end{aligned} \tag{3.4.3}$$

All notation of the BC was defined in equation 1.2.1

The source term $f(\boldsymbol{x}) \equiv f(x,y)$ is chosen so that the exact solution of the problem is

$$u(x,y) = 5 \cdot x^2 \cdot (1-x)^2 \cdot (e^{10x^2} - 1) \cdot y^2 \cdot (1-y)^2 \cdot (e^{10y^2} - 1), \tag{3.4.4}$$

where e is the mathematical constant, not an error. Hence

$$\begin{aligned} f(x,y) := \; & 5 \cdot \Big[e^{10x^2} \cdot (400x^6 - 800x^5 + 580x^4 - 280x^3 + 112x^2 - 12x + 2) - \\ & -12x^2 + 12x - 2\Big] \cdot \Big[y^2 \cdot (1-y)^2 \cdot (e^{10y^2} - 1)\Big] + \\ & 5 \cdot \Big[e^{10y^2} \cdot (400y^6 - 800y^5 + 580y^4 - 280y^3 + 112y^2 - 12y + 2) - \\ & -12y^2 + 12y - 2\Big] \cdot \Big[x^2 \cdot (1-x)^2 \cdot (e^{10x^2} - 1)\Big]. \end{aligned} \tag{3.4.5}$$

The weak form of this problem is exactly equation 1.2.2 with $C = 1$. As a result, the short definition of the bilinear form (equation 1.2.3) is maintained for this specific diffusion problem.

3.5 Results for the FGMRES with error estimators as preconditioners

Figure 3.1 shows excellent performance for the problem version where Dirichlet BC are applied to all the boundary. On the contrary, when Neumann BC are applied

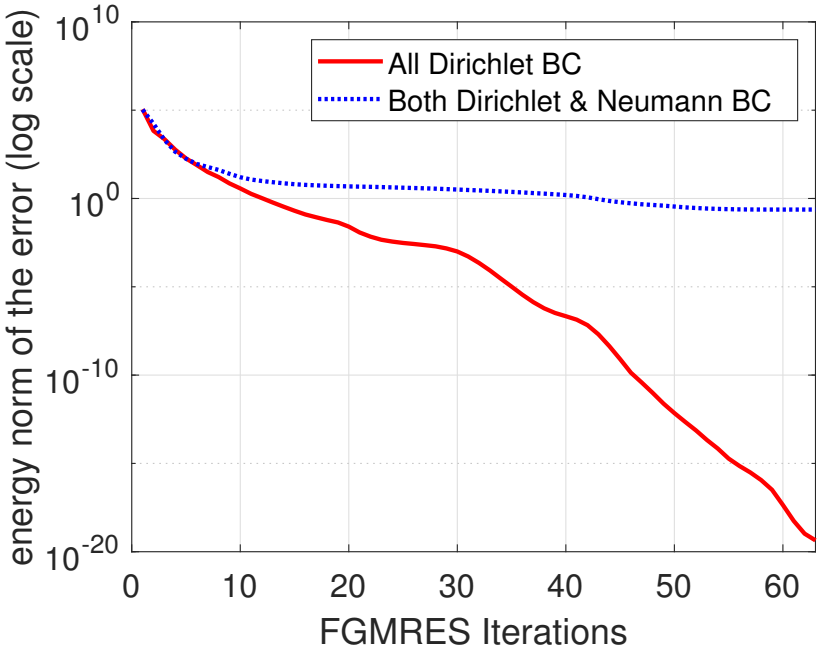

Figure 3.1: Convergence of FGMRES with error estimation as left preconditioner

to one of the edges, the convergence reaches a plateau. Apparently, error estimators based on the residual do assimilate to preconditioners. However, if Neumann BC are included, the approximation of the residual becomes orthogonal to certain search directions in the iterative solver algorithm. As a result, after some iterations the algorithm is unable to find the right direction to decrease the error. Despite the error is still reduced at each iteration, its reduction becomes negligible and not worthy compared to the computational cost of a new step in the algorithm.

Chapter 4

A-posteriori error estimation based on the residual and Dirichlet boundary conditions

4.1 Introduction

A review of different error estimators is presented in chapter 1. There, the concept of patch as a partition of unity is also introduced assuming that all patches $\mathbb{P}_{\mathbb{p}}$ are invariantly defined as the union of elements containing a vertex (*i.e.* to compute the smooth reconstruction of the stress/flux in a super patch recovery method, to create a kinematically admissible solution from the statically admissible one in constitutive relation estimate method, and to equilibrate the residual and overcome the zero mode solutions in residual estimators with Neumann Boundary Conditions, BC).

One of the purposes of the present work is to evidence the influence that patch definition has upon the accuracy of any estimation method and also that the decreased efficiency can be overcome by using p refinement. Although omitted in chapter 1, the literature presents some choice for patch definition even though only within the framework of residual estimators with Dirichlet BC. Consequently, this kind of a-posteriori estimator is used in this chapter.

The first goal is to assess the effectivity in the range of existing patch options and the new alternatives developed for this dissertation. In order to do so, the assessed estimators are reformulated in a common framework. Because of this common framework, hybrid versions of the assessed estimators can be produced and added to the comparison.

Another aim of the chapter is to decouple the patch definition from the residual distribution, which is a novel contribution. The idea comes from the existence of FE techniques that couple an element with its adjacent through ghost penalties [37]. An example is cutFEM elements [38], where moving interfaces are captured by some elements in a non-moving mesh and then cut across the interface and coupled to avoid condition number instabilities. Regardless of the original purpose, which is not included in this work, decoupling allows the improvement and stabilisation of some of the methods included in the assessment.

The present chapter is organised as follows: In section 4.2, a common framework for error estimators based on residual reduction to local problems is presented. The existing methods reformulated in this framework can be found in section 4.3 while the novel methods are formulated in section 4.4. The following section 4.5 defines the practical problem and assessment criteria employed to test the methods. Section 4.6 is devoted to analyse the soundness of the Saint-Venant assumption used to formulate the novel methods. The results of all variations of patch definition are displayed in section 4.7 for the diffusion problem and in section 4.8 for the convection-diffusion problem. Finally, section 4.9 lists the conclusions of the chapter.

4.2 Framework for error estimation based on the residual

Recall the linear elliptic abstract problem over a bounded domain introduced in equations 1.2.1 and 1.2.2, which leads to the bilinear equation 1.3.12 for the error e and the residual equation 1.3.13.

Since the error $e(\boldsymbol{x})$ belongs to the space $\mathcal{V}$ on non-discrete functions, its compu-

tation is as difficult as the resolution of the exact solution $u(\boldsymbol{x}) \in \mathcal{U}$. Furthermore, it is obvious that the cost of computing equations 1.2.2 and 1.3.12 has an equivalent cost for any given discrete subspace of $\mathcal{V}$ and $\mathcal{U}$ defined by the same mesh. It is know from Galerkin orthogonality that the solution $u^{\mathbb{h}}(\boldsymbol{x})$ is the best possible solution that belongs to the space of discrete functions $\mathcal{U}^{\mathbb{h}}$. Then, in order to compute any error using only the residual equation, a pair discrete spaces richer than $\mathcal{V}^{\mathbb{h}}$ and $\mathcal{U}^{\mathbb{h}}$ is needed.

With the purpose of avoiding this computational cost, a-posteriori error estimators based on the residual approximates this global problem in a richer subspace to a set of local subspaces. Consequently, this dissertation considers a discrete solution $\widehat{e}(\boldsymbol{x}) = \widehat{u}(\boldsymbol{x}) - u^{\mathbb{h}}(\boldsymbol{x})$ in a rich discrete space $\widehat{\mathcal{V}} \subset \mathcal{V}$ as a reference solution close enough to $e(\boldsymbol{x}) \in \mathcal{V}$. Since it is known that convergence towards the analytical solution is asymptotic with mesh refinement, for easiness of implementation, an over-discretised mesh is used in order to act as analytical solution in the verification of the results. The notation for the pseudo-analytical solution, error and space of errors is $\widetilde{u}$, $\widetilde{e}$ and $\widetilde{\mathcal{V}}$ respectively.

Formally, in order to compute discrete errors such as $\widehat{e}(\boldsymbol{x}) = \widehat{u}(\boldsymbol{x}) - u^{\mathbb{h}}(\boldsymbol{x})$, the coarse field $u^{\mathbb{h}}(\boldsymbol{x})$ must be interpolated to the fine space through the shape functions (see equation 1.2.7). In other words, the interpolator operator for a field $v^{\mathbb{h}} \in \mathcal{V}^{\mathbb{h}}$ to the fine space $\widehat{\mathcal{V}}$ reads

$$\underset{\mathcal{V}^{\mathbb{h}}}{\overset{\widehat{\mathcal{V}}}{I}}(v^{\mathbb{h}}) = \underset{\mathcal{V}^{\mathbb{h}}}{\overset{\widehat{\mathcal{V}}}{I}}([v^{\mathbb{h}}]\psi^{\mathbb{h}}) = [\widehat{v}^{*}]\widehat{\psi}, \tag{4.2.1}$$

where

$$[\widehat{v}^{*}] \begin{cases} [\widehat{v}^{*}_{i_{\text{DOF}}}] = [v^{\mathbb{h}}{}_{i_{\text{DOF}}}] & \text{if } i_{\text{DOF}} \in \mathcal{V}^{\mathbb{h}} \;\&\; i_{\text{DOF}} \in \widehat{\mathcal{V}}; \\ [\widehat{v}^{*}_{i_{\text{DOF}}}] = \displaystyle\sum_{i'_{\text{DOF}} \in \mathcal{V}^{\mathbb{h}}} \psi^{\mathbb{h}}_{i'_{\text{DOF}}}(\boldsymbol{x}_{i_{\text{DOF}}})[v^{\mathbb{h}}_{i'_{\text{DOF}}}] & \text{if } i_{\text{DOF}} \notin \mathcal{V}^{\mathbb{h}} \;\&\; i_{\text{DOF}} \in \widehat{\mathcal{V}}. \end{cases} \tag{4.2.2}$$

This thesis abuses notation and just write $v^{\mathbb{h}}(\boldsymbol{x})$ even if referring to its interpolation to a fine space.

Through error estimation, a pre-computed coarse solution $u^{\mathbb{h}}(\boldsymbol{x}) \in \mathcal{U}^{\mathbb{h}} \subset \widehat{\mathcal{U}} \subset \mathcal{U}$ is reused to compute an estimated error $\widehat{\varepsilon}(\boldsymbol{x}) \in \widehat{\mathcal{V}} \subset \mathcal{V}$ as an approximation of the reference error $\widehat{e}(\boldsymbol{x}) \in \widehat{\mathcal{V}}$. It is in this frame that patch definition has practical use

as a set of discrete elements. Nevertheless, since the error equation and derivation of local problems are satisfied at a continuum level, $\varepsilon(\boldsymbol{x}) \in \mathcal{V}$ is also defined as the approximation of $e(\boldsymbol{x})$ through patches applied to the continuum space.

In this chapter, the initial coarse space is defined by the characteristic length $\mathbb{h}$ of its elements. Since a regular quadrilateral mesh is employed, $\mathbb{h}$ stands for the length of the edges in the mesh. The reference space is defined by $\mathbb{h}$ and the number of refinements R in each direction for every element. For instance, figure 4.1.d shows a particular case of a 2 dimensional coarse domain of 1×1.25 units of length. The domain is regularly meshed by means of $1/\mathbb{h} \times 1.25/\mathbb{h} = 4{\times}5$ quadrilateral elements, where a refinement of $R \times R{=}4{\times}4$ is applied creating a reference space of $(1/\mathbb{h})^{*}R$ $\times$ $(1.25/\mathbb{h})^{*}R = 16{\times}20$ sub-elements.

4.2.1 Reduction to local Dirichlet sub-domains

The main purpose of this family of error estimators is to subdivide the global problem in a set of local problems, where contributions outside of the sub-domains are either null or negligible.

The common way of doing this is by reducing the tests functions' support to the interior of each sub-domain so that $v(\boldsymbol{x}) = 0$, on $\Omega \setminus \Omega_{\mathbb{p}}$. That creates a set of "bubble sub-domains" that may intersect each other. Then, BC are applied to the sub-domains to estimate each patch's error.

The way of splitting the global domain determines each local sub-domain's shape. Three different published methods using this technique are presented and compared in section 4.3.

This work introduces a new way of reducing the global residual in section 4.4. It is named "additive subdomains" and it is based on Saint-Venant's Principle [49]. It considers the locally applied residuals as equilibrated loads, therefore its contribution becomes negligible if far enough from the application point. This allows local domains to be arbitrary large.

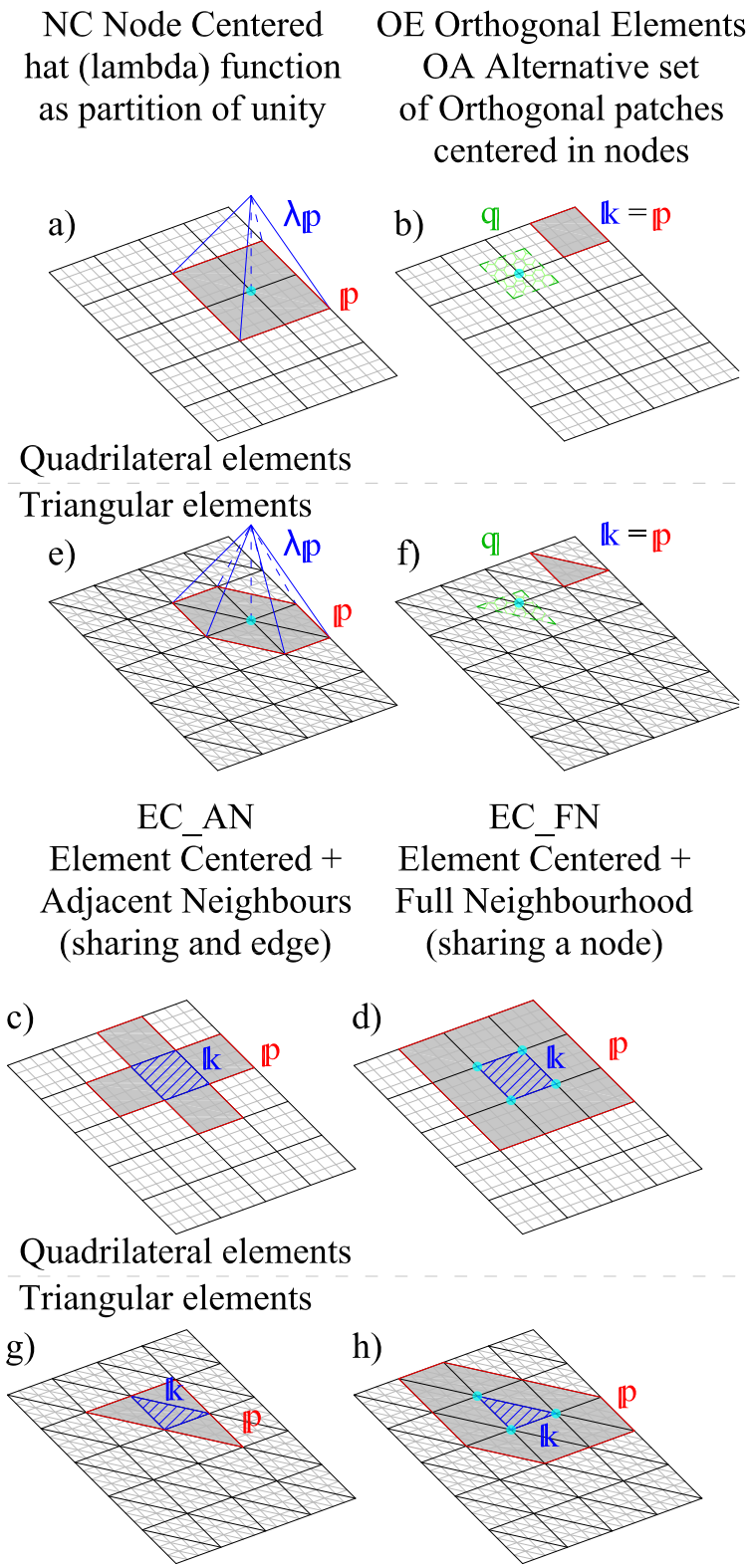

Figure 4.1: Types of patch definition used in this dissertation

Red lines are the boundary of local patches also indexed by symbol $\mathbb{p}$

Blue colour indicates the residual part applied to an additive sub-domain

Symbols $\mathbb{k}$ and $\mathbb{q}$ stand for element and alternative orthogonal patch indexes

4.3 Sub-domain bubble methods

The common idea behind these methods is to split the global finer space into a set of local subspaces with no support outside the sub-domain. This produces a set of local problems transforming equation 1.3.12 into

$$a^D_{\mathbb{p}}(e_{\mathbb{p}}(\boldsymbol{x}), v(\boldsymbol{x})) = \mathcal{R}^D_{\mathbb{p}}(v(\boldsymbol{x})), \qquad \forall\, v(\boldsymbol{x}) \in \mathcal{V}, \qquad v(\boldsymbol{x}) = 0,\ on\, \Omega \setminus \Omega_{\mathbb{p}}, \tag{4.3.1}$$

where $a^D_{\mathbb{p}}(\cdot,\cdot)$, $\mathcal{R}^D_{\mathbb{p}}(\cdot)$ and $e_{\mathbb{p}}(\boldsymbol{x})$ stand for local versions of $a^D(\cdot,\cdot)$, $\mathcal{R}^D(\cdot)$ and $e(\boldsymbol{x})$ excluding elements outside each patch $\mathbb{P}_{\mathbb{p}}$, and $\Omega_{\mathbb{p}}$ stands for the subdomain resulting from the union of all elements in the patch. Different ways to get to this equation are detailed in each of the methods.

Since the partition is applied directly to all test functions, the change affects both sides of the equation. Therefore, each patch approximates the whole error but only where the local subspace has support. The consequence of this approach is that a discontinuous approximated error field is generally recovered from the union of all patches. Then, some sort of averaging for the different results is needed to recover a continuous and global estimation for the error field. The exception of a continuous recovered error field requires the patches not to intersect each other.

This might not be a disadvantage if the only aim of using error estimation is to compute a bound or to guide an adaptive refinement strategy.

4.3.1 Elemental bubble (uses Orthogonal Element patches, OE)

The simplest way to define a set of local subspaces for $\mathcal{V}$ is to restrict its support to the interior domain of each element $\mathbb{e}^{\mathbb{k}}$ denoted $\Omega_{\mathbb{k}}$. The nomenclature OE comes from Orthogonal Element patches and examples can be found in figures 4.1.b,f delimited in red. In this set of subspaces $\{\mathcal{V}_{\mathbb{k}}\}_{\mathbb{k}=1}^{n_{\mathbb{e}}}$ each subspace fulfils the following condition $\mathcal{V}_{\mathbb{k}} \subset \mathcal{V} = \{v(\boldsymbol{x}) \in \mathcal{V}_{\mathbb{k}} \,|\, v(\boldsymbol{x}) = 0\, in\, \Omega \setminus \Omega_{\mathbb{k}}\}$, and all subspaces are orthogonal with respect to $a^D(\cdot,\cdot)$ by definition, due to the fact that their intersection is empty. Figures 4.1.b and 4.1.f show these patches $\mathbb{P}_{\mathbb{k}}$ in red. Consequently, using

the equation 1.3.12 on each discrete subspace $\widehat{\mathcal{V}_{\mathbb{k}}} \subset \mathcal{V}_{\mathbb{k}}$ with homogeneous Dirichlet BC, a projection $\widehat{\varepsilon_{\mathbb{k}}}$ of $e(\boldsymbol{x})$ can be obtained. Furthermore, by Bessel's inequality, this projection is a local lower bound that verifies

$$\sum_{\mathbb{k}=1}^{\mathbb{k}=n_{\mathbb{e}}} a^D(\widehat{\varepsilon_{\mathbb{k}}}(\boldsymbol{x}), \widehat{\varepsilon_{\mathbb{k}}}(\boldsymbol{x})) = a^D(\widehat{\varepsilon}(\boldsymbol{x}), \widehat{\varepsilon}(\boldsymbol{x})) \leq a(e(\boldsymbol{x}), e(\boldsymbol{x})). \tag{4.3.2}$$

Moreover, by the definition of $a^D(\cdot,\cdot)$, $\varepsilon_{\mathbb{k}}(\boldsymbol{x})$ (and any discrete approximation $\widehat{\varepsilon_{\mathbb{k}}}(\boldsymbol{x})$) is also orthogonal to $e(\boldsymbol{x}) - \varepsilon_{\mathbb{k}}(\boldsymbol{x})$. In addition, since the support of $\varepsilon_{\mathbb{k}}(\boldsymbol{x})$ lives only in the interior of $\mathcal{V}_{\mathbb{k}}(\boldsymbol{x})$, it can be proved that this orthogonality also stands for the local form $a^D_{\mathbb{k}}(\cdot,\cdot)$.

These local bubble problems are estimators for the error directly. These estimations stand even locally. However, only the interior nodes of the elements make contributions to the estimate, since $\varepsilon(\boldsymbol{x}) = \sum_{\mathbb{k}=1}^{\mathbb{k}=n_{\mathbb{e}}} \varepsilon_{\mathbb{k}}(\boldsymbol{x})$ vanishes on all elemental boundaries.

Since the local estimations of the error do not intersect each other, exceptionally in this case, a continuous field is recovered. In this field, the value is equal to zero in all edges of any original coarse element. Furthermore, the FE solution at the degrees of freedom (DOF) initially belonging to $\mathcal{V}_{\mathbb{k}}$ is never updated.

4.3.2 Subspace projection (uses Orthogonal Element and Orthogonal Alternative patches, OE+OA)

This method was presented by A. Huerta and co-workers [88]. It is based on the elemental bubbles orthogonality seen in the previous section. Its aim is to enrich the elemental bubble estimation by computing missing contributions hidden to the initial projection.

Figures 4.1.b and 4.1.f show two examples where the original set of orthogonal patches in red coincides with the elements (OE), and the alternative orthogonal patches in green are centred in the vertexes of the element (OA).

The global error field $e(\boldsymbol{x})$ can be split into the projection $\varepsilon(\boldsymbol{x})$ and the part omitted by the projection $e^{\perp\varepsilon}(\boldsymbol{x})$, which is orthogonal to the projection subspaces

$\mathcal{V}_{\mathbb{k}}$ and hence to $\varepsilon(\boldsymbol{x})$. By the Pythagoras theorem $||e(\boldsymbol{x})||_E^2 = ||\varepsilon||_E^2 + ||e^{\perp\varepsilon}||_E^2$ being $||\cdot||_E^2$ the energy norm $a^D(\cdot,\cdot)$.

This method defines a way to estimate $e^{\perp\varepsilon}(\boldsymbol{x})$ and to add this contribution to the first estimate.

Algorithm 4 Subspace projection estimate and approximative computational cost

1:	Interpolation to rich space	# Not considered	
	BUBBLE PART		
2:	**for** $\mathbb{k} = 1$ to $n_{\mathbb{e}}$ **do**	# Loop on elements = patches	$n_{\mathbb{e}}$ iterations
3:	Global to local indexes	# Comparison sort · loop	$DOF_{\mathbb{P}_{\mathbb{k}}} \cdot \mathcal{O}(DOF_{\mathbb{P}_{\mathbb{k}}} \cdot log(DOF_{\mathbb{P}_{\mathbb{k}}}))$
4:	Assemble FEM local system	# Not considered	
5:	Apply boundary conditions	# Direct access	$\mathcal{O}(DOF_{\partial\Omega_{\mathbb{k}}})$
6:	Solve system of equations	# Krylov methods	$K \cdot \mathcal{O}(DOF^2_{\mathbb{P}_{\mathbb{k}}})$
7:	**end for**		
	PROJECTION PART		
8:	**for** $\mathbb{q} = 1$ to $n_{\mathbb{Q}}$ **do**	# Loop on alternative patches	$n_{\mathbb{Q}}$ iterations
9:	Global to local indexes	# Comparison sort · loop	$DOF_{\mathbb{Q}} \cdot \mathcal{O}(DOF_{\mathbb{Q}} \cdot log(DOF_{\mathbb{Q}}))$
10:	Assemble FEM local system	# Not considered	
11:	Enforce orthogonality	# Add row and column to matrix	$\mathcal{O}(2 \cdot DOF_{\mathbb{Q}} + 1)$
12:	Apply boundary conditions	# Direct access	$\mathcal{O}(DOF_{\partial\Lambda_{\mathbb{q}}})$
13:	Solve system of equations	# Krylov methods	$K \cdot \mathcal{O}(DOF^2_{\mathbb{Q}})$
14:	**end for**		
			$n_{\mathbb{Q}} \approx n_{\mathbb{e}}$; $DOF_{\mathbb{Q}} = DOF_{\mathbb{P}_{\mathbb{k}}}$; $DOF_{\partial\Omega_{\mathbb{k}}} = DOF_{\Lambda_{\mathbb{q}}}$
	Total approximative cost		$\mathcal{O}(2 \cdot n_{\mathbb{e}} \cdot (K + log(DOF_{\mathbb{P}_{\mathbb{k}}})) \cdot DOF^2_{\mathbb{P}_{\mathbb{k}}})$

LEGEND

$\mathbb{e}$ = Elements, $\mathbb{P}_{\mathbb{k}}$ = Elemental patches (coarse elements refined), $\mathbb{k}$ = index for the elements,
$\mathbb{Q}$ = Alternative Patches, $\mathbb{q}$ = index for the alternative patches, DOF = Degrees of freedom,
K number of basis functions used in Krylov method (depends on the condition number),
n_* = number of, $*_{\partial\Omega_{\mathbb{k}}}$ = elemental patch's boundary, $*_{\partial\Lambda_{\mathbb{q}}}$ = alternative patch's boundary

Consider another projection of $e(\boldsymbol{x})$ named $\zeta(\boldsymbol{x})$ analogous to $\varepsilon(\boldsymbol{x})$, but into a different set of $n_{\mathbb{Q}_{\mathbb{q}}}$ alternative orthogonal subspaces $\{\mathcal{V}_{\mathbb{q}}\}_{\mathbb{q}=1}^{n_{\mathbb{Q}}}$ fulfilling the same condition $\mathcal{V}_{\mathbb{q}} \subset \mathcal{V} = \{v(\boldsymbol{x}) \in \mathcal{V}_{\mathbb{q}} \,|\, v(\boldsymbol{x}) = 0 \, in \, \Omega \setminus \Lambda_{\mathbb{q}}\}$. In the last sentence, $\mathbb{Q}$ stands for alternative patch, $\mathbb{q}$ is the index identifying each alternative patch and $\Lambda_{\mathbb{q}}$ denotes the sub-domain corresponding to the alternative patch $\mathbb{q}$. All subspaces $\mathbb{Q}_{\mathbb{q}}$ overlap partially with at least one of the elemental patches $\mathbb{P}_{\mathbb{k}}$ (*i.e.* $\delta\Lambda\mathbb{q} \neq \partial\Omega\mathbb{k}\,, \forall\mathbb{q}, \mathbb{k}$).

Because of the orthogonality enforced by means of homogeneous Dirichlet BC, $\zeta(\boldsymbol{x}) = \sum_{\mathbb{q}=1}^{\mathbb{q}=n_{\mathbb{P}_{\mathbb{q}}}} \zeta_{\mathbb{q}}(\boldsymbol{x})$ as in the original set.

Provided that both sets of discrete subspaces $\{\widehat{\mathcal{V}_{\mathbb{k}}} \subset \mathcal{V}_{\mathbb{k}}\}_{\mathbb{k}=1}^{n_{\mathbb{e}}}$ and $\{\widehat{\mathcal{V}_{\mathbb{q}}} \subset \mathcal{V}_{\mathbb{q}}\}_{\mathbb{q}=1}^{n_{\mathbb{Q}}}$ share the same discretisation (nodes and shape functions), it is possible to compute locally the orthogonal part of the discrete new field $\widehat{\zeta}(\boldsymbol{x})$ with respect to $\widehat{\varepsilon}(\boldsymbol{x})$ on the local energy norm, for instance with Lagrange multipliers enforcing $a_{\mathbb{q}}^D(\widehat{\zeta_{\mathbb{q}}^{\perp}}(\boldsymbol{x}), \widehat{\varepsilon_{\mathbb{q}}}(\boldsymbol{x})) = 0$.

This set of new fields $\widetilde{\zeta_{\mathbb{q}}^{\perp}}(\boldsymbol{x})$ can be added to the first estimator keeping the lower bound property stated by Bessel inequality

$$\sum_{\mathbb{q}=1}^{\mathbb{q}=n_{\mathbb{Q}}} a^D(\widehat{\zeta_{\mathbb{q}}^{\perp}}(\boldsymbol{x}), \widehat{\zeta_{\mathbb{q}}^{\perp}}(\boldsymbol{x})) + a^D(\widehat{\varepsilon}(\boldsymbol{x}), \widehat{\varepsilon}(\boldsymbol{x})) \leq a^D(e(\boldsymbol{x}), e(\boldsymbol{x})). \tag{4.3.3}$$

4.3.3 Node Centred sub-domains (NC patches)

An extended alternative way to divide the domain into patches is to make use of the partition of unity through the first-order Lagrange basis function $\lambda_{\mathbb{p}}$ in every nodal point $np_{\mathbb{p}}$ that is a vertex of the coarse discretisation. Figures 4.1.a and 4.1.e are examples of this NC patches. Then,

$$\lambda_{\mathbb{p}}(\boldsymbol{x}_j) = \delta_{\mathbb{p}j}, \tag{4.3.4}$$

where $\delta_{\mathbb{p}m}$ stands for the Kronecker delta and

$$\sum_{\mathbb{p}=1}^{\mathbb{p}=n_{\mathbb{P}}} \lambda_{\mathbb{p}}(\boldsymbol{x}) \equiv 1, \qquad x \in \Omega. \tag{4.3.5}$$

From equation 1.3.12 the following equation is obtained

$$\begin{array}{ll} a^D(e(\boldsymbol{x}), \sum_{\mathbb{p}=1}^{\mathbb{p}=n_{\mathbb{P}}} \lambda_{\mathbb{p}} \cdot v(\boldsymbol{x})) = \mathcal{R}^D(\sum_{\mathbb{p}=1}^{\mathbb{p}=n_{\mathbb{P}}} \lambda_{\mathbb{p}} \cdot v(\boldsymbol{x})), & \forall\, v(\boldsymbol{x}) \in \mathcal{V}. \\ \sum_{\mathbb{p}=1}^{\mathbb{p}=n_{\mathbb{P}}} a^D(e(\boldsymbol{x}), \lambda_{\mathbb{p}} \cdot v(\boldsymbol{x})) = \sum_{\mathbb{p}=1}^{\mathbb{p}=n_{\mathbb{P}}} \mathcal{R}^D(\lambda_{\mathbb{p}} \cdot v(\boldsymbol{x})), & \forall\, v(\boldsymbol{x}) \in \mathcal{V}. \end{array} \tag{4.3.6}$$

Note that $\lambda_{\mathbb{p}} \cdot v(\boldsymbol{x})$ fulfils all the criteria to be a test function in any subspace limited to the patch, but it is a different function from $v(\boldsymbol{x})$.

From this equation, the original method converts $\lambda_{\mathbb{p}} \cdot v(\boldsymbol{x})$ into a regular test function in both sides of the equation. As advanced in previous sections, this produces different nodal solutions for the estimation of $e(\boldsymbol{x})$ from each local patch problem:

$$a_{\mathbb{p}}^D(\phi_{\mathbb{p}}(\boldsymbol{x}), v(\boldsymbol{x})) = \mathcal{R}_{\mathbb{p}}^D(v(\boldsymbol{x})), \qquad \forall v(\boldsymbol{x}) \in \mathcal{V}, \tag{4.3.7}$$

Algorithm 5 Node centred subdomains and approximative computational cost

1:	**for** $\mathbb{p} = 1$ to $n_{\mathbb{P}}$ **do**	# Loop on vertexes = patches	$n_{\mathbb{P}}$ iterations
2:	Select sub-elements in patch	# Comparison sort	$\mathcal{O}(SubE_T \cdot log(SubE_T))$
3:	Interpolation to rich space	# Not considered	
4:	Global to local indexes	# Comparison sort · loop	$DOF_{\mathbb{P}} \cdot \mathcal{O}(DOF_{\mathbb{P}} \cdot log(DOF_{\mathbb{P}}))$
5:	Assemble FEM local system	# Not considered	
6:	Apply boundary conditions	# Direct access	$\mathcal{O}(DOF_{\partial\Omega_{\mathbb{p}}})$
7:	Solve system of equations	# Krylov methods	$K \cdot \mathcal{O}(DOF_{\mathbb{P}}^2)$
8:	Multiplication by hat function	# Multiplication by hat function	$\mathcal{O}(DOF_{\mathbb{P}})$
9:	**end for**		
	Total approximative cost		$\mathcal{O}(n_{\mathbb{P}} \cdot (K + log(DOF_{\mathbb{P}})) \cdot DOF_{\mathbb{P}}^2)$

LEGEND

$n_{\mathbb{P}}$ = Number of patches, $\mathbb{p}$ = Index identifying a patch, $SubE$ = Sub-elements, DOF = Degrees of freedom, K number of basis functions used in Krylov method (depends on the condition number), $*_T$ = total, $*_{\mathbb{P}}$ = in patch, $*_{\partial\Omega_{\mathbb{p}}}$ = in patch's boundary

where $\phi_{\mathbb{p}}(\boldsymbol{x})$ is the complete local approximation of $e(\boldsymbol{x})$ computed from patch $\mathbb{P}_{\mathbb{p}}$.

The original published method proposes the addition of this local quantities $||e(\boldsymbol{x})||_E^2 \approx \sum_{\mathbb{p}=1}^{\mathbb{p}=n_{\mathbb{P}}} ||\phi_{\mathbb{p}}(\boldsymbol{x})||_E^2$ as estimator. However, this addition results in duplicating the contribution of several nodes that belong to more than one patch. This is useful just if the only goal of using this method is to compute an indicator of the local energy in order to mark which elements should be refined in an adaptive refinement scheme.

Details of this original method and how to compute bounds can be found in I. Babuška and A. Miller [14].

If on the contrary, the interest is to obtain a sharper approximation of the whole energy field, an averaging is needed. One averaging option is to make use of the same $\lambda_{\mathbb{p}}$ that is defined to partition the domain initially. Then, this set of different averaged $\phi_{\mathbb{p}}(\boldsymbol{x})$ leads to $e(\boldsymbol{x}) \approx \varepsilon(\boldsymbol{x}) = \sum_{\mathbb{p}=1}^{\mathbb{p}=n_{\mathbb{P}}} \lambda_{\mathbb{p}} \cdot \phi_{\mathbb{p}}(\boldsymbol{x})$. However, this requires a global assembly of the field.

Another suggestion made in this thesis is to compute a local density of energy norm $\rho_{\mathbb{p}} = ||\phi_{\mathbb{p}}(\boldsymbol{x})||_E^2 / |\Omega_{\mathbb{p}}|$ which is completely local, and then integrate it across the whole domain with the already computed coarse shape functions $||e(\boldsymbol{x})||_E^2 \approx \int_\Omega \rho_{\mathbb{p}}$.

As it is shown in section 4.7.1, both ways of averaging are viable although the

first one is more accurate.

4.3.4 Element Centred sub-domains (EC patches)

The extension to larger sub-domains as the ones displayed in figures 4.1.c, 4.1.d, 4.1.g and 4.1.h (EC patches), requires further assumptions. This is due to two reasons. Firstly, the orthogonality is lost if more than one element is included in the sub-domain. Secondly, there is no obvious continuous function that forms a partition of unity and can modify the test functions in order to define the patch. Furthermore, an average rule, generally difficult to define, is also needed to recover a global field.

Algorithm 6 Element centred estimate and approximative computational cost

1:	**for** $\mathbb{k} = 1$ to $n_{\mathbb{e}}$ **do**	# Loop on elements = patches	$n_{\mathbb{e}}$ iterations
2:	Select sub-elements in patch	# Comparison sort	$\mathcal{O}(SubE_T \cdot log(SubE_T))$
3:	Interpolation to rich space	# Not considered	
4:	Global to local indexes	# Comparison sort $\cdot$ loop	$DOF_{\mathbb{P}} \cdot \mathcal{O}(DOF_{\mathbb{P}} \cdot log(DOF_{\mathbb{P}}))$
5:	Assemble FEM local system and residual Not considered		#
6:	Apply boundary conditions	# Direct access	$\mathcal{O}(DOF_{\partial\Omega_{\mathbb{k}}})$
7:	Solve system of equations	# Krylov methods	$K \cdot \mathcal{O}(DOF_{\mathbb{P}}^2)$
8:	Multiplication by hat function	# Multiplication by hat function	$\mathcal{O}(DOF_{\mathbb{P}})$
9:	**end for**		
	Total approximative cost		$\mathcal{O}(E_T \cdot (K + log(DOF_P)) \cdot DOF_P^2)$

LEGEND

$n_{\mathbb{e}}$ = Number of elements, $\mathbb{k}$ Index identifying an element, $SubE$ = Sub-elements, DOF = Degrees of freedom, K number of basis functions used in Krylov method (depends on the condition number), $*_T$ = total, $*_{\mathbb{P}}$ = in patch, $*_{\partial\Omega_{\mathbb{k}}}$ = in patch's boundary

A possible way to partially mitigate the lack of orthogonality is to fix the DOF corresponding to both coarse and enhanced space. Any solution $\widehat{u}(\boldsymbol{x}) \in \widehat{\mathcal{V}}$ can be decomposed into $\widehat{u}(\boldsymbol{x}) = \widehat{u_1}(\boldsymbol{x}) \in \mathcal{V}^{\mathbb{h}} + \widehat{u_2}(\boldsymbol{x}) \in \triangle\widehat{\mathcal{V}}$ being $\triangle\widehat{\mathcal{V}} = \{v(\boldsymbol{x}) \in \widehat{\mathcal{V}}, v(\boldsymbol{x}) = 0\}$ at each node in $\mathcal{V}^{\mathbb{h}}\}$. Then the approximation $\widehat{u_1} \approx u^{\mathbb{h}}$ is introduced to solve the equation 1.3.12 in the subspace $\widehat{\mathcal{V}}$ as previously seen.

Note that this last assumption becomes less sound as the spaces $\widehat{\mathcal{V}}$ and $\mathcal{V}^{\mathbb{h}}$ are further from each other, which is not a desirable property and it rapidly makes the

method unstable as it is shown in the results section.

Remark. The particular case of adjacent elements and coarse order 1 elements to order 2 serendipity elements was presented by K. Runesson and co-workers [109]. In this case, there are only enhanced DOF on the boundary, and only non-zero in 2 contiguous elements so the averaging rule is obvious. Also, in this particular case, the 2 spaces are close enough so that the method is stable.

4.4 Sub-domain additive methods

This novel approach to the sub-domain partition is based on Saint-Venant principle [49]. The partitioning is applied only to the right hand side of the error equation 1.3.12, leading to a sum of $n_{\mathbb{P}}$ local terms of the form

$$a^D(e(\boldsymbol{x}), v(\boldsymbol{x})) = \mathcal{R}^D(v(\boldsymbol{x})) = \sum_{\mathbb{i}=1}^{n_{\mathbb{P}}} \mathcal{R}^D_{\mathbb{i}}(v(\boldsymbol{x})), \qquad \forall\, v(\boldsymbol{x}) \in \mathcal{V}. \tag{4.4.1}$$

All local partitions of the residual $\mathcal{R}^D_{\mathbb{i}}(v(\boldsymbol{x}))$ can be defined totally arbitrary (being $\mathbb{i}$ a mere sequential index to identify them, unlinked to any geometric feature). Each local residual is applied to a patch $\mathbb{P}_{\mathbb{p}=\mathbb{i}}$. For the moment they are not defined, so consider that all of the patches equal the global domain Ω.

Solving independently for each $\mathcal{R}^D_{\mathbb{i}}$ term originates a number of $\varepsilon_{\mathbb{i}}(\boldsymbol{x})$ contributions to the whole domain equal to the number of patches. And it is known that

$$e(\boldsymbol{x}) = \sum_{\mathbb{i}=1}^{n_{\mathbb{P}}} \varepsilon_{\mathbb{i}}(\boldsymbol{x}), \tag{4.4.2}$$

with no approximation for any combination of $\mathcal{R}^D_{\mathbb{i}}$ that adds up to the original global residual. The several solutions $\varepsilon_{\mathbb{i}}(\boldsymbol{x})$ are global fields computed through the local residuals.

Provided that each of these $\mathcal{R}^D_{\mathbb{i}}$ terms is defined locally and is equilibrated, by Saint-Venant principle [49] there exists a limit beyond which the contribution $\varepsilon_{\mathbb{i}}(\boldsymbol{x})$ is negligible. Due to this assumption, it is possible to approximate the sum of global

problems to a sum of local ones.

$$a^D(\varepsilon_{\mathbb{i}}(\boldsymbol{x}), v(\boldsymbol{x})) = \mathcal{R}^D_{\mathbb{i}}(v(\boldsymbol{x})) \approx a^D_{\mathbb{p}=\mathbb{i}}(\varepsilon_{\mathbb{p}}(\boldsymbol{x}), v(\boldsymbol{x})) = \mathcal{R}^D_{\mathbb{p}=\mathbb{i}}(v(\boldsymbol{x})), \qquad \forall\, v(\boldsymbol{x}) \in \mathcal{V}. \tag{4.4.3}$$

The form $a^D_{\mathbb{p}=\mathbb{i}}(\cdot,\cdot)$ is nothing but $a^D(\cdot,\cdot)$ excluding all elements outside the patch $\mathbb{P}_{\mathbb{p}=\mathbb{i}}$, and $\mathcal{R}^D_{\mathbb{p}=\mathbb{i}}$ is a particular case of $\mathcal{R}^D_{\mathbb{i}}$ distribution that must be applied to a sub-domain equal or smaller than the patch so that the assumption is fulfilled. Note that in contrast to the former methods, here the local patch size can be arbitrary large, as long as it is larger than the aforementioned limit.

This new variant of patch definition overcomes the necessity of averaging different solutions, allowing the use of any h or p-refinement. In contrast to the traditional case, the global estimated field must be computed adding local terms, since each local quantity is incomplete.

4.4.1 Node and element centred additive variants

In order to obtain Node Centred patches (NC) as in figures 4.1.a and 4.1.e, it is possible to utilise the Lagrange polynomial of order 1 $\lambda_{\mathbb{p}}(\boldsymbol{x}_j) = \delta_{\mathbb{p}j}$ defined in section 4.3.3 to obtain the local residuals from the global residual equation. $\mathcal{R}^D = \sum_{\mathbb{p}=1}^{n_{\mathbb{P}}} \lambda_{\mathbb{p}}(\boldsymbol{x}_m) \cdot \mathcal{R}^D = \sum_{\mathbb{p}=1}^{n_{\mathbb{P}}} \mathcal{R}^D_{\mathbb{p}=\mathbb{i}}$. The $\lambda_{\mathbb{P}}(\boldsymbol{x}_j)$ function already concentrates the residual in the centre of the patch, but any larger patch could be designated with no residual applied to the rest of elements in it.

Unfortunately, following a similar approach for element centred patches with the indicator function breaks the C0 continuity requirement for the shape functions. The indicator function reads $\mathbb{1}_{\Omega_{\mathbb{k}}}(\boldsymbol{x}) := \{1 \text{ if } (\boldsymbol{x}) \in \Omega_{\mathbb{k}}\,;\, 0 \text{ if } (\boldsymbol{x}) \notin \Omega_{\mathbb{k}}\}$, being $\Omega_{\mathbb{k}}$ the central element defining the patch $\mathbb{P}_{\mathbb{k}}$ and $\mathbb{k}$ the index identifying it. An alternative to split the right hand side (r.h.s.). is needed.

The additivity property of the integrals can be exploited to achieve a similar result. It says that if c is an element of the domain $[a, b]$ then $\int_a^b f(x) = \int_a^c f(x) + \int_c^b f(x)$. Splitting all the integrals in the residual and using each element $\mathbb{e}^{\mathbb{k}}$ with associated subdomain $\Omega_{\mathbb{k}}$ as a local domain of additivity integration leads to the

transformation of the residual expression below

$$\mathcal{R}^D(v(\boldsymbol{x})) = \int_\Omega v(\boldsymbol{x})\cdot f(\boldsymbol{x})\,d\Omega + \int_{\Gamma_n} v(\boldsymbol{x})\cdot g_n(\boldsymbol{x})\,d\Gamma_n - \int_\Omega (\nabla v(\boldsymbol{x})\cdot(C\nabla u^{\mathbb{h}}(\boldsymbol{x}))\,d\Omega \quad (4.4.4)$$

into

$$\mathcal{R}^D(v(\boldsymbol{x})) = \sum_{\mathbb{k}=1}^{n_{\mathbb{e}}} \mathcal{R}^D_{\mathbb{p}=\mathbb{i}=\mathbb{k}} = \sum_{\mathbb{k}=1}^{n_{\mathbb{e}}} \left(\int_{\Omega_{\mathbb{k}}} v(\boldsymbol{x})\cdot f(\boldsymbol{x})\,d\Omega + \int_{\Gamma_n^{\mathbb{k}}} v(\boldsymbol{x})\cdot g_n(\boldsymbol{x})\,d\Gamma_n - \int_{\Omega_{\mathbb{k}}} \nabla v(\boldsymbol{x})\cdot(C\nabla u^{\mathbb{h}}(\boldsymbol{x}))\,d\Omega \right). \quad (4.4.5)$$

It is possible then to apply only an additive part of the residual on the central element, which defines a patch around it in an analogy with distributed loads. Examples are shown in blue in figures 4.1.c, 4.1.d, 4.1.g and 4.1.h.

4.4.2 Hybrid estimators

Let the purpose be to estimate the error in an h-refined rich space $\widehat{\mathcal{V}}^{p1:\frac{\mathbb{h}}{R}}$ but also to reduce the cost of solving a large additive version of the local patch of several elements with a high number of sub-refinements R. In this subsection p1 stands for order 1 shape functions and p2 for order 2 shape functions.

The proposed idea is to employ an additive sub-domain estimator with p-refinement as a first step. This is easily done for any residual error estimator (*e.g.* [131] for the subspace projection method). After that, only the solution in those boundaries is taken into account and extended to the interior through orthogonal elemental bubbles and h-refinement.

The initial computation creates a solution in space $\widehat{\mathcal{V}}^{p2}$ that is far cheaper than solving for $\widehat{\mathcal{V}}^{p1:\frac{\mathbb{h}}{R}}$ with high R.

Finally, this preliminary solution is applied as Dirichlet BC for each local bubble problem in $\widehat{\mathcal{V}}_{\mathbb{k}}^{p1:\frac{\mathbb{h}}{R}}$. Since the subset of interior spaces is orthogonal to $a^D(\cdot,\cdot)$, this process is equivalent to projecting the preliminary solution to the desired subspace. The cost of this secondary stage is also cheaper than solving multi-element local patches directly in $\widehat{\mathcal{V}}^{p1:\frac{\mathbb{h}}{R}}$ since the support is a single element.

4.5 Posed problems, bounds and assessment criteria

This section is devoted to define the problems posed and the assessment criteria to compare the aforementioned methods.

4.5.1 Diffusion problem

The first proposed problem is the diffusion one already mentioned in equation 3.4.1 with BC 3.4.3 that will be rewritten for chapter compactness.

$$\begin{aligned} -\triangle u(\boldsymbol{x}) &= f(\boldsymbol{x}) \quad in\, \Omega = \{(x,y):\, 0 \leq x \leq 1\,,\, 0 \leq y \leq 1\}, \\ u(\boldsymbol{x}) &= 0 \qquad on\, \Gamma_d = \{(x,y) : 0 < x < 1,\, y = 0\}, \\ \tfrac{\delta u(\boldsymbol{x})}{\delta \overrightarrow{n}} &= 0 \qquad on\, \Gamma_n = \{\partial\Omega \setminus \Gamma_d\}. \end{aligned} \tag{4.5.1}$$

where $f(\boldsymbol{x}) \equiv f(x,y)$ is chosen so that the analytical solution of the problem is

$$u(x,y) = 5 \cdot x^2 \cdot (1-x)^2 \cdot (e^{10x^2} - 1) \cdot y^2 \cdot (1-y)^2 \cdot (e^{10y^2} - 1), \tag{4.5.2}$$

being e the mathematical constant for natural logarithms. The explicit $f(\boldsymbol{x})$ formulation can be found in equation 3.4.5.

This problem's strong and weak forms are equations 1.2.1 and 1.2.2 with $C = 1$ respectively.

4.5.2 Convection diffusion problem

The second problem was originally proposed at [159]. It includes a reactive term and a rotational field that turns the problem into a non-symmetric problem. This term must be added to the strong form of the equation defined at 1.2.1 leading to the expansion of the weak form 1.2.3 into

$$a^C(u(\boldsymbol{x}), v(\boldsymbol{x})) := \int_\Omega (\nabla v(\boldsymbol{x}) \cdot (C \nabla u(\boldsymbol{x})) + v(\boldsymbol{x}) \cdot (\alpha(\boldsymbol{x}) \cdot \nabla u(\boldsymbol{x})) + v(\boldsymbol{x}) \cdot b \cdot u(\boldsymbol{x}))\, d\Omega, \tag{4.5.3}$$

being $\alpha(\Omega)$ the convective velocity and b a constant parameter for the reaction term.

The proposed problem is restricted to a unit square domain $\Omega = [0,1] \times [0,1]$ with homogeneous Dirichlet conditions in the whole boundary $\partial\Omega$. Parameters are $C = 1$, $\alpha(x,y) = 250(y - \frac{1}{2}, \frac{1}{2} - x)$, $b = 10$, a forced input of $f(x,y) = 1000$ in the square region $\Omega_{f=1000} = [0.7, 0.8] \times [0.7, 0.8]$, and $f = 0$ on the rest of the domain $\Omega_{f0} = \Omega \setminus \Omega_{f1000}$.

Figure 4.2 depicts a solution for the problem posed for a 80x80 elements direct computation. The peak in concentration corresponds to the forced input and the rotational field distributes it clockwise.

Note that the convective term makes the stiffness matrix non-symmetric. [103] defines a weighted energy norm that takes this into account in order to define a better suited norm to estimate the error for convective problems. Its expression for a solution in the space $H_0^1(\Omega)$ is

$$| \, ||e(\boldsymbol{x})|| \, |^2_{\Lambda,\mu,\Omega} := \Lambda \int_\Omega |\nabla e(\boldsymbol{x})|^2 dx + \mu \int_\Omega \tilde{b}(\boldsymbol{x}) \cdot e(\boldsymbol{x})^2 dx, \tag{4.5.4}$$

being $\tilde{b}(\boldsymbol{x}) := b(\boldsymbol{x}) - \frac{1}{2}\nabla \cdot \alpha(\boldsymbol{x}) \geq 0$ the condition for a well suited problem, and Λ, μ weights defined in the aforementioned paper to tune the estimation norm. However, the problem posed is a particular case where $\nabla \cdot \alpha(\boldsymbol{x}) = 0$. Consequently, the energy norm based on the bilinear form can be used, which is the standard for symmetric problems. Note that this norm is a particular case of the weighted norm satisfying $||e(\boldsymbol{x})||^2_E = | \, ||e(\boldsymbol{x})|| \, |^2_{C,1,\Omega} = a^C(e(\boldsymbol{x}), e(\boldsymbol{x}))$.

4.5.3 Assessment criteria

A verification and quality indicator is needed in order to assess and compare the different methods tested. Since the solutions are approximated in a Sobolev space $\mathcal{V}$ and the bilinear form is bounded and coercive, the energy norm (equation 1.2.4) holds. Henceforth, this chapter assesses the accuracy of any estimated solution through the quotient between its energy norm and a pseudo-analytical or a reference energy norm both a richer space. Using the notation introduced in section 4.2, the different spaces used in the assessment are $\mathcal{V}^{\mathrm{h}} \subset \widehat{\mathcal{V}} \subset \widetilde{\mathcal{V}} \subset \mathcal{V}$, denoting the coarse, reference, pseudo-analytical and analytical spaces of error solutions.

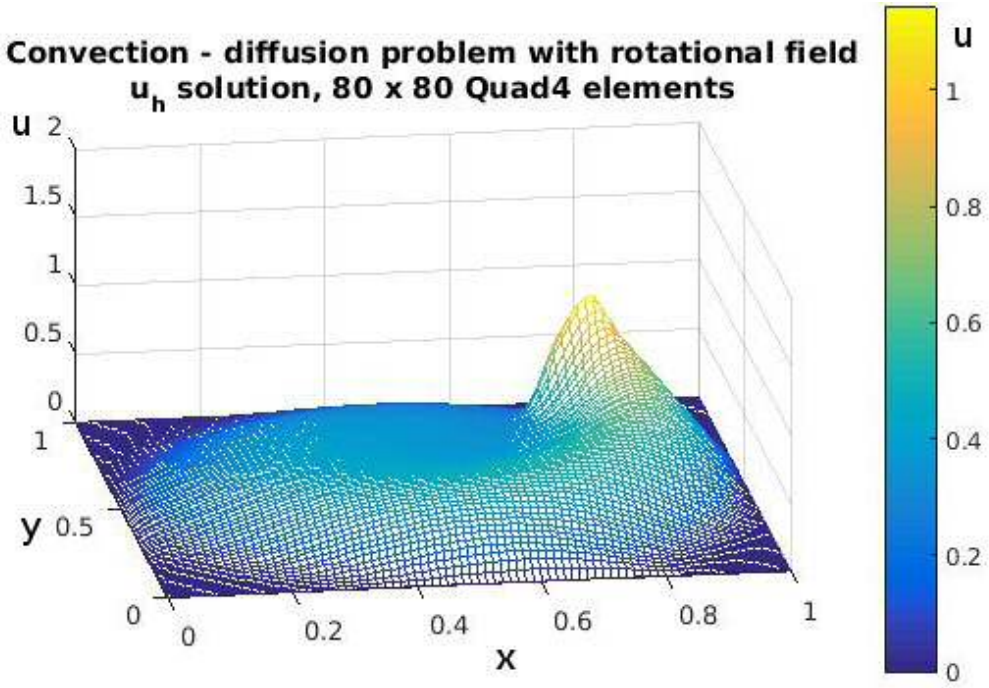

Figure 4.2: Solution to the Convection-Diffusion problem: rotational field

The effectivity index is then introduced as the ratio between the energy norm of the estimated solution and the pseudo-analytical one. Namely

$$\varpi = ||\widehat{\varepsilon}(\boldsymbol{x})||_E / ||\widetilde{e}(\boldsymbol{x})||_E. \tag{4.5.5}$$

This magnitude is a normalised indicator that tends to 1 as the computed solution gets closer to the pseudo-analytical one. It is greater than 1 if there is overestimation and lower than 1 if there is underestimation.

In order to assess the estimation of the computable part of the discretisation error, the *relative effectivity index* is introduced as

$$\varpi_R = ||\widehat{\varepsilon}(\boldsymbol{x})||_E / ||\widehat{e}(\boldsymbol{x})||_E. \tag{4.5.6}$$

In this case, both solutions belong to the same space, so it is assumed and never checked that the reference solution is close enough to the analytical one. In common FEM practise a convergence analysis between different stages of mesh refinement refinement is conducted to avoid the computation of $\widetilde{e}$, and if there is enough confidence in the estimator or it provides guaranteed bounds even the computation of $\widehat{e}$ can be skipped.

In the case of the index ϖ_R, both energy norms involved in its computation depend on the parameters defining the coarse and reference solution spaces. As mentioned in section 4.2, $\mathbb{h}$ defines the coarse space, and $\mathbb{h}$ and R the reference space. Error estimation is employed to guide the mesh refinement of any finite element analysis towards a good enough discrete solution. As a consequence, the estimation is used in a multiple step process where the coarse and reference solution spaces vary with each refinement.

The estimators must become at least independent of $\mathbb{h}$, so that they do not loose effectivity with the refinement. Independence of R is also desirable so that any distance between $\widehat{\mathcal{V}}$ and $\mathcal{V}^{\mathbb{h}}$ can be selected. The fact that an estimator tends to effectivity 1 with any of the parameters is not essential, but obviously, the closer it gets the better.

As a general rule, this work includes results of the effectivity's evolution versus R and relative effectivity compared to $\mathbb{h}$. The reason is that non-relative effectivity in comparison with $\mathbb{h}$ is assured due to the convergence of the FEM. For each method tested it is verified that the effectivity is asymptotic with respect to R and that the relative effectivity does not grow without control. Then, the final effectivity index is chosen as indicator of the method's performance. Plots also include guaranteed lower bound effectivities for the estimated solution defined in the following subsection.

4.5.4 Guaranteed Lower Bounds

In any engineering computation, guaranteeing bounds for the problems to be solved is even more important than improving the accuracy of the computations. These bounds ensure the reliability of any approximated solution in the worst case scenario, while an improved accuracy does not.

As advanced in chapter 1, only the equilibrated residual method first mentioned by Kelly [98] and Ladevèze [106] guarantees that the computed solution is an upper bound. On the other hand, it is possible to define a lower bound for any finite element solution making use of Cauchy-Schwarz inequality.

Since all possible solutions are vectors of an inner product space, it is true that

$$|a^{\odot}(e(\boldsymbol{x}),\widehat{\varepsilon}(\boldsymbol{x}))|^2 \leq a^{\odot}(e(\boldsymbol{x}),e(\boldsymbol{x}))\cdot a^{\odot}(\widehat{\varepsilon}(\boldsymbol{x}),\widehat{\varepsilon}(\boldsymbol{x})). \tag{4.5.7}$$

Rearranging and using the definition of energy norm we obtain

$$||e(\boldsymbol{x})||_E \geq \frac{|a^{\odot}(e(\boldsymbol{x}),\widehat{\varepsilon}(\boldsymbol{x}))|}{||\widehat{\varepsilon}||_E}, \tag{4.5.8}$$

being the second term the lower bound of the first one.

Despite $e(\boldsymbol{x})$ can not be computed in a general case, using the residual definition with $\widehat{\varepsilon}(\boldsymbol{x})$ as test function leads to the rewriting of the now computable expression from the discrete space as

$$||e(\boldsymbol{x})||_E \geq \frac{|\mathcal{R}^{\odot}(\widehat{\varepsilon}(\boldsymbol{x}))|}{||\widehat{\varepsilon}(\boldsymbol{x})||_E}. \tag{4.5.9}$$

It is known that some error estimation methods are also a lower bound for the error. In order to find the needed relation between $e(\boldsymbol{x})$ and $\widehat{\varepsilon}(\boldsymbol{x})$ so that they produce a guaranteed lower bound, the bilinear form can be transformed into $a^{\odot}(e(\boldsymbol{x}),\widehat{\varepsilon}(\boldsymbol{x})) = a^{\odot}(e(\boldsymbol{x})-\widehat{\varepsilon}(\boldsymbol{x}),\widehat{\varepsilon}(\boldsymbol{x})) + a^{\odot}(\widehat{\varepsilon}(\boldsymbol{x}),\widehat{\varepsilon}(\boldsymbol{x}))$. Then, the lower bound expression 4.5.8 becomes

$$||e(\boldsymbol{x})||_E \geq \frac{|a^{\odot}(e(\boldsymbol{x})-\widehat{\varepsilon}(\boldsymbol{x}),\widehat{\varepsilon}(\boldsymbol{x})) + a^{\odot}(\widehat{\varepsilon}(\boldsymbol{x}),\widehat{\varepsilon}(\boldsymbol{x}))|}{||\widehat{\varepsilon}(\boldsymbol{x})||_E} = \frac{|\,a^{\odot}(e(\boldsymbol{x})-\widehat{\varepsilon}(\boldsymbol{x}),\widehat{\varepsilon}(\boldsymbol{x})) + ||\widehat{\varepsilon}(\boldsymbol{x})||_E^2\,|}{||\widehat{\varepsilon}(\boldsymbol{x})||_E}. \tag{4.5.10}$$

Consequently, if the computed error field $\widehat{\varepsilon}(\boldsymbol{x})$ and the error in its approximation $e-\widehat{\varepsilon}(\boldsymbol{x})$ are orthogonal i.e. $a^{\odot}(e(\boldsymbol{x})-\widehat{\varepsilon}(\boldsymbol{x}),\widehat{\varepsilon}(\boldsymbol{x})) = 0$, then 4.5.8 becomes :

$$||e||_E \geq \frac{|\,0+||\widehat{\varepsilon}||_E^2\,|}{||\widehat{\varepsilon}||_E} = ||\widehat{\varepsilon}||_E. \tag{4.5.11}$$

Therefore, this orthogonality is the condition for an error estimator to directly produce a lower bound.

4.6 Verification of the Saint-Venant assumption

Once a problem has been defined, the main assumption made for the new additive approach must be verified. In order to do so, the first diffusion problem is used.

Elemental local residuals are defined as $\mathcal{R}^D_{\mathbb{p}=\mathbb{i}} := \mathcal{R}^D_{\mathbb{k}}$ where $\mathbb{k}$ is the central element of each patch. Then, equation 4.4.3 becomes

$$a^D(\varepsilon_{\mathbb{i}}(\boldsymbol{x}), v(\boldsymbol{x})) = \mathcal{R}^D_{\mathbb{i}}(v(\boldsymbol{x})) \approx a^D_{\mathbb{p}=\mathbb{i}}(\varepsilon_{\mathbb{p}=\mathbb{i}}(\boldsymbol{x}), v(\boldsymbol{x})) = \mathcal{R}^D_{\mathbb{k}}(v), \qquad \forall\, v(\boldsymbol{x}) \in \mathcal{V}. \tag{4.6.1}$$

Defining the whole domain as patch for each local residual along with the initial BC leads to an exact solution. Taking this into account, it is possible to define the elemental contribution $\varepsilon_{\mathbb{p}=\mathbb{i}}(\boldsymbol{x})$ to the error for any element. This definition is achieved by reducing the right hand side of the global problem to $\mathcal{R}^D_{\mathbb{k}}(v(\boldsymbol{x}))$. The gradient of $\varepsilon_{\mathbb{p}=\mathbb{i}}(\boldsymbol{x})$ is more interesting though, since it is what influences the initial equation 4.5.1.

Nevertheless, discretisation is needed to compute any result with FEM and error estimation. Subsequently, $\widehat{\varepsilon}_{\mathbb{p}=\mathbb{i}}(\boldsymbol{x})$ and $\widehat{v}(\boldsymbol{x})$ are employed to check the actual discrete distribution of the elemental error. Figure 4.3 displays these two fields solved exactly throughout the whole domain, but colouring differently the elements that would be part of a `EC_AN` patch definition (see figure 4.1.c). The element selected for these plots has both analytical and reference values close to the maximum for the error field $e(\boldsymbol{x})$ and its gradients. All other patches show similar response, with smaller values.

Even though the computed elemental contribution to the error is larger at the defining element where the partial residual is applied, as expected, its order of magnitude is similar to other parts of the domain. On the other hand, the computed gradient shows that after a transitional element, the order of magnitude has descended significantly. This transition happens in all directions, so including only adjacent neighbours (sharing an edge) to the patch does not account for diagonal transition. Figure 4.3.b shows that in this diagonal neighbour elements the gradient is also relevant (green peaks). The larger the patch definition, the better its local approximation. However, increasing the patch size increases the computational cost exponentially.

The numerical part of the verification is included in section 4.7.1, since element

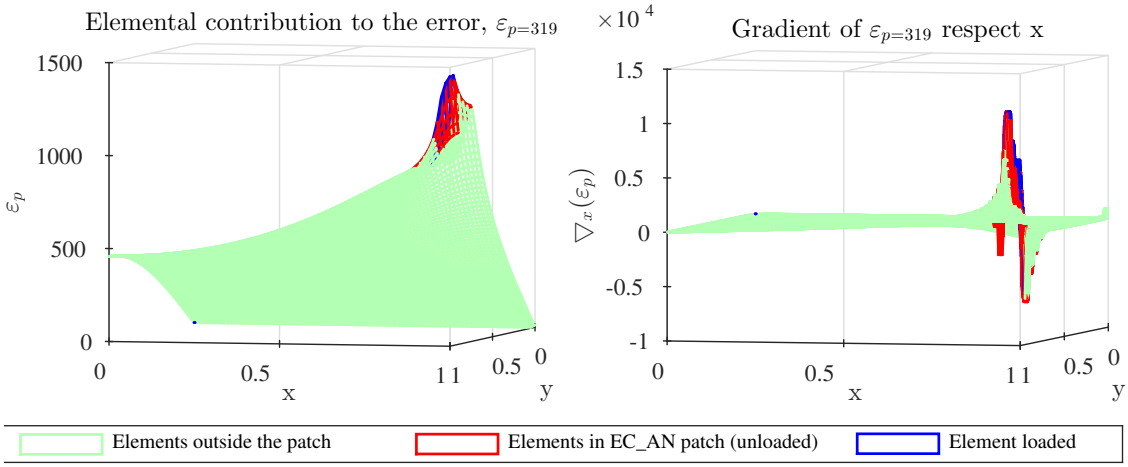

Initial mesh: structured quad4 20×20 elements, R=4×4. Element $\mathbb{e}^{\mathbb{k}}$ *loaded* $\mathbb{k}$*=319 => row 15, column 19. Full domain as patch. What would be approximated in an element centred patch including only adjacent elements is coloured in red and blue (fig. 4.1.c)*

Figure 4.3: Elemental Contribution to the error and its gradient

centred approach is adopted in figure 4.3 to plot the contribution of local residuals to the global patch.

4.7 Results for the diffusion problem

All methods for error estimation formulated in the previous sections belong to the residual family. In particular, to the subfamily where Dirichlet BC are applied to the patches. They differ in how the reduction to local sub-domains is done. Furthermore, some of the patch types have more than one method (standard bubble sub-domains and the novel additive approach). In order to perform the comparison between methods, a two step analysis is performed.

As a first step, effectivity results are presented together for each method, grouping all the methods that share the same sort of patches. They are grouped by patch type because the computational time of the classical bubble or average sub-domains and the new additive sub-domain approaches are of the same order.

Combinations of $1/\mathbb{h}$ from 5 to 160 elements and R from 2 to 8 refinements are computed for all the methods. Only the most relevant of these results are included

for the sake of clarity.

Once the representative version of each sort of patch is selected, the second step consists on evaluating the efficiency rather than the effectivity. This efficiency accounts for the computational cost, which greatly differs for each patch category.

4.7.1 Effectivity of the methods

Elemental bubbles and subspace projection

As seen in sections 4.3.1 (OE patches) and 4.3.2 (OE+OA patches), the results for this methods are guaranteed lower bounds.

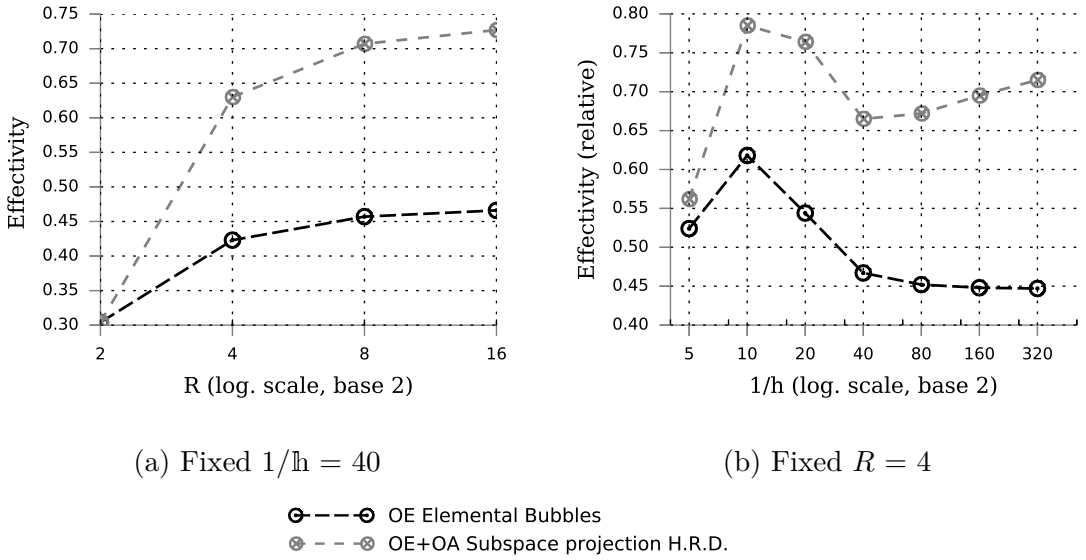

(a) Fixed $1/\mathbb{h} = 40$ (b) Fixed $R = 4$

Figure 4.4: Effectivity for bubble methods

Figure 4.4.a includes results for effectivity index ϖ and an initial mesh of $1/\mathbb{h} \times 1 \times \mathbb{h} = 40 \times 40$ elements, with a fixed semi-analytical solution of 1280×1280 elements and different R refinements (see equation 4.5.5). On the other hand, figure 4.4.b includes results for a relative effectivity index ϖ_R (equation 4.5.6) fixing R to 8 refinements for each direction, where the reference solution varies R respect to the number of elements in the initial coarse mesh.

These methods are really cheap, but their performance is worse than that of the other methods presented, not reaching 0.8 effectivity. It is interesting to see that even in this method, where a lower bound is guaranteed mathematically, the relative effectivity respect $\mathbb{h}$ is not asymptotic. The reason is that both the estimation method and the reference solution depend on $\mathbb{h}$, so the accuracies of the estimated and reference energy norms race one against the other.

Node centred patches

Since the $\lambda_{\mathbb{p}}$ function already concentrates the local residual around the central node of the NC patches, extra elements are not needed to fulfil Saint-Venant assumption. As a result, the same number of elements are employed in the classical average and additive approaches. Furthermore, since the computational cost of the lower bound process is negligible compared to the error estimator, all the versions have a roughly equivalent computational cost.

With regard to the direct effectivity versus R refinement, using the same $\lambda_{\mathbb{p}}$ function to average the local fields produces better approximations than defining a local density of energy norm and integrating it. However, the additive method outperforms both averaging variants. Figure 4.5 is an example of this. As advanced in section 4.3.3, the original estimator adds repeated whole estimations on the nodes belonging to more than one patch, leading to overestimation unless an average rule is defined (there are 4 elements in each patch if a quadrilateral structured mesh is used).

On the contrary, figure 4.6.a shows again that fixing R and allowing the reference solution to move with initial $1/\mathbb{h}$ generates more uncertainty. Despite the lack of clear asymptotic behaviour, the effectivity fluctuates but does not grow without control. Applying the lower bound process mitigates the fluctuation, as can be seen in figure 4.6.b. Regarding the patch central node's fixation, all cases show worse effectivity index so it is not advantageous in the node centred patches methods.

From the former comparison, the bubble sub-domain method averaged through the $\lambda_{\mathbb{p}}$ function with the lower bound process is selected as representative for the

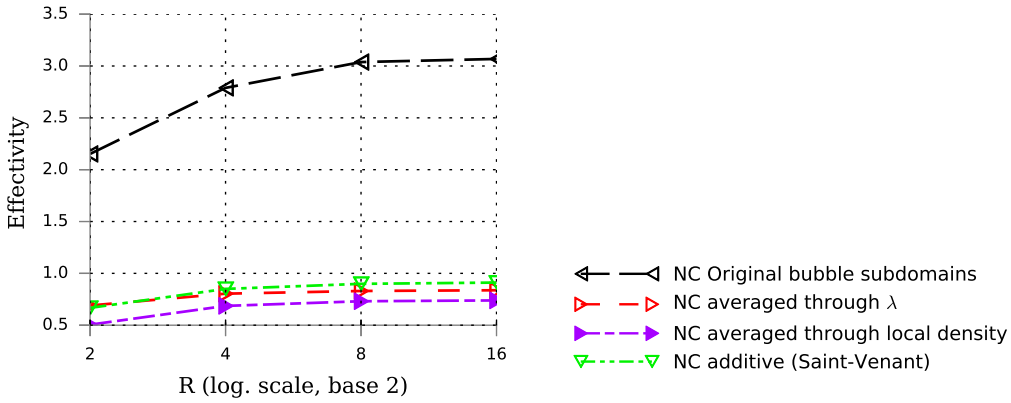

Figure 4.5: Effectivity for node centred methods. Fixed $1/\mathbb{h} = 40$

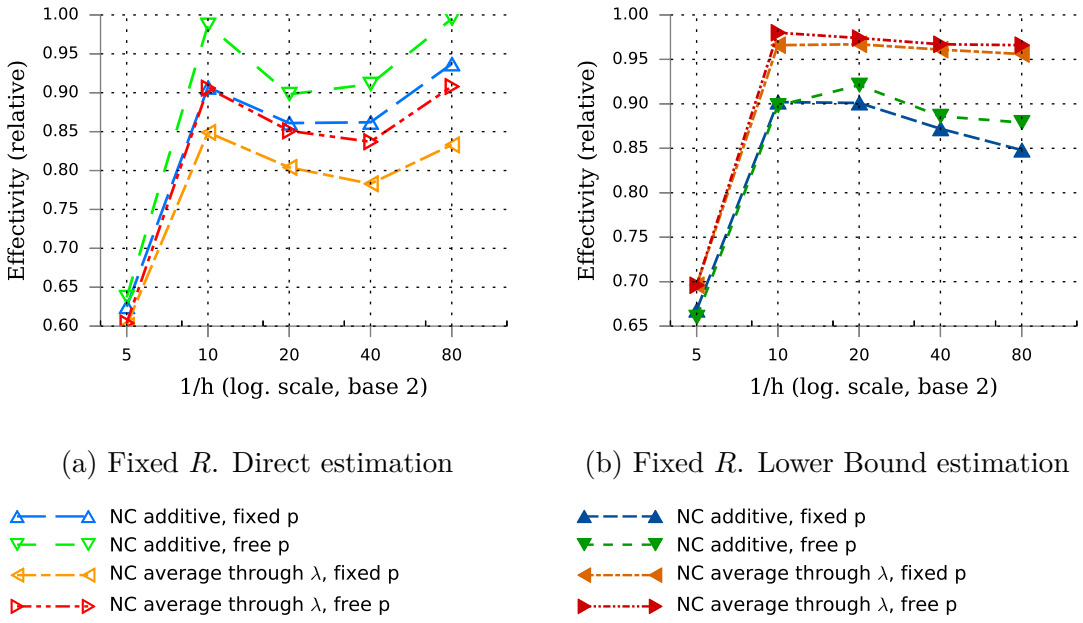

(a) Fixed R. Direct estimation

(b) Fixed R. Lower Bound estimation

Figure 4.6: Effectivity for node centred methods. Fixed R

node centred patches in the efficiency comparison between different type of patches.

Element centred patches

Since elemental contributions to the global domain are used in section 4.6 to verify the Saint-Venant assumption, this subsection includes also numerical results of the soundness of this assumption for different sizes of element centred patches (figures 4.1.b,c,d).

Comparison between the classical bubble and new additive sub-domains is only performed for p-refinement, since apart from the Quad4 to Quad8 refinement presented in [109] there is no easy average rule available. Besides, finer p-refinement proves the point made in section 4.3.4 that the longer the distance between the coarse and fine spaces, the worse the hypothesis performs in the bubble sub-domain. How the additive sub-domains overcome this issue is also shown.

h-refinement additive estimation

Figure 4.7 shows effectivity's evolution for different patch definitions. It can be seen that all methods show an asymptotic behaviour when fixing $\mathbb{h}$ and refining R (figure 4.7.a). This behaviour is constant for all estimators tested, even though results for only for this case are included. Conversely, fixing R shows that the element centred patch with adjacent elements only does not work. The finer $\mathbb{h}$ initial mesh is used, the worse relative effectivity index is obtained, both for direct estimation (figure 4.7.b) and the Lower Bound counterpart (figure 4.7.c)

These results confirm that, as a general rule, an element in every direction is needed to consider that Saint-Venant assumption holds (including the elements that only share a corner, *i.e.* EC_FN patches). Otherwise, the gradient transition is not high enough and the quality of the approximation is not guaranteed. Nonetheless, it is interesting to see that the elemental bubble OE patches work better than EC_AN patches (which include just adjacent neighbours). Furthermore, OE patches show the desired asymptote as $\mathbb{h}$ decreases for a fixed R. This comes from the fact that solutions from OE patches are the only ones fulfilling the orthogonality condition seen in section 4.5.4.

Fixing the coarse solution as suggested in [109] improves the performance for full neighbourhood patches (EC_FN).

These results suggest that the assumption of considering local residuals as self equilibrated loads, whose contribution to the error vanish as the distance from its application point increases, is reasonable. However, the patch definition needs to include at least all the neighbour elements sharing a node with the loaded element

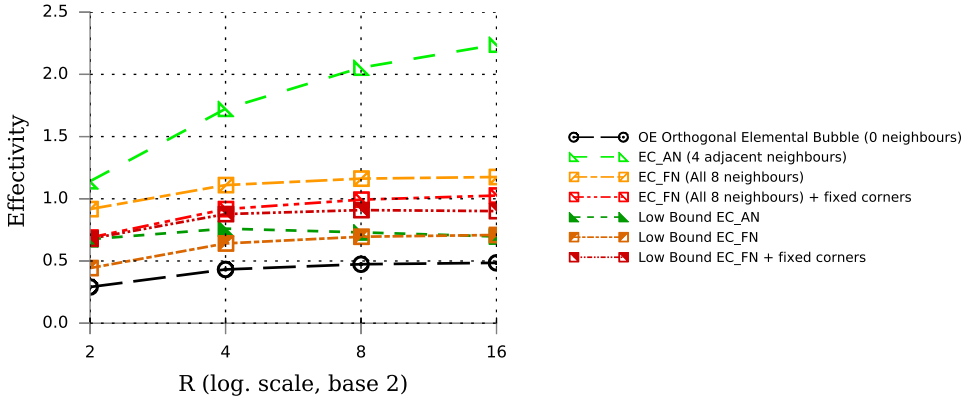

(a) Effectivity, fixed $1/\mathbb{h}$=40x40 vs R

(ref. solution 640x640)

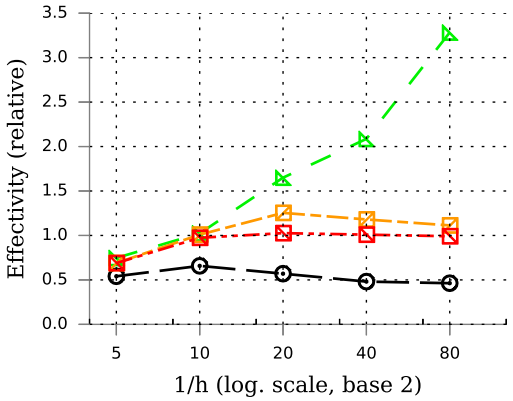

(b) Effectivity Direct, fixed R=8x8 vs $\mathbb{h}$

(ref. solution varies with $\mathbb{h}$)

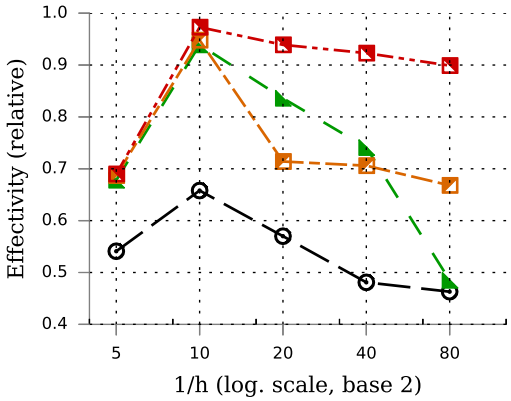

(c) Effect. LowBound, fixed R=8x8 vs $\mathbb{h}$

(ref. solution varies with $\mathbb{h}$)

Inital mesh: structured quad4 $1/\mathbb{h} \times 1/\mathbb{h}$ elements

Finer space: elemental $\mathbb{h}$ refinement $R \times R$

Figure 4.7: Effectivity evolution considering different element centred patches

defining the patch. Otherwise, the distance is not enough to consider Saint-Venant principle and thus, the effectivity worsens as refinements $\mathbb{h}$ are applied.

p-refinement additive estimation

Only EC_AN patches with serendipity refinement are tested for classical bubble sub-domains, since they are the only ones with a clear average rule. The serendipity Quad8 element is also the particular case presented in [109]. Quad9 and Quad16 elements p-refinement are also tested for additive patches since no average rule is needed.

The new DOF are significantly reduced if a polynomial order increase is exploited as enrichment instead of h-refinement. Therefore, the computational cost (algorithm number 6) is also reduced. Since the number of elements does not vary with p-refinement, the initial $1/\mathbb{h}$ number of elements and the distance from p to h are the only parameters that can influence the effectivity.

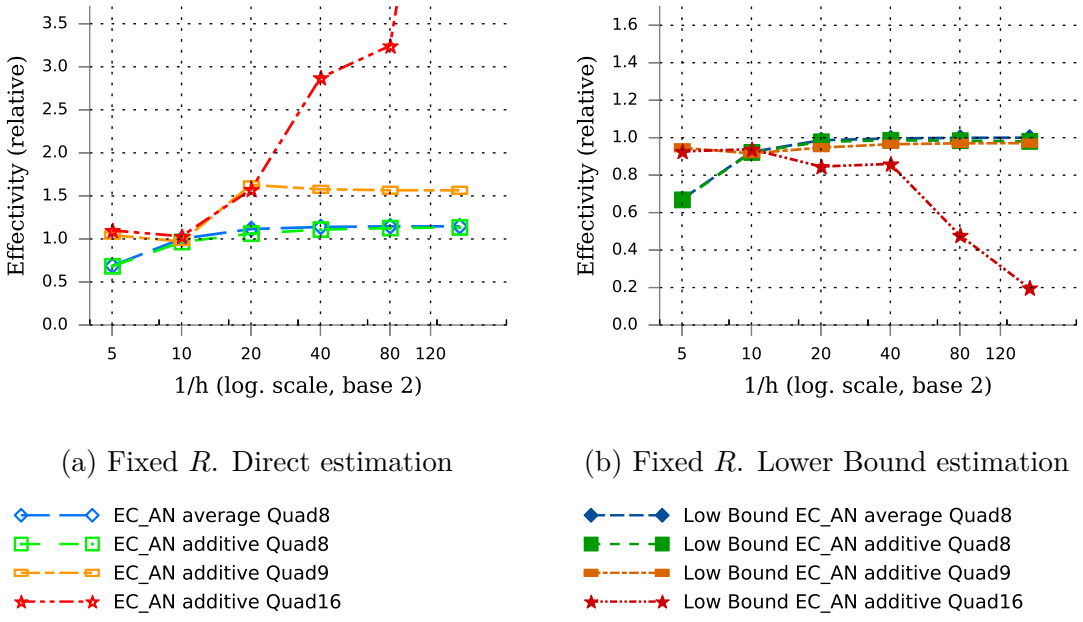

(a) Fixed R. Direct estimation

(b) Fixed R. Lower Bound estimation

X axis corresponds to the initial mesh with structured quad4 $1/\mathbb{h} \times 1/\mathbb{h}$ elements

Figure 4.8: Effectivity for Space enhancement and p-refinement

Figure 4.8 reveals that for EC_AN patches, the farther the shape function of the original and enhanced elements, the worse performance. Both Quad8 versions of p-refinement show good results, Quad9 elements reveal worse performance but still stable, and Quad16 turns the method to unstable. For the sake of clarity, the figure

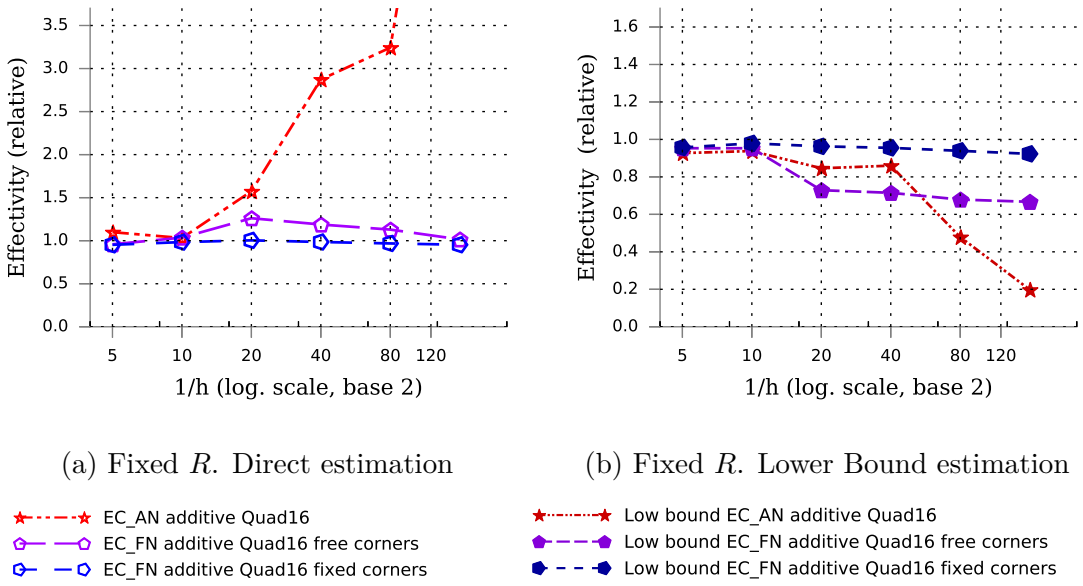

(a) Fixed R. Direct estimation

(b) Fixed R. Lower Bound estimation

Figure 4.9: Influence of patch selection for space enhancement estimator

is cut excluding the last value for Quad16 refinement and initial 160x160 elements which is effectivity 7.976.

These results are consistent with the ones obtained for h-refinement, evidencing that the adjacent elements alone are not enough to guarantee that Saint-Venant principle holds in element centred patches.

The application of this kind of EC_AN or EC_FN local patches, in addition to any of the assumptions that lead to homogeneous Dirichlet BC, is equivalent to enforce that the solution at the shared boundary nodes does not vary from the coarse to the fine spaces. Thus, in the refined problem, the shape function of higher order in $\widehat{\mathcal{V}}$ is effectively approximated as the one of lower order in $\mathcal{V}^{\mathbb{h}}$. So it seems reasonable that as the spaces and associated shape functions differ, this approximation becomes cruder making the method fail eventually.

Despite the drawbacks, EC_AN patches are still stable and useful for one level of p serendipity refinement in either average or additive variants. For other refinements, at least EC_FN and additive sub-domains must be used. Hence, the latter are selected as representative of the element centred patches method.

Hybrid estimators

Figure 4.10 shows that computing the additional bubble problem always results in a higher energy norm. This is only useful if paired with the lower bound process, since it assures that the estimated solution is closer to the reference solution. However, this is not necessarily an improvement for the direct estimation.

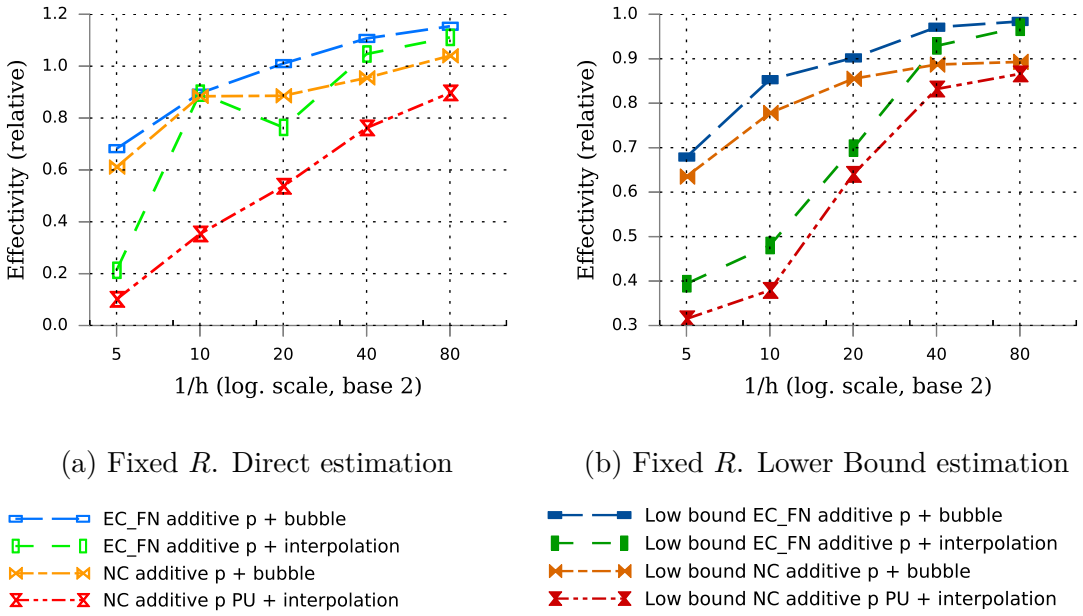

(a) Fixed R. Direct estimation

(b) Fixed R. Lower Bound estimation

Figure 4.10: Effectivity for hybrid methods

The plot on the right of figure 4.10 shows that when $\mathbb{h}$ is refined, the interpolated and the projected solutions get closer to each other. Since the computational cost of the additional problem escalates with h-refinement, the benefits of the hybridisation might be worth only for a few $\mathbb{h}$ refinements.

4.7.2 Efficiency of the methods

Up to this point, only the effectivity has been considered to evaluate the methods. Nevertheless, efficiency is as important as accuracy for the comparison.

The Poisson problem 4.5.1 is solved with a common reference space of $1/(\mathbb{h} \cdot R)$ $\times$ $1/(\mathbb{h} \cdot R)$ linear elements. The computational time expended in each case is normalised by taking the direct computation of the problem as measure of scale.

Against this normalised time in the abscissae, the corresponding corrected effectivity $|\nu - 1|$ is plotted in the ordinate of figure 4.11 to have a map of the methods where the origin would be the ideal estimator.

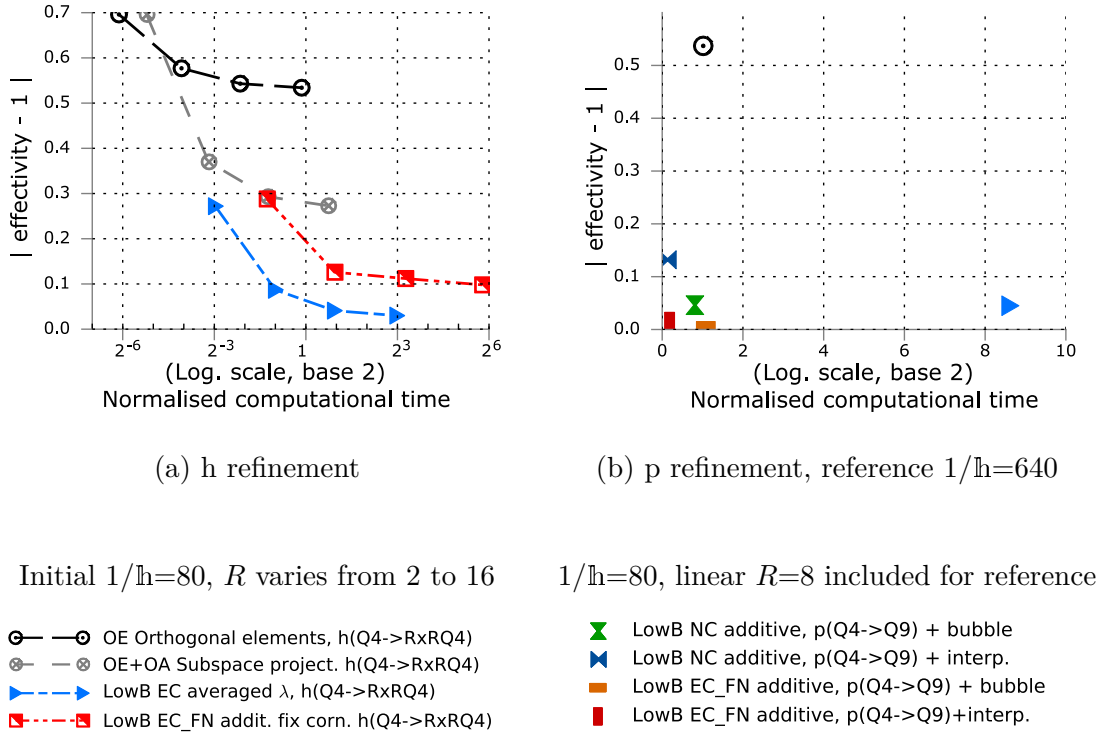

(a) h refinement

(b) p refinement, reference 1/h=640

Figure 4.11: Efficiency of the methods compared

The results in figure 4.11.a reflect that for all methods using only h-refinement and extended patches, the computational cost of refining the initial coarse problem is exponential, and it is not worthy for R>8. Cost growth in 3D would be magnified because local problems have more elements as neighbours and more nodes per element scaling at power 3 instead of 2.

Node centred sub-domains show the best efficiency for h-refinement. Element centred sub-domains achieve a similar accuracy but at a bigger cost. Subspace projection (OE+OA patches) is on a lower accuracy level.

On the contrary, for p-refinement, element centred sub-domains show better accuracy for a cost in the same order of magnitude than node centred patches.

The use of element centred patches with p-refinement boosts effectivity avoiding

the additional cost of multiple nodes in neighbour elements. Extended patch problem's cost with p-refinement is significantly inferior than the bubble problem with R=8 and achieves better effectivity than the node centred patches (see figure 4.11.b). Since only low order polynomials are considered, there is no risk of ill-conditioning the problem as documented by Babuška et al. at [13].

Regarding hybrid methodology, it improves both node and element centred estimator's accuracy. However, the increase of computational cost exceeds the benefits of the improved accuracy.

4.8 Results for a convection diffusion problem

The aim of this section is to verify that additive methods with p-refinement also work for non-symmetric problems, and that by using p-refinement they are more efficient than classical averaged methods. Consequently, only the best choice is adopted for p and h-refinement respectively. Effectivity results included in figure 4.12.a show that

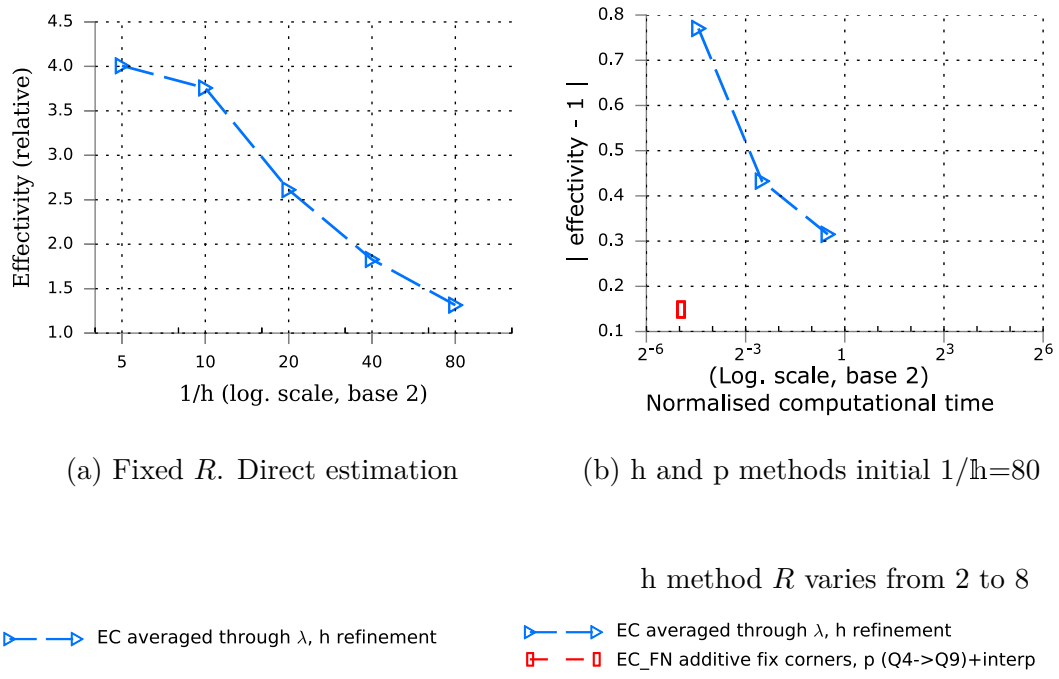

(a) Fixed R. Direct estimation

(b) h and p methods initial $1/\mathbb{h}$=80

Figure 4.12: Effectivity and efficiency for a convection diffusion problem

the asymptotic behaviour for a fixed R is not as clear for the convection diffusion

problem as it is for the diffusion problem. Nevertheless, the efficiency approaches 1 as the initial coarse mesh is refined. As for efficiency results, figure 4.12.b reproduces the pattern seen for symmetric problems.

In the convective problem, coarser meshes overestimate the error in opposition to the only diffusive problem. It is known that for linear parabolic problems the FEM adds stiffness when reducing the DOFs. Therefore, overestimation appears only due to singularities. There is not a known direction of the error for the convective contribution. Furthermore, if convection strongly dominates (Péclet number is sufficiently small) the used Galerkin method turns unstable and the upwind approach is needed to compute reliable solutions.

4.9 Conclusion

The reformulation of the different a-posteriori error estimators based on the residual with Dirichlet BC under a common framework allows not only their assessment, but also their hybridisation.

Subsequently, a novel approach to the definition of these patches based on the Saint-Venant principle allows total freedom in the definition of the patches. The principle holds directly for node centered patches, but needs all adjacent elements for element centered ones. This novel additive patches technique improves the element centred patches present in literature.

Results show that the computational cost of the methods depends mainly on the DOF of the local patch in the rich space, while their accuracy depends on the shape of this patch in relation to the residual considered. Efficiency is achieved by using p-refinements, which reduce the DOF of the local enriched system of equations and allows a cheap computation of patches including the full neighbourhood of a coarse element.

Finally, there is evidence that the new proposed additive estimators work for non-symmetric problems as well, and that by using p-refinement they are not only more effective, but also more efficient.

Chapter 5

Goal-oriented finite element adaptivity in a stochastic model for vibrating structures

5.1 Introduction

Adaptivity algorithms allow to optimise computational resources by constructing a mesh where all local contributions to the discretisation error are of the same order. They are driven by error estimation which is discussed in chapters 1 and 4. However, a stochastic process introduces new sources of error that have nothing to do with discretisation. This errors are due to finite sampling of the parameter space and optionally to the construction of a surrogate model that reduces the computational cost of evaluating multiple times the full numerical model.

In order to optimise the solution of problems with parametric uncertainty, the same principle of making all errors of the same order holds. Nevertheless, errors introduced by parametric uncertainty cannot be measured in the same way as the errors coming from discretisation. Because of that, research about how to design combined adaptive processes is scarce.

This chapter is devoted to link all the different errors and control the level of refinement for the FE approximation of the spatial fields and Monte-Carlo sampling

of the probability distribution of the quantity of interest (QoI). The control strategy will be driven by the will to calculate statistics of the QoI at minimum cost, given the margin of error that the user is willing to accept. The approach to this complex minimisation problem is greedy-based in space and strictly incremental in the global complexity of the surrogate model that is only employed to reduce the computational cost of producing outcomes.

At each stage of the greedy algorithm, the FE mesh is refined in the regions of space that contribute most to the error in the expectation of the quantity of interest. The meta-modelling error (due to a standard polynomial chaos expansion in this dissertation) is automatically controlled by enforcing that its order of magnitude is smaller than the finite element error at each refinement stage, the exact balance between the two sources of error being a parameter of the algorithm.

Finally, the number of Monte-Carlo samples is chosen such that either (a) the overall precision of the chain of approximations can be ascertained with sufficient confidence, or (b) the fact that the computational model requires further refinement is statistically established.

The efficiency of the approach is discussed for frequency-domain vibration problems that are relevant to the field of structural reliability assessment, and show difficulties in determining beforehand the areas of the mesh that need refinement. Uniformly refined spatial grids are used as benchmarks of the locally adapted FE solutions.

The chapter is organized as follows. Section 5.2 introduces all the formulation and notation for both spatial and stochastic frameworks, ending with an explicit definition of all the errors involved in the problem posed. In section 5.3 the interaction between the errors is explored, as well as the algorithm that decides which error is larger and how to reduce it. Section 5.4 is an extension of the algorithm to a general case were the variation of the response PDF is taken into account for the stopping criterion. Finally, section 5.5 displays and discusses the results for the problem posed, with the aim to verify that the algorithm controls all different sources of error.

5.2 Reference parametrised vibration problem and notation

This section introduces the model problem to be parametrised in the stochastic framework. The stochastic process is introduced through the Young's modulus, which is a function of space and is parametrised as a finite set of real-valued variables, but could be introduced through parametrised boundary data (*e.g.* to model aleatoric earthquake imposed displacements), geometry or mass densities (*e.g.* to model manufacturing defects), or excitation frequency ω (*e.g.* to model periodic loads imposed by wind of ocean waves).

The present work focuses on the interaction of model errors and therefore assumes simple models and does not study the modelling error with respect the reality. In particular the probabilistic characterisation of the Young's modulus of the structure is considered perfectly modelled by means of a normal distribution. In reality, the primary probabilistic characterisation is a field of research on his own where several complex models to capture the global and local variation of material properties have been proposed. These models are usually distinct for a vast range of scales and materials considered. A non-exhaustive list of examples include modelling of macro scale global material properties of concrete and steel [122, 128, 128] and aluminium alloys [69, 161], macro-scale masonry brick-mortar distributions [68, 112], multi-scale homogenisation models [1, 130], multi-scale of granular materials [113], multi-scale fibre reinforced concrete [80, 43], meso-scale orientation of timber fibres [173, 124], meso-scale fracture considered in concrete [60], micro-scale graded composites [70] or nano-scale graphene [143].

5.2.1 Parametrised frequency-domain structural vibration problem

The specific model consists in an undamped, steady-state vibration of a structure occupying a bounded domain $\Omega \subset \mathbb{R}^d$, with d spatial dimensions considered. The deformations of the structure are modelled upon the equations of isotropic linear

elasticity, under the classical assumption of small perturbations. As advanced, the parametric variation is ruled by the random variable $\boldsymbol{\mu}(\theta) \in \Theta \subset \mathbb{R}^r$ which is a r-dimensional vector of real parameters that fully characterises the field of Young's modulus $E(\boldsymbol{x}, \boldsymbol{\mu})$.

In this context, the conservation of the linear momentum is the differential equation that reads

$$\begin{aligned} \left(\rho \frac{\partial^2}{\partial t^2} - \nabla_s \cdot (C(\boldsymbol{x}, \boldsymbol{\mu}) \nabla_s)\right) U(\boldsymbol{x}, \boldsymbol{\mu}, t) &= F(\boldsymbol{x}, t) && \text{in } \Omega, \\ U(\boldsymbol{x}, \boldsymbol{\mu}, t) &= U_d(\boldsymbol{x}, t) && \text{on } \Gamma_d, \\ (C(\boldsymbol{x}, \boldsymbol{\mu}) \nabla_s U(\boldsymbol{x}, \boldsymbol{\mu}, t)) \cdot \overrightarrow{n} &= G_n(\boldsymbol{x}, t) && \text{on } \Gamma_n. \end{aligned} \tag{5.2.1}$$

In the previous equations, the boundary $\partial\Omega$ is split into the complementary subsets Γ_n and Γ_d where Neumann and Dirichlet conditions are prescribed respectively. Furthermore, Γ_d is not empty and contains enough points distributed in such a way that the problem is well posed (all zero energy modes are constrained, for instance rotation over a fixed set of points). $F(\boldsymbol{x}, t) : \Omega \times \mathcal{T} \to \mathbb{R}^d$ is a given vector-valued forcing function that depends on space and time. $\mathcal{T}$ denotes a bounded time interval. $U_d(\boldsymbol{x}, t) : \Gamma_d \times \mathcal{T} \to \mathbb{R}^d$ is a prescribed boundary displacement. $G_n(\boldsymbol{x}, t) : \Gamma_n \times \mathcal{T} \to \mathbb{R}^d$ stands for the prescribed traction on the boundary. Symbol ρ denotes the mass density, which is assumed to be constant. $C(\boldsymbol{x}, \boldsymbol{\mu}) \equiv C(E(\boldsymbol{x}, \boldsymbol{\mu}), \nu)$ is the fourth order Hooke tensor classically utilised to describe isotropic linear elasticity, where ν is the parameter-independent Poisson's ratio. Finally, the displacement $U(\boldsymbol{x}, t, \boldsymbol{\mu}) : \Omega \times \Theta \times \mathcal{T} \to \mathbb{R}^d$ is a vector-valued field that is time-dependent and parametrised by $\boldsymbol{\mu}$.

Shifting the interest towards frequency-domain solutions and assuming that the loading functions are time-harmonic allows transforming equation 5.2.1 into a time independent one. Technically speaking, the time-harmonic loading functions read $F(\boldsymbol{x}, t) = f(\boldsymbol{x})\, e^{i\omega t}$, $U_d(\boldsymbol{x}, t) = u_d(\boldsymbol{x})\, e^{i\omega t}$, $G_n(\boldsymbol{x}, t) = g_n(\boldsymbol{x})\, e^{i\omega t}$, and a steady-state wave takes the form $U(\boldsymbol{x}, t, \boldsymbol{\mu}) = u(\boldsymbol{x}, \boldsymbol{\mu})\, e^{i\omega t}$. Here symbol $i = \sqrt{-1}$ is employed, and ω is the circular frequency associated with the harmonic loading function.

The steady harmonic strong form of the wave equation for vibrating structures is obtained from equation 5.2.1 by substituting all time-harmonic expressions, cal-

culating the partial derivative $\frac{\partial^2}{\partial t^2} e^{i\omega t} \cdot u(\boldsymbol{x}, \boldsymbol{\mu}) = -\omega^2 e^{i\omega t} \cdot u(\boldsymbol{x}, \boldsymbol{\mu})$, and dividing all terms by $e^{i\omega t} \cdot u(\boldsymbol{x}, \boldsymbol{\mu})$. This leads to the following problem

$$\begin{aligned} -\left(\rho\omega^2 + \nabla_s \cdot (C(\boldsymbol{x}, \boldsymbol{\mu})\nabla_s)\right) u(\boldsymbol{x}, \boldsymbol{\mu}) &= f(\boldsymbol{x}) && \text{in } \Omega, \\ u(\boldsymbol{x}, \boldsymbol{\mu}) &= u_d(\boldsymbol{x}) && \text{on } \Gamma_d, \\ (C(\boldsymbol{x}, \boldsymbol{\mu})\nabla_s u(\boldsymbol{x}, \boldsymbol{\mu})) \cdot \overrightarrow{n} &= g_n(\boldsymbol{x}) && \text{on } \Gamma_n. \end{aligned} \tag{5.2.2}$$

In an analogous way as the variational form 1.2.2 is obtained from 1.2.1, to formulate the variational form of 5.2.2 the test and trial Sobolev spaces are needed. Recalling, their definitions are $\mathcal{V} = \{v \in \mathcal{H}^1(\Omega) \,|\, v = 0 \; on \; \Gamma_d\}$ and $\mathcal{U} = \{u \in \mathcal{H}^1(\Omega) \,|\, u = u_d \text{ on } \Gamma_d\}$ respectively, where both are spaces of functions with square integrable derivatives. Any test function $v \in \mathcal{V}$ is then multiplied at both sides of equation 5.2.2.a. Lastly, after integration by parts, the weak form of the problem is obtained. It reads: find $u \in \mathcal{U}$ such that

$$\begin{aligned} \int_\Omega \left(\rho\omega^2 v(\boldsymbol{x}) \cdot u(\boldsymbol{x}, \boldsymbol{\mu}) + \nabla v(\boldsymbol{x}) \cdot (C(\boldsymbol{x}, \boldsymbol{\mu})\nabla_s u(\boldsymbol{x}, \boldsymbol{\mu}))\right) d\Omega \\ = \int_\Omega v(\boldsymbol{x}) \cdot f(\boldsymbol{x})\, d\Omega + \int_{\Gamma_n} v(\boldsymbol{x}) \cdot g_n(\boldsymbol{x})\, d\Gamma_n, \qquad \forall\, v(\boldsymbol{x}) \in \mathcal{V}. \end{aligned} \tag{5.2.3}$$

The notation $a^\omega(\cdot, \cdot; .)$ is introduced to match the left side of equation 5.2.3. Using the definition of $l(\cdot)$ (as in equations 1.2.2 and 1.2.3) the variational form simply reads

$$a^\omega(u, v; \boldsymbol{\mu}) = l(v), \qquad \forall\, v \in \mathcal{V}. \tag{5.2.4}$$

The definition of energy norm (equation 1.2.4) uses $a^\omega(\cdot, \cdot)$ instead of $a^\odot(\cdot, \cdot)$ for the problem posed in this chapter.

Vibration problems literature commonly poses the problem in terms of mass and stiffness matrices. Using the definition of shape functions in 1.2.8 and any discrete space $\mathcal{V}^{\mathbb{h}}$, the concepts of mass matrix M and stiffness matrix K are introduced as

$$M := \rho \cdot \omega^2 \int_\Omega \left(\psi \cdot \psi\right) d\Omega \tag{5.2.5}$$

and

$$K := \int_\Omega \left(\nabla\psi \cdot (C\nabla\psi)\right) d\Omega \tag{5.2.6}$$

respectively.

Then, the left hand side of the system of equations derived from discretisation of equation 5.2.3 can be rewritten as

$$a^{\omega}(u^{\mathbb{h}}, v^{\mathbb{h}}) = [v^{\mathbb{h}}]^T K[u^{\mathbb{h}}] + [v^{\mathbb{h}}]^T \rho \cdot \omega^2 M[u^{\mathbb{h}}] = [v^{\mathbb{h}}]^T (K + \rho \cdot \omega^2 M)[u^{\mathbb{h}}] = [v^{\mathbb{h}}]^T A_{\omega}[u^{\mathbb{h}}], \tag{5.2.7}$$

where $[v^{\mathbb{h}}]$ and $[u^{\mathbb{h}}]$ stand for the coefficients multiplying the shape functions of the fields $v^{\mathbb{h}}$ and $u^{\mathbb{h}}$ respectively (c_i in equation 1.2.7).

Remark. In the presented problem, the only parametrised quantity is the field of Young's moduli. However, parametric uncertainty can be considered on any physical quantity modelled upon the mathematical model. Some examples would be parametrised boundary data, mass densities or the excitation frequency ω.

All the discussion and algorithmic propositions presented in this chapter can be applied regardless of the physical quantity where the stochastic process is implemented to consider its parametric uncertainty. Even a combination of stochastic processes can be considered, although in that case correlation may arise and should be taken into account to build the surrogate model.

5.2.2 Parametrised problem of interest

Once defined the general framework, this section introduces the specific structural vibration parametrised problem under consideration. In order to guide the reader a visual generalisation is included in figure 5.1. The figure includes graphical representation of the geometry, load cases and known stochastic parameters.

P1, P2 and P3 are different loading cases, being the load $f(\boldsymbol{x})$ uniformly distributed and of unitary value in the direction of the arrows. Load P1 excites the 1st natural frequency of the structure, load P2 produce horizontal displacement only due to the parametric uncertainty and load P3 is included only to test the indicator of refinement, which should concentrate in the lower half of the structure.

In the proposed examples, the j^{th} component μ^j of parameter vector $\boldsymbol{\mu}$ represents the logarithm of the Young's modulus in domain Ω_j (represented in grey in figure

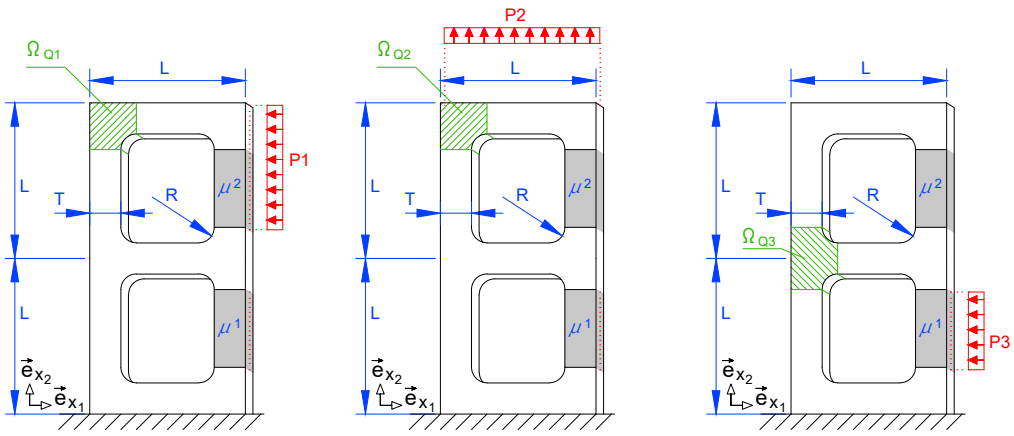

Figure 5.1: Geometry parameters for the numerical examples

5.1). In the rest of the domain $\Omega_0 = \Omega \backslash \bigcup_{i=j}^{r} \Omega_j$, the value of the Young's modulus is set to reference value 1.

The Hooke tensor field $C(\boldsymbol{x}, \boldsymbol{\mu})$ is then a function of the space and the parameters. Its definition reads

$$C(\boldsymbol{x}, \boldsymbol{\mu})\nabla_s(\,.\,) = \frac{e^{\mu^j}\nu}{(1+\nu)(1-2\nu)}\mathrm{Tr}(\nabla_s(\,.\,))\,\mathbb{I} + \frac{e^{\mu^j}}{(1+\nu)}\nabla_s(\,.\,) \qquad \text{if } \boldsymbol{x} \in \Omega_j,\ j \geq 1 \tag{5.2.8}$$

where $\mathbb{I}$ is an identity fourth order tensor of appropriate dimension.

Notice that this framework ensures that the $C(\boldsymbol{x}, \boldsymbol{\mu})$ remains strictly positive, irrespectively of $\boldsymbol{\mu}$.

In this thesis the Quantity of Interest (QoI) is defined as the displacement in horizontal direction $\overrightarrow{e}_{x_1} \in \mathbb{R}^d$, averaged over a subdomain $\Omega_Q \subset \Omega$, as represented in figure 5.1:

$$q(u(\boldsymbol{x}, \boldsymbol{\mu})) := \frac{1}{|\Omega_Q|}\int_{\Omega_Q} \overrightarrow{e}_{x_1} \cdot u(\boldsymbol{x}, \boldsymbol{\mu})\, d\boldsymbol{x}. \tag{5.2.9}$$

5.2.3 Goal-oriented error estimation

Discrete approximations of the parametrised posed problem of interest is computed through the FEM. Section 1.3.4 introduced how error estimators based on the residual assess the discretisation error, which is discussed further in chapter 4. However, the error and residual equations 1.3.12 and 1.3.13 must be formally redefined in view

of the changes in the problem.

The redefined bilinear form of the error equation over $\mathcal{V}$ for the parametrised harmonic vibration problem reads

$$a^{\omega}(e, v; \boldsymbol{\mu}) = l(v) - a^{\omega}(u^{\mathbb{h}}, v; \boldsymbol{\mu}), \qquad \forall\, v \in \mathcal{V}, \tag{5.2.10}$$

which leads to the definition of residual form over $\mathcal{V}$ for the same problem as

$$\mathcal{R}^{\omega}(v; \boldsymbol{\mu}) := l(v) - a^{\omega}(u^{\mathbb{h}}, v; \boldsymbol{\mu}). \tag{5.2.11}$$

For the concern that lack of precision of any a-posteriori error estimator might interfere with the assessment in the relation between the discretisation error and the error coming from the stochastic process, the present work approximates the discretisation error by actually computing the reference solution $\widehat{u} \in \widehat{\mathcal{U}}$. This is still an approximation, since $\widehat{u} \neq u$ even if $\widehat{u}$ is much closer to u than $u^{\mathbb{h}} \in \mathcal{U}^{\mathbb{h}} \subset \widehat{\mathcal{U}} \subset \mathcal{U}$. Usually, error estimation based on the residual approximates the solution in the reference space by means of patches as seen in chapter 4.

The discrete spaces $\mathcal{U}^{\mathbb{h}}, \widehat{\mathcal{U}}, \mathcal{V}^{\mathbb{h}}, \widehat{\mathcal{V}}$ are defined by the coarse and reference mesh as seen in section 1.2.1.

For the present project, all coarse meshes are defined by means of a mesh $\mathcal{M}i$ (where i stands for the sequential number of refinements) of non-overlapping linear (p1) triangular elements that cover all domain Ω except for the curved areas that cannot be captured through linear triangles. The coarse solution and test FE fields are then piecewise linear in a tessellated domain $\Omega_{\mathbb{h}} \approx \Omega$. The influence of the geometrical error is neglected and $\Omega \equiv \Omega_{\mathbb{h}}$ is abusively considered even in the context of non-polygonal domains.

Regarding the reference space, it consists in the same mesh $\mathcal{M}i$ with quadratic (p2) triangles and the edge nodes exactly at the midpoint of the edges. The solution $\widehat{u}$ is computed and considered close enough to u. This leads to the following approximation

$$e(\boldsymbol{x}, \boldsymbol{\mu}) = u(\boldsymbol{x}, \boldsymbol{\mu}) - u^{\mathbb{h}}(\boldsymbol{x}, \boldsymbol{\mu}) \approx \widehat{e}(\boldsymbol{x}, \boldsymbol{\mu}) := \widehat{u}(\boldsymbol{x}, \boldsymbol{\mu}) - u^{\mathbb{h}}(\boldsymbol{x}, \boldsymbol{\mu}), \tag{5.2.12}$$

which is directly computable through the FEM without any other error estimation technique.

The derivation described in section 1.4 leads to the dual-weighted form of the adjoint problem

$$\mathcal{R}^{\omega}(e;\boldsymbol{\mu}) = q(e(\boldsymbol{x},\boldsymbol{\mu})) = a^{\omega}(e(\boldsymbol{x},\boldsymbol{\mu}), z(\boldsymbol{x},\boldsymbol{\mu})). \tag{5.2.13}$$

The field $z(\boldsymbol{x},\boldsymbol{\mu})$ is known as the *influence field* or *influence function* since it reflects how the residual influences the QoI. Discrete approximations can be computed through equation

$$a^{\omega}(v(\boldsymbol{x},\boldsymbol{\mu}), z(\boldsymbol{x},\boldsymbol{\mu})) := q(v(\boldsymbol{x},\boldsymbol{\mu})) = \mathcal{R}^{\omega}(z;\boldsymbol{\mu}), \qquad \forall\, v(\boldsymbol{x},\boldsymbol{\mu}) \in V. \tag{5.2.14}$$

Most importantly, any partition of unity $\phi_{\mathbb{p}=\mathbb{i}}$ can be applied to obtain a local indicator of the influence of the local residual.

$$\mathcal{R}^{\omega}(z;\boldsymbol{\mu}) = \sum_{\mathbb{p}=1}^{\mathbb{p}=n_{\mathbb{p}}} \mathcal{R}^{\omega}(\phi_{\mathbb{p}} z;\boldsymbol{\mu}). \tag{5.2.15}$$

As seen in chapters 1 and 4, the index $\mathbb{p} = \mathbb{i}$ can designate patches of arbitrary form.

5.2.4 Measures of the discretisation error extended to the parameter space

Any stochastic error (including the surrogate error) is defined in the parameter space, whereas the discretisation error is defined for a single sampling point. Therefore, the latter must be extended to the parameter space for obtaining a suitable measure to compare the errors.

For a given mesh $\mathcal{M}_i$, discretisation error $\widehat{\epsilon}_{is}$ in any sampling point s reads $|\widehat{Q}_{is} - Q^{\mathbb{h}}_{i\,s}|$. Some of the options to extend $\widehat{Q}_{is}$, which is different at each sampling point, to the parameter space Θ are:

$$\text{the maximum} \qquad \widehat{\epsilon}^{\Theta}_i = \max_{\Theta} |\widehat{Q}_{is} - Q^{\mathbb{h}}_{i\,s}|, \tag{5.2.16a}$$

$$\text{statistical moment of order } \tilde{o} \qquad \widehat{\epsilon}^{\Theta}_i = \int_{\Theta} |(\widehat{Q}_{is} - Q^{\mathbb{h}}_{i\,s})|^{\tilde{o}} f_{\boldsymbol{\mu}}(\boldsymbol{\mu}) d\boldsymbol{\mu}, \tag{5.2.16b}$$

$$\text{the average} \qquad \widehat{\epsilon}^{\Theta}_i = \frac{1}{n}\sum_{s=1}^{n_s} |\widehat{Q}_{is} - Q^{\mathbb{h}}_{i\,s}|, \tag{5.2.16c}$$

where each s is an individual sampling point, and n is the total number of sampling points evaluated in a discrete approximation.

The present work considers the error in the expectation of the QoI $\mathcal{E}[]$ as measure in the probabilistic space (see equations 2.3.1 and 5.2.9). Selecting other measure does not affect any of the algorithmic propositions of this chapter. The reader interested in delving into mathematical description of random fields is referred to [169].

5.2.5 Stochastic model for the parameters

Chapter 2 includes several ways to build surrogates and sample the parameter space. Despite the model is able to incorporate arbitrary large number of parameters, for the present work only two parametric Young's moduli are considered. Due to this small number of parameters, the computational cost of building a surrogate with Polynomial Chaos Expansion (PCE) is expected to be smaller in relation to sampling the FEM model with brute force Monte Carlo.

Even though PCE introduces a new error and contradicts the criterion of not polluting neither the discretisation nor the stochastic error, it can be fully controlled before the construction of the surrogate. Since the cost of evaluating PCE is negligible compared to the evaluation of the FEM numerical model, the sampling of the surrogate is performed with brute force Monte Carlo without any local enhancement.

5.2.6 Sources of error

Once all the ingredients of the computation are defined, the equation for the total error in the QoI reads

$$\epsilon := \mathcal{E}[Q] - \overline{\mathcal{E}}[Q^{\mathbb{h}}_{PC}], \tag{5.2.17}$$

where $\mathcal{E}[Q]$ stands for the exact expectation of the QoI (*i.e.* Monte Carlo with an infinity of simulated samples; with no discretisation error, that is to say, infinitely fine mesh; and no approximation of the QoI by PCE). Superindex $\mathbb{h}$ denotes the approximation of the QoI belonging to the discrete coarse space $\mathcal{V}^{\mathbb{h}}$. Subindex

PC denotes the PCE approximation. Remember that operator $\overline{\mathcal{E}}[\cdot]$ introduced in equation 2.3.1 refers to the expectation evaluated with a finite number of Monte Carlo samples. In this chapter, the rich spaces $\widehat{\mathcal{V}}$ or $\widehat{\mathcal{U}}$ are always the p2 enrichment space of p1 spaces $\mathcal{V}^{\mathbb{h}} \subset \widehat{\mathcal{V}} \subset \mathcal{V}$ or $\mathcal{U}^{\mathbb{h}} \subset \widehat{\mathcal{U}} \subset \mathcal{U}$ respectively. Henceforth, the symbol $\widehat{\ }$ denotes all magnitudes belonging to those rich spaces.

The total error produced at each step of the computation process can be split, reading

$$\epsilon = \underbrace{(\mathcal{E}[Q] - \mathcal{E}[\widehat{Q}])}_{\widetilde{\epsilon}} + \underbrace{(\mathcal{E}[\widehat{Q}] - \overline{\mathcal{E}}[\widehat{Q}])}_{\overline{\epsilon}} + \underbrace{\underbrace{(\overline{\mathcal{E}}[\widehat{Q}] - \overline{\mathcal{E}}[\widehat{Q}_{PC}])}_{\epsilon_{PC}} + \underbrace{(\overline{\mathcal{E}}[\widehat{Q}_{PC}] - \overline{\mathcal{E}}[Q^{\mathbb{h}}_{PC}])}_{\widehat{\epsilon}}}_{\epsilon_{NM}}, \tag{5.2.18}$$

where $\overline{\epsilon}$ stands for the Monte Carlo (*i.e.* statistical sampling error), ϵ_{PC} for the PCE error, and $\widehat{\epsilon}$ for the computable part of discretisation error. The remaining non-computable part of the discretisation error is denoted by $\widetilde{\epsilon}$ and assumed to be negligible in the proposed approach.

Finally, the definition of ϵ_{NM} as the *numerical approximation error* is introduced. ϵ_{NM} is fully controlled by mesh refinement. In fact, its PCE component is pre-calibrated for each mesh and impossible to assess separately after the calibration (see section 5.3.1 for details).

5.3 Simultaneous evaluation and control of Monte Carlo, surrogate and FE numerical errors with relative error stopping criterion

The purpose of the algorithm presented in this section is to deliver an optimised computational mesh, with minimum computational effort and for a given accuracy of the expectation of the engineering QoI. The refinement algorithm is iterative for each mesh $\mathcal{M}_i$. Each iteration leads to a local refinement of mesh $\mathcal{M}_i$ and the construction of the new mesh $\mathcal{M}_{i+1}$ until one of the meshes produces a solution fulfilling the stopping criterion. Crucial details that need to be addressed at each

step of the algorithm are:

- How to control the quality of the PCE surrogate so it does not pollute the rest of errors.
- How to compare the statistical error $\bar{\epsilon}$ and the numerical approximation error ϵ_{NM} (PCE surrogate + FEM discretisation) and subsequently decide which of the two needs to be reduced.
- How to perform local mesh adaptivity if the algorithm dictates that numerical error is larger and must be reduced.
- Which criterion needs to be checked to make the algorithm stop satisfactorily.

The algorithm proposed in this section adopts the relative error as stopping criterion. This approach is problem dependent and requires a good understanding of the problem, especially to determine the mean that centres the stochastic dispersion. From a statistical perspective, a stopping criterion which takes into account the variance is more useful. Section 5.4 presents a stopping criterion where the error in the expectation is normalised by means of the standard deviation, which is problem independent.

5.3.1 Adaptive surrogate model strategy

As a step towards a full adaptive uncertainty propagation algorithm, this subsection explains how to jointly control errors due to PCE and FE discretisation.

The precision of the PCE depends on the maximum unidimensional order $\mathfrak{O}_{Max}$ of the polynomial considered in the multidimensional basis $\mathscr{Z} = \{Z_1, ..., Z_{i_Z}, ..., Z_{n_Z}\}$ (see equation 2.4.11). In turn, the maximum order $\mathfrak{O}_{Max}$ determines the number of quadrature points needed to integrate these polynomials with no error. For the sake of simplicity in notation, the scalar $\mathfrak{O}^{\#}$ is defined to refer to the maximum combination of unidimensional order of polynomials allowed in the PCE basis. Its definition includes implicitly the selection of the general truncation scheme for the

tensor product and all steps explained in section 2.4.1 to obtain a truncated multidimensional PCE basis $\mathscr{Z}$, where the maximum polynomial order in any of the parametric dimensions is Φ_{Max}.

Ideally, exactly the same discretisation error would be recovered for a given mesh. That would mean that the surrogate model behaves precisely as the full FE model. Taking this into account, the accuracy of the PCE surrogate is subordinated to the discretisation error. If the error introduced by PCE is of smaller order than the discretisation one, there is no need to increase its precision and hence the maximum order in the polynomial expansion.

Calibration of the polynomial chaos expansion

In section 5.2.4 the expectation of the QoI is selected as measure of the stochastic process. Consequently, to calibrate PCE surrogate, it is natural to choose the same measure defined in equation 5.2.16c even if it is not a norm.

Sampling for the calibration. To assess PCE accuracy, the needed number of evaluations of the full FE model is the sum of two different set of samples. The first one is the number of Gauss-Hermite quadrature points required to fit PCE through the least squares process (equation 2.4.12) up to an order Φ_{Max} in any parametric direction. The second one is a set of samples needed to assess the measure 5.2.16c. The latter is called *set of control points* and needs to be independent of the set of samples in the MC process even if they are also drawn from the primary PDF.

To ensure the minimum number of evaluations of the full FE model, the proposed subalgorithm 7 checks the PCE accuracy for an increasing order $\Phi^{\#}$ of polynomials. Once the relative error in the measure 5.2.16c is smaller than a 10%, the algorithm stops and the order $\Phi^{\#}$ is stored as the starting point for future meshes. The 10% limit enforces the initial goal, that is to say, that the order of magnitude of PCE is lower than the discretisation error.

Regarding the control points, this work proposes that the set size is defined by the larger of two criteria. The first criterion is user defined and represents the

estimated minimum number of control samples to have at least one evaluation from all relevant regions in the sampling space. The second criterion equals the number of Gauss-Hermite quadrature points. The latter, links the increase of variation in the surrogate outcomes to the increase of control evaluations. At the same time, it ensures that the cost of the control phase does not exceed the cost of the fitting phase.

Calibration sub-algorithm. Putting all together, the measure $\widehat{\epsilon}_i^{CP}$ related to the discretisation error extended to the parameter space reads

$$\begin{aligned} &\widehat{\epsilon}_i^{CP} = \frac{1}{n_{CP}} \sum_{s=1}^{n_{CP}} |\widehat{Q}_{i\,s'} - Q^{\mathbb{h}}_{i\,s'}|, \\ &\text{where } \theta_{s'} \neq \theta_s, \quad \forall s' \in S' = \{1, ..., n_{CP}\}, \forall s \in S = \{1, ..., n_s\}, \end{aligned} \tag{5.3.1}$$

being n_{CP} the number of control sampling points $\theta_{s'} \in \Theta$ and n_s the number of sampling points $\theta_s \in \Theta$ used in Monte Carlo.

Exactly the same measure is then approximated through two different PCE so that the quality of the approximation can be assessed. One expansion is the reduced meta model of the QoI in the coarse p1 mesh and the other the reduced meta model of the QoI in the rich p2 space.

$$\widehat{Q}_{i\,s',PC^{\mathfrak{o}^\#}} = \sum_{j_Z=1}^{j_Z=n_Z} \widehat{\mathbb{c}}_{j_Z} Z_{j_Z}(\theta_{s'}), \qquad 1^{st} \text{ PCE approximating } \widehat{Q}_i, \tag{5.3.2a}$$

$$Q^{\mathbb{h}}_{i\,s',PC^{\mathfrak{o}^\#}} = \sum_{j_Z=1}^{j_Z=n_Z} \mathbb{c}^{\mathbb{h}}{}_{j_Z} Z_{j_Z}(\theta_{s'}), \qquad 2^{nd} \text{ PCE approximating } Q^{\mathbb{h}}_i, \tag{5.3.2b}$$

$$\widehat{\epsilon}^{CP}_{i\,PC^{\mathfrak{o}^\#}} = \frac{1}{n_{CP}} \sum_{s'=1}^{n_{CP}} |\widehat{Q}_{i\,s',PC^{\mathfrak{o}^\#}} - Q^{\mathbb{h}}_{i\,s',PC^{\mathfrak{o}^\#}}| \qquad \text{approximated measure,} \tag{5.3.2c}$$

where $\widehat{\mathbb{c}}$ and $\mathbb{c}^{\mathbb{h}}$ are two different sets of coefficients $\{\widehat{\mathbb{c}}_{j_Z}\}_{j_Z=1}^{j_Z=n_Z}$ and $\{\mathbb{c}^{\mathbb{h}}_{j_Z}\}_{j_Z=1}^{j_Z=n_Z}$ weighting the basis $\{Z_{j_Z}\}_{j_Z=1}^{j_Z=n_Z}$ determined by the maximum multidimensional order $\mathfrak{o}^\#$ considered for PCE truncation. These coefficients are obtained through least squares fitting at the quadrature points (different from the control points). The minimisation process is explained in section 2.4.2.

Subalgorithm 7 Calibration of the polynomial chaos for mesh $\mathcal{M}_i$

1: **while** $|\widehat{\epsilon}_{i\,PC^{\mathfrak{o}^\#}}^{CP} - \widehat{\epsilon}_i^{CP}|/|\widehat{\epsilon}_i^{CP}| > 10\%$ and $1/n_{CP}\sum_{s'=1}^{n_{CP}}(|\widehat{Q}_{i\,s',PC^{\mathfrak{o}^\#}} - \widehat{Q}_{i\,s'}|/|\widehat{Q}_{i\,s'}|) > 10\%$ **do**
2: Increase order $\mathfrak{o}^\#$ of the maximum polynomial ▷ Increased quadrature and control points
3: Compute solution at new quadrature and control points
4: Update $\widehat{\epsilon}_{iCP}$ with new samples
5: Least squares to update the coefficients of polynomial chaos
6: Compute approximation at control points and $\widehat{\epsilon}_{i\,PC^{\mathfrak{o}^\#}}^{CP}$
7: **end while**

The condition to ensure that PCE error does not pollute the discretisation error reads

$$|\widehat{\epsilon}_{i\,PC^{\mathfrak{o}^\#}}^{CP} - \widehat{\epsilon}_i^{CP}|/|\widehat{\epsilon}_i^{CP}| < 10\%. \tag{5.3.3}$$

However, there exists the possibility that both PCE surrogate models produce very inaccurate approximations, but in the same direction. In that case, by compensation of errors, the relative error of the difference is reduced as individual approximations worsen. To avoid this possibility, an extra condition is introduced.

$$\frac{1}{n_{CP}}\sum_{s'=1}^{n_{CP}}(|\widehat{Q}_{i\,s',PC^{\mathfrak{o}^\#}} - \widehat{Q}_{i\,s'}|/|\widehat{Q}_{i\,s'}|) < 10\%. \tag{5.3.4}$$

Once both PCE set of coefficients are calibrated, they produce outcomes of $\widehat{Q}_{i\,s',PC^{\mathfrak{o}^\#}}$ and $Q^{\mathbb{h}}_{i\,s',PC^{\mathfrak{o}^\#}}$ with a 10% error at most, compared to $\widehat{Q}_{i\,s'}$ and $Q^{\mathbb{h}}_{i\,s'}$ in the desired norm. Then, $\epsilon_{PC} << \widehat{\epsilon}$ and they are never assessed independently again for mesh $\mathcal{M}_i$. All MC outcomes are computed only through the surrogate model since calibration ensures $\epsilon_{NM} \approx \widehat{\epsilon}$.

The subindex i will be omitted from now on, unless different quantities belonging to different meshes in the refinement process are compared.

5.3.2 Link between uncertainty and discretisation error

Once the PCE has been calibrated, the task that motivates the present work must be faced. At each point of the refinement strategy, a mechanism must be implemented to ascertain if a refinement of the mesh is needed, the desired accuracy has been achieved, or more samples are required to provide more certainty in the choice.

In section 2.3.1 the expectations of $\widehat{Q}$ and $Q^{\mathbb{h}}$ are chosen as measures for the stochastic spaces of the reference and coarse discretisations. However, these mea-

sures vary depending on the set of samples employed in its computation. Indeed, due to the discrete MC approximation, $\overline{\mathcal{E}}[\widehat{Q}]$ and $\overline{\mathcal{E}}[Q^{\mathbb{h}}]$ are also response random variables where the sets $\widehat{\mathscr{Q}_{\mathscr{b}}} = \{\widehat{Q}_1, ..., \widehat{Q}_{n_s}\}$ and $\mathscr{Q}^{\mathbb{h}}_{\mathscr{b}} = \{Q^{\mathbb{h}}_1, ..., Q^{\mathbb{h}}_{n_s}\}$ are the samples producing an outcome indexed with the integer $\mathscr{b}$. Each pair of arbitrary sets $\widehat{\mathscr{Q}_{\mathscr{b}}}$ and $\mathscr{Q}^{\mathbb{h}}_{\mathscr{b}}$ produce outcomes $\overline{\mathcal{E}}[\widehat{Q}]_{\mathscr{b}}$ and $\overline{\mathcal{E}}[Q^{\mathbb{h}}]_{\mathscr{b}}$ respectively. All different sets $\widehat{\mathscr{Q}_{\mathscr{b}}}$ and $\mathscr{Q}^{\mathbb{h}}_{\mathscr{b}}$ have exactly n_s samples but all of them are generally different for each random combination $\mathscr{b}$.

Bootstrapping

The bootstrapping methods based on the works of Efron [59] allow the estimation of uncertainty related magnitudes of any quantity computed through evaluation of a number of samples, as is the case of $\overline{\mathcal{E}}[\widehat{Q}]$ and $\overline{\mathcal{E}}[Q^{\mathbb{h}}]$. The core idea is to estimate the PDF of a magnitude computed through several original set of samples by means of constructing alternative sets. The alternative construction uses different random combinations of the outcomes already evaluated in the original set, with replacement or repetition. It has been proved that the variance observed in the distribution of the magnitude computed using original sets and the variance computed using artificially constructed sets are equivalent [177].

The easier way of bootstrapping is based on reusing the samples. Let $n_s = 5$ be the number of samples considered in the primary stochastic process to compute the MC expectation. Then, the first sample for the discrete coarse expectation $\overline{\mathcal{E}}[Q^{\mathbb{h}}]_{\mathscr{b}=1}$ is obtained after evaluating the first set of random samples of the primary stochastic process $\mathscr{Q}^{\mathbb{h}}_{\mathscr{b}=1} = \{Q^{\mathbb{h}}_1, Q^{\mathbb{h}}_2, Q^{\mathbb{h}}_3, Q^{\mathbb{h}}_4, Q^{\mathbb{h}}_5\}$ by means of the numerical model. For the second sample $\overline{\mathcal{E}}[Q^{\mathbb{h}}]_{\mathscr{b}=2}$ instead of computing a new set of samples $\mathscr{Q}^{\mathbb{h}}_{\mathscr{b}=2} = \{Q^{\mathbb{h}}_6, ..., Q^{\mathbb{h}}_{10}\}$ which can be computationally expensive, an aleatoric re-sampling allowing repetition is exploited $\mathscr{Q}^{\mathbb{h}}_{\mathscr{b}^*=2} = \{Q^{\mathbb{h}}_4, Q^{\mathbb{h}}_1, Q^{\mathbb{h}}_4, Q^{\mathbb{h}}_5, Q^{\mathbb{h}}_1\} \mapsto \overline{\mathcal{E}}[Q^{\mathbb{h}}]_{\mathscr{b}^*=2}$. Evidently, the number of initially computed samples must be increased over n_s if repetition is not allowed.

After constructing the alternative sets of bootstrapped samples mapping to the set of outcomes $\{\overline{\mathcal{E}}[Q^{\mathbb{h}}]_{\mathscr{b}^*}\}_{\mathscr{b}^*=1}^{\mathscr{b}^*=n_{\mathscr{b}}}$, an estimated Confidence Interval [125] (CI) can be computed.

The present work transfers non-symmetric CI "centred" in the median of the bootstrapped set to the expectation of the initial set. As a first step, if a Confidence Level (CL) of 90% is desired, the left and right subintervals are computed as the distance between the median and the percentiles $\mathcal{C}_5$ and $\mathcal{C}_{95}$, respectively. Technically speaking,

$$CI^{\overline{\mathcal{E}}[Q^{\mathbb{h}}]}_{L,M} := [\mathcal{C}_5(\{\overline{\mathcal{E}}[Q^{\mathbb{h}}]_{\mathcal{b}^*}\}^{\mathcal{b}^*=n_{\mathcal{b}}}_{\mathcal{b}^*=1}) \ , \ \text{median}(\{\overline{\mathcal{E}}[Q^{\mathbb{h}}]_{\mathcal{b}^*}\}^{\mathcal{b}^*=n_{\mathcal{b}}}_{\mathcal{b}^*=1})], \tag{5.3.5a}$$

$$CI^{\overline{\mathcal{E}}[Q^{\mathbb{h}}]}_{R,M} := [\text{median}(\{\overline{\mathcal{E}}[Q^{\mathbb{h}}]_{\mathcal{b}^*}\}^{\mathcal{b}^*=n_{\mathcal{b}}}_{\mathcal{b}^*=1}) \ , \ \mathcal{C}_{95}(\{\overline{\mathcal{E}}[Q^{\mathbb{h}}]_{\mathcal{b}^*}\}^{\mathcal{b}^*=n_{\mathcal{b}}}_{\mathcal{b}^*=1})], \tag{5.3.5b}$$

where $[\cdot,\cdot]$ denotes a closed interval. Finally, a CI equals the union of the left and right subintervals, *i.e.*

$$CI^{\overline{\mathcal{E}}[Q^{\mathbb{h}}]} = CI^{\overline{\mathcal{E}}[Q^{\mathbb{h}}]}_{L,M} \cup CI^{\overline{\mathcal{E}}[Q^{\mathbb{h}}]}_{R,M}. \tag{5.3.6}$$

For display purposes, the CIs are "non-symmetrically centered" at the expectation computed by means of the original set. In other words, the left and right subintervals are displayed around the correspondent initial expectation instead of around the median of the set of bootstrapped expectations.

How FE refinement and addition of samples affect the distribution

Plot contents. Figures 5.2, 5.3 and 5.4 in this subsection graphically show the PDF of $\widehat{Q}_{PC}$ (in red) and $Q^{\mathbb{h}}_{PC}$ (in blue). They also show that they differ due to the difference between the spaces $\widehat{\mathcal{U}}$ and $\mathcal{U}^{\mathbb{h}}$. Standard Kernel Density Estimation (KDE) is used for estimating these PDFs. The PDFs are included for illustration purposes only, since they do not play a role in the algorithm.

The graphical representation of the discretisation error $\widehat{\epsilon}$ is the distance $\overline{\mathcal{E}}[\widehat{Q}_{PC}] - \overline{\mathcal{E}}[Q^{\mathbb{h}}_{PC}]$ (as defined in equation 5.2.18).

Regarding the graphical representation of the MC sampling error $\overline{\epsilon}$, it is included through the CI of these expectations [125]. Section 5.3.2 describes the particular bootstrapping technique selected in the present thesis. Graphically the confidence in PDF representations is included in the figures through an orange and a cyan interval on top of the corresponding PDF.

Effects of reducing MC error. Figure 5.2 shows that for a given mesh $\mathcal{M}_1$, the larger the number of samples, the thinner the CI intervals. This is due to the improved characterisation of the PDF coming from the increase of samples. In contrast, the distance between the estimated expectations is constant, since the discretisation error $\widehat{\epsilon}$ is only improved by refining the mesh. By looking at figure 5.2, it is obvious that FE refinement is needed for all meshes because the discretisation error is much larger than the CI representing the MC error.

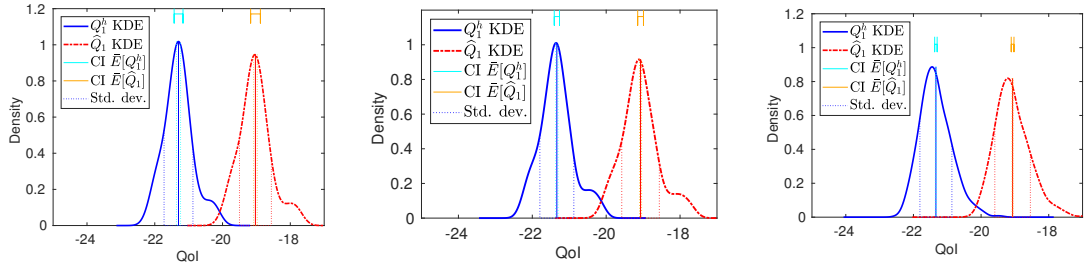

(a) 40 samples (b) 160 samples (c) 640 samples

Figure 5.2: Effects of reducing sampling error on the response PDFs error
Load case P1, mesh number 1

Effects of reducing discretisation error. Figure 5.3 shows the opposite case. The size of the CI remains of the same order of magnitude if the same number of samples is employed in different meshes. On the other hand, the distance between both PDFs and hence their expectations becomes smaller with each mesh refinement.

Need of a specific indicator of refinement. Figures 5.2 and 5.3 are produced for the loading case P1 (see figure 5.1). In loading case P1 the parametric uncertainty has a minor contribution to the QoI. It is clear in all the plots that the distance $\overline{\mathcal{E}}[\widehat{Q}_{PC}] - \overline{\mathcal{E}}[Q^{\mathrm{h}}_{PC}]$ is larger than the CI measuring MC error, even considering the best case within the two sets of CI.

Conversely, figure 5.4 , produced for the loading case P2, shows an overlap of CIs. In this case, the plot does not provide enough information to establish whether the FE error dominates or more samples are needed to reduce the uncertainty. Either

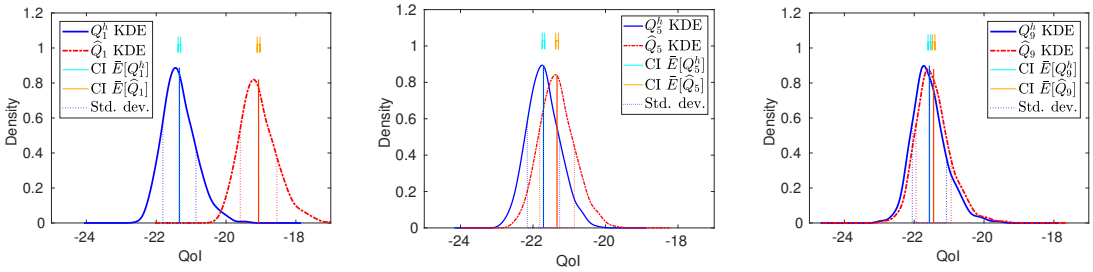

(a) Mesh num. 1 (b) Mesh num. 5 (c) Mesh num. 9

Figure 5.3: Effects of reducing discretisation error on the response PDFs error
Load case P1, 640 samples

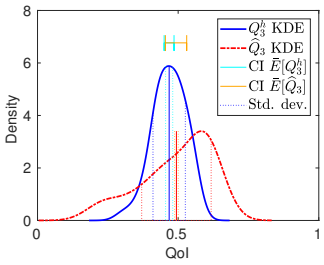

Figure 5.4: Need of a specific indicator of refinement
Load case P2, 40 samples, mesh num. 3

of the errors could be the largest considering all possibilities of $\overline{\mathcal{E}}[\widehat{Q}_{PC}]$ and $\overline{\mathcal{E}}[Q^{\mathbb{h}}_{PC}]$ within their CI.

Mechanism to ascertain whether any of the errors must be further reduced

Since the goal is to assess the uncertainty in the FE discretisation error $\widehat{\epsilon} = \overline{\mathcal{E}}[\widehat{Q}_{PC}] - \overline{\mathcal{E}}[Q^{\mathbb{h}}_{PC}]$, the logical step is to look at the distribution of the difference rather than both distributions separately. This avoids overlapping of variances as in figure 5.4.

For this section, the desired discretisation accuracy is determined by means of the introduction of a user defined maximum relative error ε_{FE} as stopping criterion.

The uncertainty in the achievement of the desired accuracy is assessed by percentiles $\mathcal{C}_{CL}^{FE}$, which are defined as percentiles of the bootstrapped distribution of the relative error.

$$\widehat{\epsilon}_{/} := \frac{|\overline{\mathcal{E}}[\widehat{Q}_{PC}] - \overline{\mathcal{E}}[Q^{\mathrm{h}}_{PC}]|}{|\overline{\mathcal{E}}[\widehat{Q}_{PC}]|}. \tag{5.3.7}$$

Figure 5.5, for instance, contains a case where the Confidence Level CL^{FE} is set to 95%, and the desired accuracy to 10% of relative error $\widehat{\epsilon}_{/}$ (*i.e.* $\widehat{\epsilon}_{/} < \varepsilon_{FE} = 0.10$ with $CL^{FE} = 95\%$).

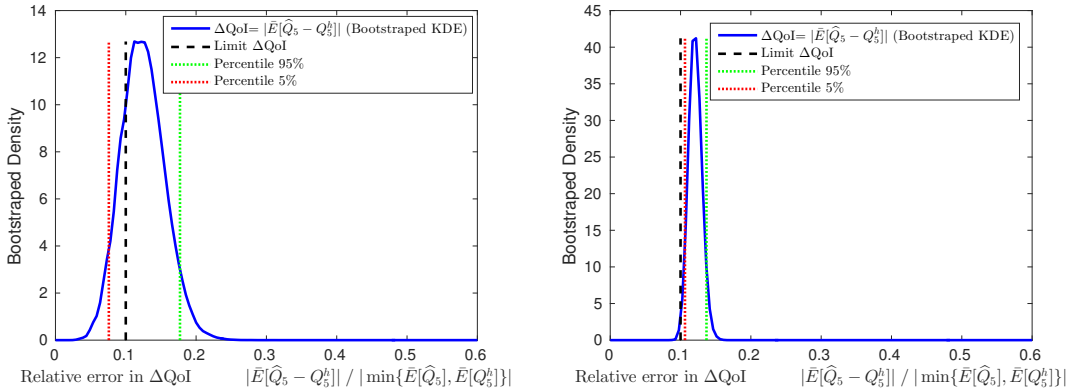

(a) Load P2, Mesh 5, 10 samples

More samples needed

(b) Load P2, Mesh 5, 160 samples

Certainty of refinement needed

Figure 5.5: KDE approximation of $\widehat{\epsilon_{\%}}$

In figure 5.5.a (produced with 10 samples) no decision can be made. According to the percentiles, if the computation is repeated with different sampling points, $\widehat{\epsilon}_{/}$ could be either larger or smaller than the limit. This means that Monte Carlo sampling error dominates and thus more samples are needed, since uncertainty is to be reduced.

On the contrary, in figure 5.5.b (produced with 160 samples) the percentile $\mathcal{C}_{(100-CL^{FE})}$ is larger than the prescribed limit. Therefore, there is certainty that 95% of the times $\widehat{\epsilon}_{/}$ will be larger than the limit. This means that discretisation error dominates the problem and consequently a finer mesh is needed to reduce this error.

Since refinement reduces the error, with each new mesh the new distribution shifts towards the left. Eventually, at one stage of the mesh refinement $\varepsilon_{FE} = 0.10$ will be larger than $\mathcal{C}_{CL^{FE}}$. At that point of mesh refinement, the error in the

expectation of the QoI will be smaller than the limit for 95% of the evaluation sets. In other words, there will be 95% certainty that the solution for the expectation of the QoI is accurate enough.

Algorithm map and severity of the certainty assessment

As presented so far, the algorithm can stagnate if the relative error in the expectation equals $\widehat{\epsilon}_{/}$ almost exactly at any point in the refinement process. In order to avoid this stagnation, a parameter Δ^{CI} is introduced as a measure of the severity imposed to the stochastic sub-loop.

If the algorithm determines that more samples are needed, before doing so, the parameter controls that the CI is not too small. The distances CI are computed by means of equation 5.3.6. The larger CI produced from the coarse and rich spaces is taken into consideration.

Then, if $CI < \Delta^{CI}$, it is considered that too much effort has been devoted to sampling and a refinement of the mesh is needed. The hypothesis for this decision is that even if the current discretisation may eventually provide certainty of having reached the final goal, the next discretisation should provide the same certainty with a smaller number of samples.

Obviously, Δ^{CI} should be very strict if the surrogate models are very cheap to compute, and loose if Monte Carlo is used with no surrogate on the original numerical model.

Algorithm map based on relative error

Figure 5.6 includes the algorithm map that dictates which error dominates and if there is a need for refinement or sampling.

5.3.3 Goal-oriented local adaptivity

Once "when to refine" is known the question of "where to" remains. The QoI is a global quantity, so it does not help in deciding where to refine. Consequently,

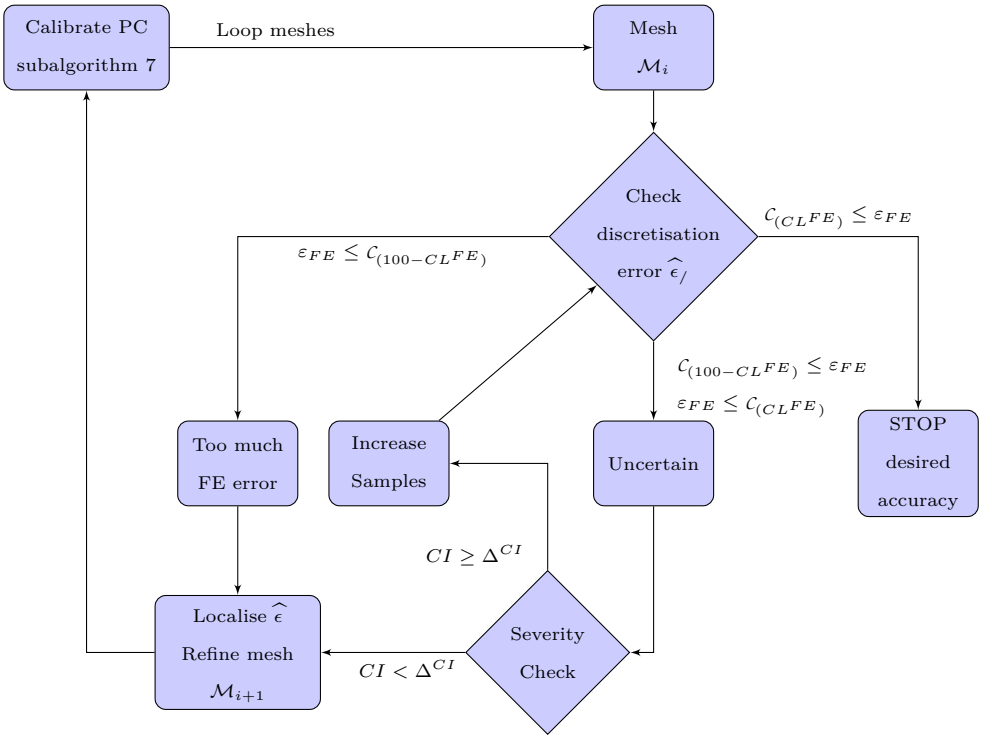

Figure 5.6: Algorithm map for relative error criterion

a localised quantity derived from the QoI must be obtained, which is not a trivial process.

Indicators based on the magnitude of the error

A naive approach to defining an indicator of refinement would be to directly use the restriction of the discrete version of equation 5.2.13 to the subdomain $\Omega_{\mathbb{k}}$ as indicator of refinement for the element $\mathbb{e}^{\mathbb{k}}$. Using the rich and coarse spaces $\widehat{\mathcal{V}}$ and $\mathcal{V}^{\mathbb{h}}$, the discrete direct local indicator $\widehat{\eta^D_{\mathbb{k}}}$ reads

$$\widehat{\eta^D_{\mathbb{k}}} := \mathcal{R}^{\omega}_{\Omega_{\mathbb{k}}}(\widehat{z}) = a^{\omega}_{\Omega_{\mathbb{k}}}(\widehat{e}, \widehat{z}). \tag{5.3.8}$$

Due to Galerkin orthogonality, the residual of any field $\zeta^{\mathbb{h}} \in \mathcal{V}^{\mathbb{h}}$ is zero (*i.e.* $\mathcal{R}^{\omega}(\zeta^{\mathbb{h}}) = 0$). So it is possible to modify 5.3.8 to compute the orthogonal part with respect to the coarse space $\mathcal{V}^{\mathbb{h}}$. Despite the localised contribution to the QoI $\widehat{\eta^{\perp}_{\mathbb{k}}}$ changes, the global QoI remains unaffected.

$$\widehat{\eta^{\perp}_{\mathbb{k}}} := \mathcal{R}^{\omega}_{\Omega_{\mathbb{k}}}(\widehat{z} - z^{\mathbb{h}}) = a^{\omega}_{\Omega_{\mathbb{k}}}(\widehat{e}, \widehat{z} - z^{\mathbb{h}}). \tag{5.3.9}$$

An estimator based on localisation of the mass norm is defined with the only purpose of showing that all the localised indices point to where the error is larger. This is not useful to drive the refinement strategy. The indicator based on the mass matrix (see equation 5.2.5) reads

$$\widehat{\eta_{\mathbb{k}}^{MN}} := \rho \cdot \omega^2 \int_{\Omega_{\mathbb{k}}} \left([\widehat{e}]^T \widehat{\psi}_v \cdot \widehat{\psi}_u [\widehat{e}] \right) d\Omega. \tag{5.3.10}$$

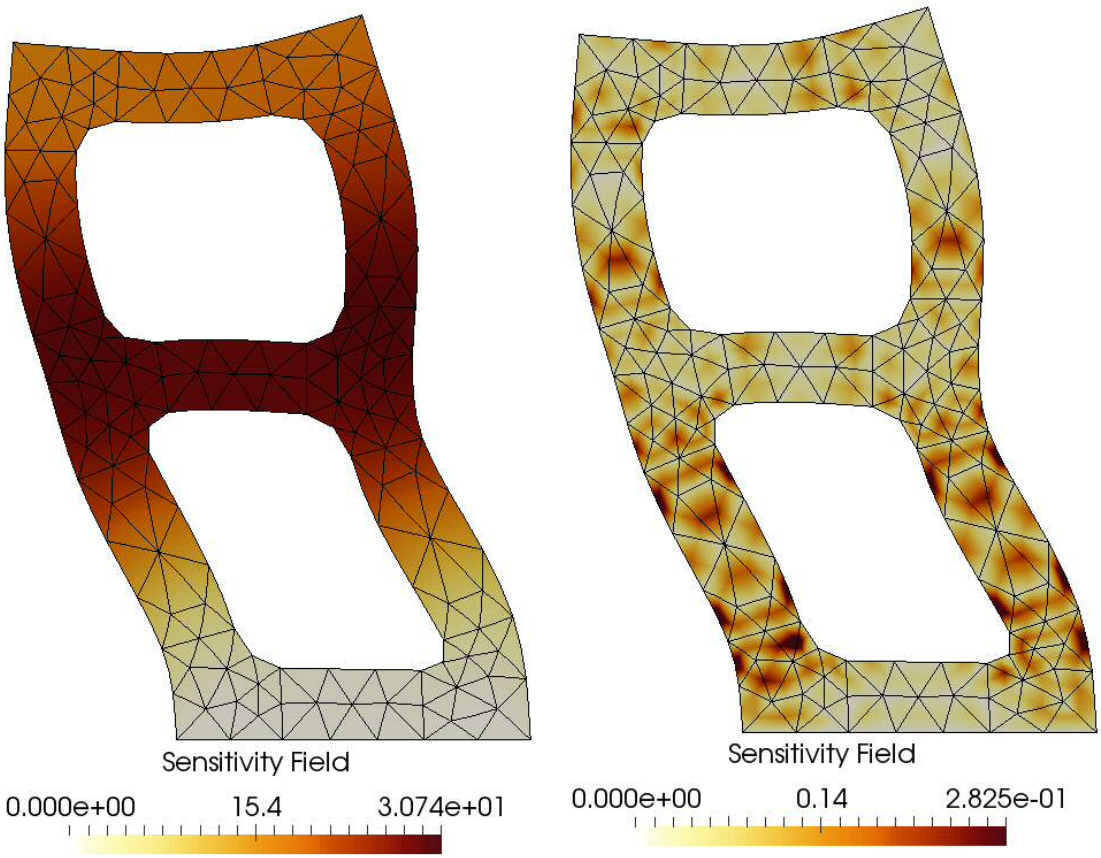

(a) z (b) $z - \widehat{\pi}^{\mathcal{V}^h}_{\widehat{\mathcal{V}}}(z)$

Figure 5.7: Sensitivity fields for the QoI, load P1, ω between 1st and 2nd natural frequency

It is clear that, for the posed problem, the indicator $\widehat{\eta_{\mathbb{k}}^{MN}}$ always points to the top part of the structure, since it is where the displacement and the error are larger (see horizontal deformation in figure 5.7). The indicators based on the QoI introduce the

sensitivity field z which modifies this focus (coloured field in figure 5.7.a), but they are still based on the magnitude of the error. Section 5.3.3 shows that this leads to very poor refinement strategies.

Indicators based on the variation of the error

Refinement indicators based on the energy norm usually lead to excellent convergence. Due to the definition of the energy norm, those indicators take into account the gradient. The mentioned indicator reads

$$\widehat{\eta_{\mathbb{k}}^{EN}} := a^{\omega}_{\Omega_{\mathbb{k}}}(\widehat{e},\widehat{e}). \tag{5.3.11}$$

Including the gradient in the indicator means that it points to where the error changes the most, so where there is more probability of improvement.

The goal is then to define an indicator of refinement $\widehat{\eta_{\mathbb{k}}^{\partial}}$ based on the QoI that points to the elements where the error varies the most, and not where it is larger as is the case of $\widehat{\eta_{\mathbb{k}}^{EN}}$.

Oden [129] proposes an indicator equivalent to $\widehat{\eta_{\mathbb{k}}^{\partial}} = \widehat{\eta_{\mathbb{k}}^{EN}} \cdot \widehat{\eta_{\mathbb{k}}^{D}}$, where one term of the product accounts for influence field and the other for the energy of the system. Another technique is to define a QoI that involves a gradient, *e.g.* an indicator based on the stress [75]. Later works, as the one by Rognes [150], base the indicator on the equilibrated residual, integration by parts and redistribution of the normal derivative, which accounts for the contribution of the rest of the domain in the element $\mathbb{e}^{\mathbb{k}}$.

The present work relies on Galerkin orthogonality and the utilisation of p-refinement to achieve the same goal in a much simpler discrete way. The idea is to subtract all the coarse FE component of the error interpolated to the rich space from the influence field. As already mentioned, subtracting any coarse field from equations 5.2.13 has no influence on the global QoI but affects the local contributions.

Then, the projection of a field $\widehat{v} \in \widehat{\mathcal{V}}$ to the space $\mathcal{V}^{\mathbb{h}} \subset \widehat{\mathcal{V}}$ is defined as in equation 1.4.6. After projected, the field must be interpolated back to space $\widehat{\mathcal{V}}$ using the coarse shape functions (see equation 4.2.1).

Therefore, the proposed indicator based both on the variation of the error and the influence field reads

$$\widehat{\eta}^{\partial}_{\mathbb{k}} := \mathcal{R}^{\omega}_{\Omega_{\mathbb{k}}}(\widehat{z} - \overset{\nu^{\mathbb{h}}}{\underset{\widehat{\nu}}{\pi}}(\widehat{z})) = a^{\omega}_{\Omega_{\mathbb{k}}}(\widehat{e}, \widehat{z} - \overset{\nu^{\mathbb{h}}}{\underset{\widehat{\nu}}{\pi}}(\widehat{z})). \tag{5.3.12}$$

Figure 5.7.b clearly shows that by removing completely any contribution belonging to $\mathcal{V}^{\mathbb{h}}$, the only local contributions to the global QoI are those where the p2 shape functions capture better the error than the p1 shape functions. Indeed, these contributions are larger where the error varies the most, which was the goal in the first place.

Effectivity of the different indicators of refinement

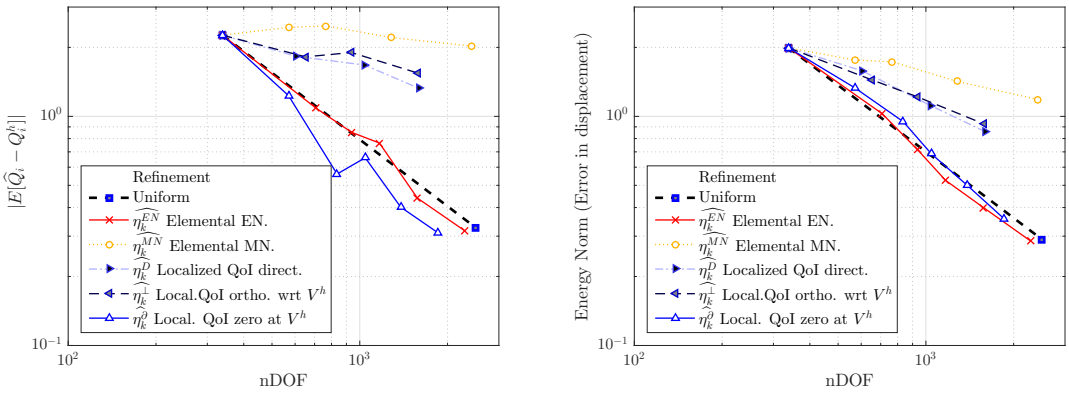

(a) Convergence of $|\overline{\mathcal{E}}[\widehat{Q}] - \overline{\mathcal{E}}[Q^{\mathbb{h}}]|$ (b) Convergence of $\overline{\mathcal{E}}[\int_\Omega (\nabla_s \widehat{e}) \cdot (C(\boldsymbol{x}, \boldsymbol{\mu}) \nabla_s \widehat{e}]$

Load case P1. Random parameters μ_1 and μ_2

Figure 5.8: Convergence depending on the refinement criteria

Figure 5.8 shows that indicators based on the magnitude of the error have poor performance. Indicators $\widehat{\eta}^{D}_{\mathbb{k}}$ and $\widehat{\eta}^{\perp}_{\mathbb{k}}$ improve in relation to $\widehat{\eta}^{MN}_{\mathbb{k}}$ because the influence field weights the new area of interest farther from the top, where the magnitude of the error is larger.

On the contrary, indicators based on the variation of the error $\widehat{\eta}^{EN}_{\mathbb{k}}$ and $\widehat{\eta}^{\partial}_{\mathbb{k}}$ show similar convergence, which in both cases is faster than uniform refinement. Besides this good performance, the proposed estimator $\widehat{\eta}^{\partial}_{\mathbb{k}}$ contains the influence field in its

definition. Therefore, its convergence is slightly slower than $\widehat{\eta_{\mathbb{k}}^{EN}}$ for the energy error but slightly better for the QoI.

Concentration of refinements check

When presenting the benefits of local refinement, it is common to pose a problem where the error is highly localised, for instance a steady flow over a notch. This is not the case of the vibration of structures. In the problem posed, displacements and hence errors due to harmonic loads tend to propagate. Consequently, concentration of local refinements is not as acute as in other problems. In addition, checking the correct placement of the local refinement is not always intuitive. Nevertheless, the ability to capture these local phenomena is needed to validate a refining indicator. As a consequence, the case of load P3 and $\omega = 0$ is introduced as a test for the refinement indicator.

In this test the natural frequencies are almost not excited. Then, if both the load P3 and the domain Ω_{Q3} are defined in the lower part of the structure, there should be concentration of refinement on the lower part. Figure 5.9 shows an acute concentration of refinement at stage 7.

Considering the good convergence and the ability to concentrate refinements, it can be concluded that, from the presented indicators, $\widehat{\eta_{\mathbb{k}}^{\partial}}$ is the most suitable to lead the goal-oriented refinement process.

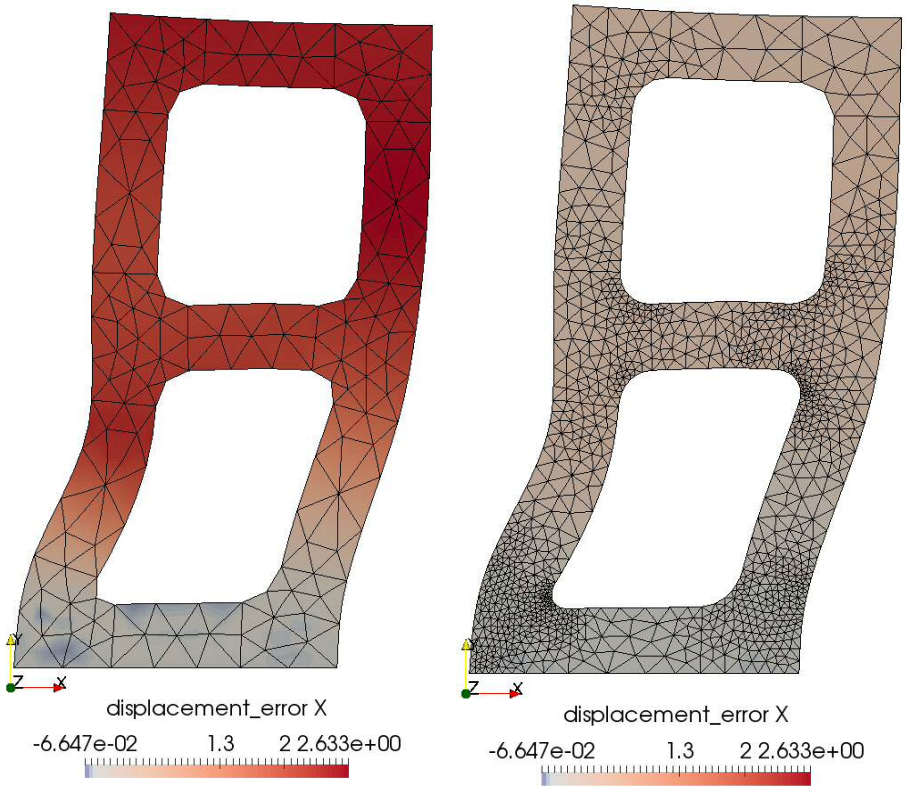

(a) mesh num 1

(b) mesh num 7

Figure 5.9: Localisation of local refinement

Error in X displacement, load P3, $\omega = 0$

5.4 Stopping criterion based on the standard deviation of the quantity of interest

The algorithm proposed in section 5.3.2 ensures that the relative error in the expectation of a QoI is small enough. However, the interest is often in quantifying how much it varies around the expectation (or the designed measure characterising the stochastic process), as well as knowing its value. For instance, if a structure can occasionally enter the plastic regime but not on a regular basis to avoid fatigue, the relative error in the expectation of the maximum stress suffices. On the contrary, if the interest is in knowing if a crack has formed in a concrete structure, the expectation of the maximum stress is as important as its standard deviation, since the first time the ultimate stress is exceeded a crack will form.

Furthermore, if the interest is in characterising the PDF of the final stochastic process, a very small error in the expectation alone does not ensure that the PDFs of $\widehat{Q}$ and $Q^{\mathbb{h}}$ are close. In fact, if their variance is smaller, the areas under the probability curves are nothing alike.

It is possible to consider the standard deviation of the response stochastic process only in the stopping criterion without modifying any of the definitions in section 5.3. Using the standard deviation $std()$ to normalise the discretisation leads to

$$\widehat{\epsilon_\sigma} := \frac{|\overline{\mathcal{E}}[\widehat{Q_{PC}}] - \overline{\mathcal{E}}[Q^{\mathbb{h}}_{PC}]|}{std(Q^{\mathbb{h}}_{PC})}, \tag{5.4.1}$$

where $std(Q^{\mathbb{h}}_{PC})$ must be evaluated from the set of outcomes $\{Q^{\mathbb{h}}_{PC,1}, ..., Q^{\mathbb{h}}_{PC,n_s}\}$.

A limit ε_σ analogous to ε_{FE} must be specified. In this case, it represents how small the discretisation error can be in comparison with the standard deviation. The number of samples influences the CI around this ratio, exactly as in the case of $\widehat{\epsilon}_/$.

The complete algorithm map taking into account both criteria is displayed in figure 5.10. Note that if the goal is only to adequately characterise the PDFs, the relative error criterion can be omitted.

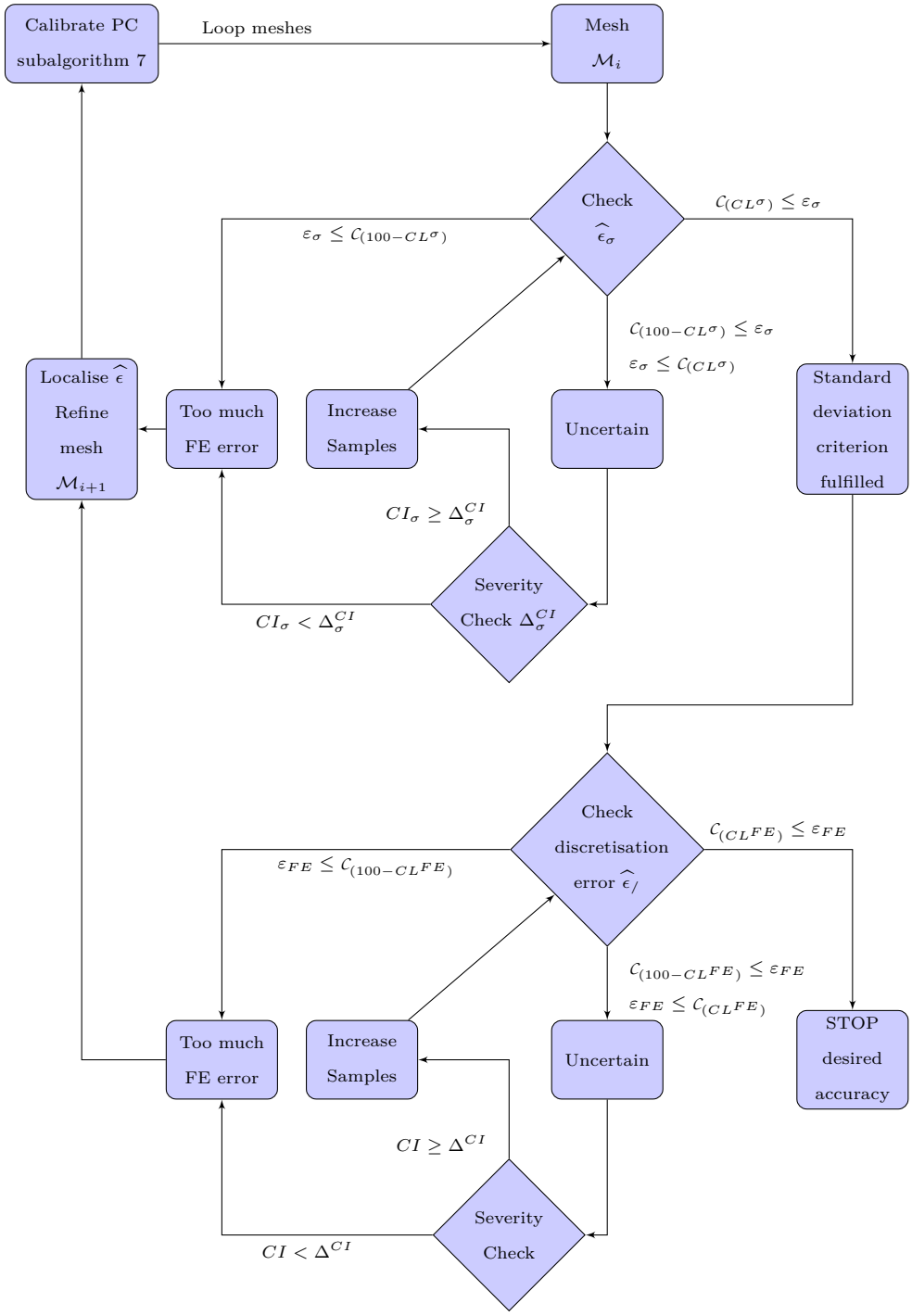

Figure 5.10: Algorithm map for double criteria

5.5 Numerical results

Based on the problem defined in section 5.2.2, the present section includes the numerical results for three different loading cases. The geometry and parameters for the structure are listed next. L=1, R=0.1, T=0.2, P1=P2=P3=1/length unit, $\boldsymbol{\mu} = \{\mu^1, \mu^2\}$, $\rho = 1$, $\omega = 0.3$ (between the first and the second natural frequency).

The results are structured in 3 subsections devoted to check the 3 different sources of error described in section 5.2.6.

5.5.1 Results for polynomial chaos expansion

The first loading case P1 consists of a horizontal load that excites the first and second natural frequencies in a direct manner. Furthermore, the QoI (defined as average of the horizontal displacement in one tip corner) is also very influenced by a direct horizontal load. Even though both parameters have also impact on the QoI, this impact is generally minor compared to the load contribution.

Figures 5.11a,b show that the error in the QoI is reduced globally in all the parameter domain where samples are approximated. It is revealed that for load P1, order 3 Hermite polynomials are accurate enough to keep polynomial chaos error below the discretisation error even for 9th stage refinement meshes.

The second loading case is vertical. In contrast to the previous case, parameter variation is now the only factor that significantly affects the QoI. Consequently, the parameter surface equals zero when the parameters are also zero. Parameter zero means Young's modulus equals 1, which is the default value for the rest of the structure.

Surface plots show similar results, except for the fact that an increasing number of polynomials is needed to keep the error below the discretisation error. Figures 5.11c-e show slices of the parameter surfaces through lines of quadrature points so that direct computations can be included.

It is interesting to notice that as the complexity of the parameter surface increases, the quadrature points cover a wider area, even farther than the high prob-

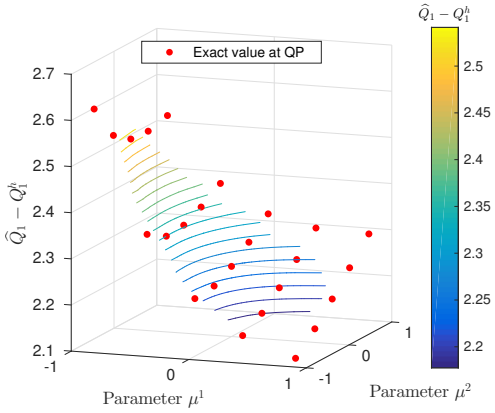

(a) Load P1, Mesh num. 1

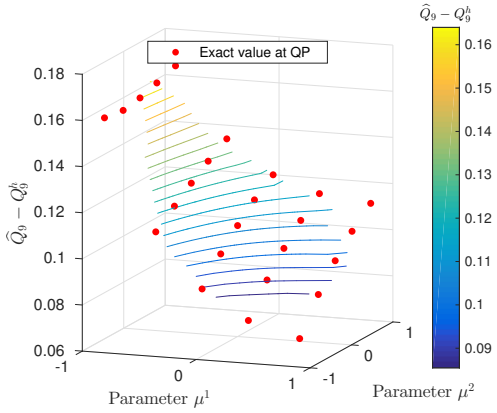

(b) Load P1, Mesh num. 9

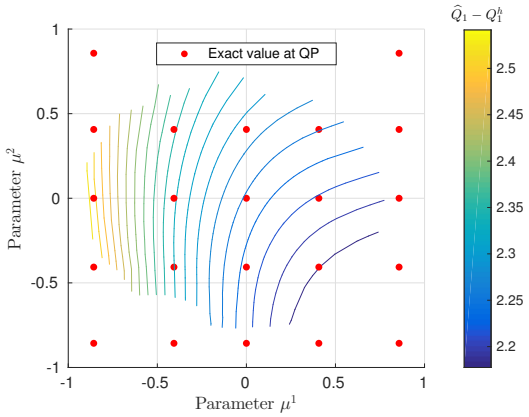

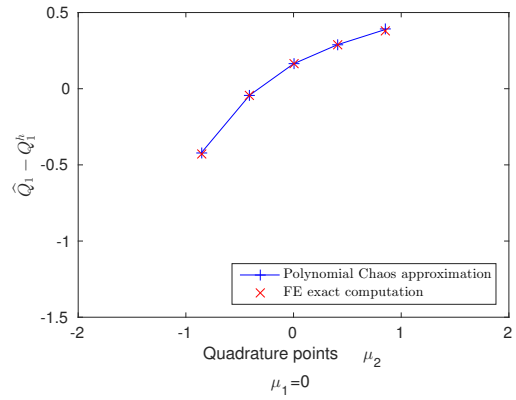

(c) Load P2, Mesh num. 1, central slice

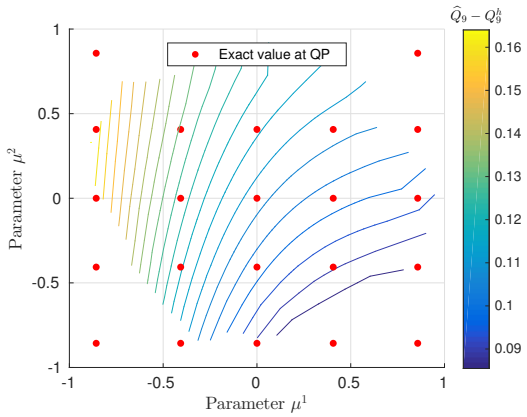

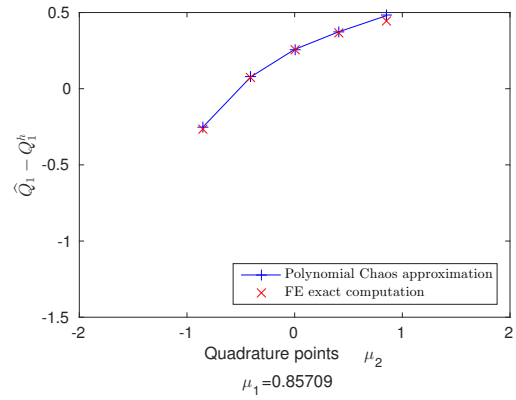

(d) Load P2, Mesh num. 1, extreme slice

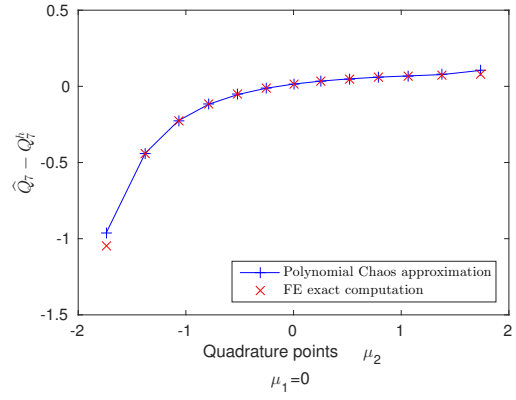

(e) Load P2, Mesh num. 7, central slice

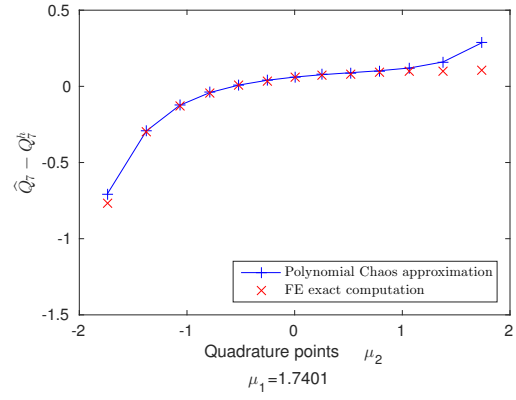

(f) Load P2, Mesh num. 7, extreme slice

Figure 5.11: Parameter response surface of the error in the QoI

ability sampling area that defined the polynomials in the first place. Of course, by increasing infinitely the number of samples, the sampling area will eventually overcome the area covered by the quadrature points regardless of their order.

Although only the central and one of the extreme slices in μ^1 direction have been included in figures 5.11c-e, it can be seen that the error of the PCE approximation is larger as the distance from the mean of the sampling distribution increases (in the present case $\mu_1 = \mu_2 = 0$ corresponding to Young's moduli =1). While the values close to this mean fit almost perfectly, there is discrepancy in the extremes of the slice plots. This behaviour is to be expected because even if the fitting process ensures that the error is minimised with an exact integration in the whole infinite parameter domain, the weights considered in the integration quadrature enhance contributions of the maximum probability region.

5.5.2 Discretisation convergence

Regarding the discretisation error, which drives the problem and serves as reference for the rest of the error, the convergence of the QoI is the best way to assess its accuracy.

The whole point of adaptive refinement is to obtain a smaller error than uniform refinement for the same number of degrees of freedom, so that computational time is saved.

Figure 5.8 shows that this is the case for load P1 where the uncertainty is small. Furthermore, figure 5.12 indicates that this better convergence is consistent for a large number of mesh refinements.

The case of load P2 produces more uncertainty. Figures 5.12.c,d manifest that local refinement still performs better than uniform refinement. However, the path to convergence has significant oscillations due to the fact that different samplings present large discrepancy in the QoI and hence its error.

In both loading cases, the gain of adaptive approach with respect to the uniform refinement approach is of the same order for the static and the $\omega = 0.3$ frequency cases (between first and second natural frequencies).

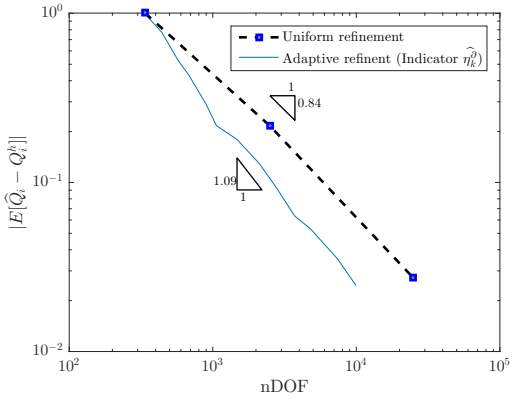

(a) Loading case P1, ω=0.0, T=0.2, R=0.1

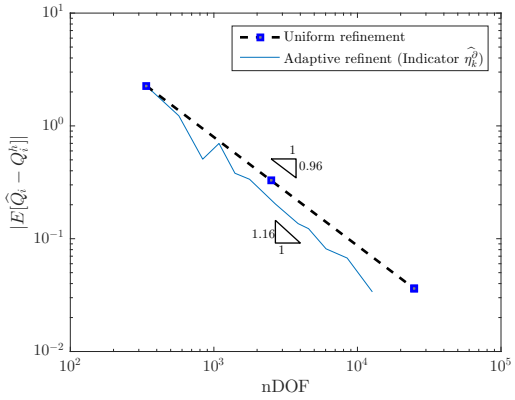

(b) Loading case P1, ω=0.3, T=0.2, R=0.1

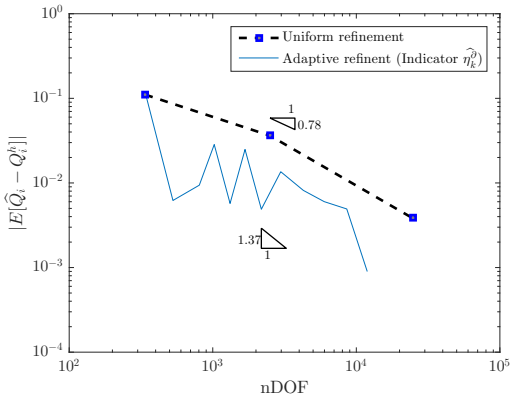

(c) Loading case P2, ω=0.0, T=0.2, R=0.1

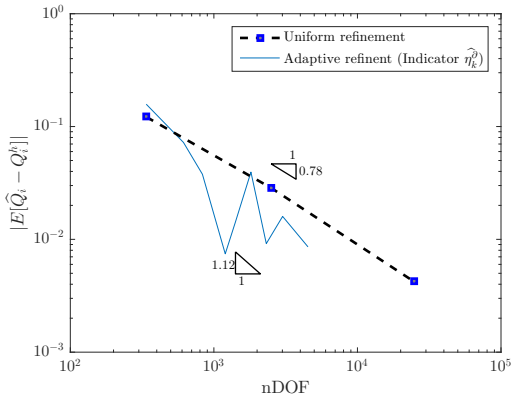

(d) Loading case P2, ω=0.3, T=0.2, R=0.1

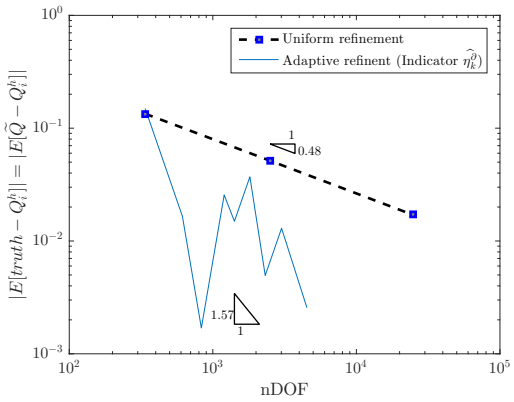

(e) Loading case P2, ω=0.3, T=0.2, R=0.1

compared vs Truth

Figure 5.12: Convergence of $|\overline{\mathcal{E}}[\widehat{Q}] - \overline{\mathcal{E}}[Q^{\mathbb{h}}]|$

The error at each step in figures 5.12.a-d is estimated as the difference between the expectation of the QoI using linear and quadratic elements ($\overline{\mathcal{E}}[Q_i^{\mathbb{h}}]$ and $\overline{\mathcal{E}}[\widehat{Q_i}]$) for the given mesh $\mathcal{M}_i$.

In order to rule out the possibility that results are polluted due to mesh dependence of the estimations, in figure 5.12.e the error is computed as the difference between the coarse solution $\overline{\mathcal{E}}[Q_i^{\mathbb{h}}]$ at each mesh and a fixed truth solution $\overline{\mathcal{E}}[\widetilde{Q}]$. The outcomes of $\widetilde{Q}$ are computed using a single highly refined mesh of quadratic elements with local refinements at the re-entrant corners. In that way, the truth is far from the solution at each step, both in an h-refinement and a p-refinement sense. The results obtained considering a fixed truth solution are even better than the ones obtained in the proposed algorithm. In the algorithm the truth is never computed. Instead, a p-refinement error estimator at each mesh refinement step is used to estimate the discretisation error. Note that any goal-oriented a-posteriori error estimator can be employed for that purpose.

5.5.3 Sampling stop criterion

This section provides evidence that the CIs serve their purpose. In other words, the stochastic error due to stop the sampling strategy early is controlled as claimed in section 5.4.

In order to perform this verification, the problem was computed 34 times allowing randomness in all samplings. The area between percentiles 5 and 95 is designated as CI, so an average of 3.4 cases are expected to be outside of the CI at each step of the mesh refinement. Certainly, the number of samples is too small in order to have conclusive results or any precision in this average. However, figure 5.13 shows that even for a small amount of computed cases, the order of magnitude of the CIs is close to 3.4.

Testing all the computed cases, the average for all cases and meshes varies from 1.6 to 4.4. Due to the low number of cases computed, the standard deviation is quite high ranging from 2.5 to 5.4.

After checking that the MC expectation of the error in the QoI is controlled

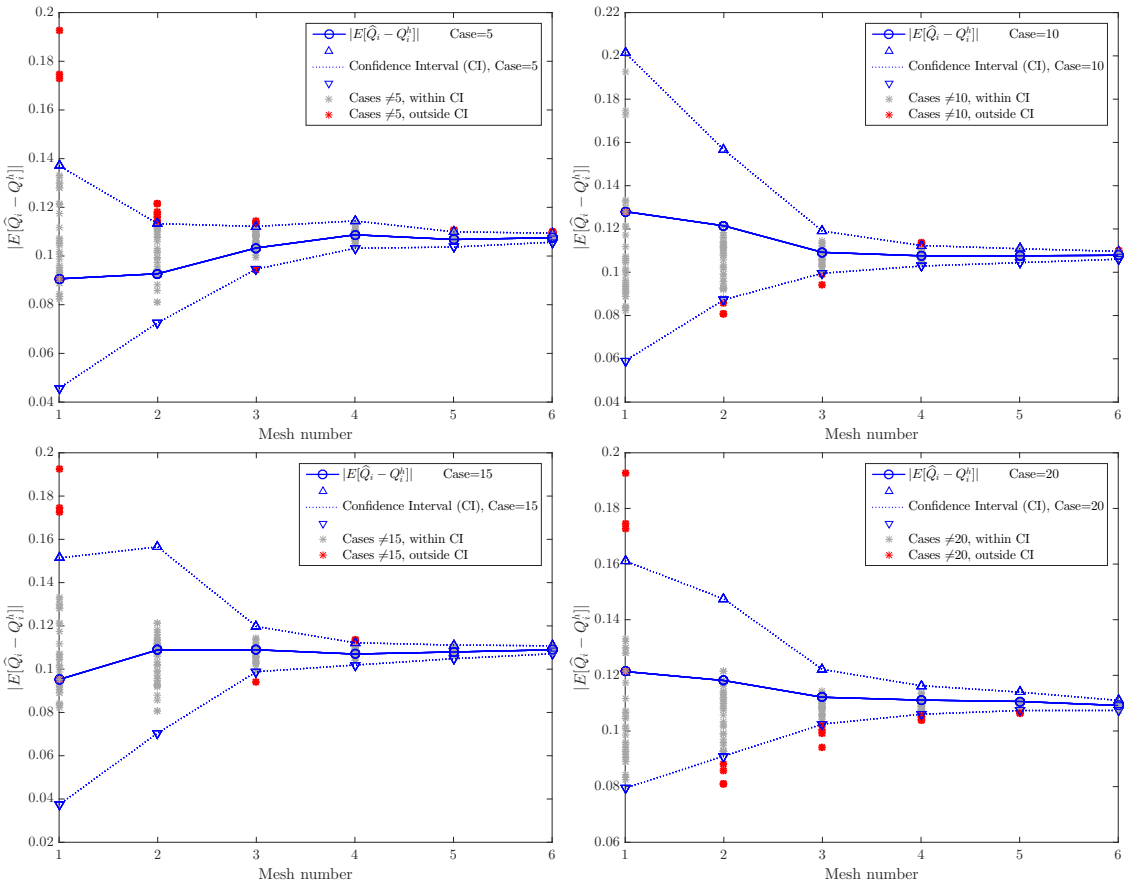

Figure 5.13: Confidence Interval validation

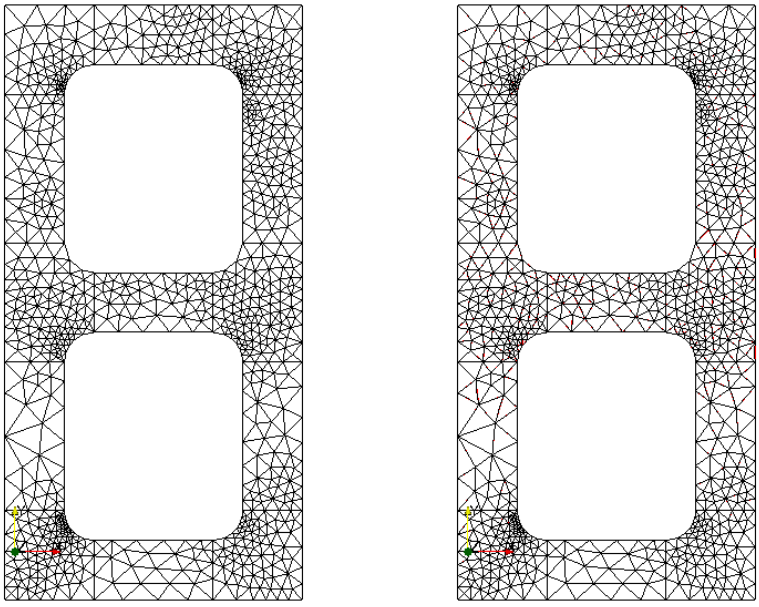

(a) Minimum 160 samples
Then check CI

(b) Minimum 40960 samples
No CI implemented

Figure 5.14: Final mesh for 6 local refinements

through CIs, the final mesh for different sampling strategies is tested. Adapted meshes are included in figure 5.14 with and without the implementation of CIs and cutting early.

It is clear that both sampling strategies lead to almost the same refined mesh. The implementation of CIs is then an excellent tool to save computational time. This is particularly helpful when PCE is not included in the algorithm, which is a sensible choice if the number of dimensions of the stochastic space is large enough. In this case, the curse of dimensionality makes evaluating the Hermite-Gauss quadrature points really expensive in computational time terms.

5.6 Conclusions

Discretisation error and parametric uncertainty can be linked under a single convergence criterion that rules the error in spatial, surrogate and parametric spaces. This

linkage allows to adaptively refine the spatial discretisation not only to produce an error scaled with the uncertainty, but also to be optimised for a QoI, which is the unknown random variable dependent of the parameters.

The indicator of refinement needs to be based on where the error varies the most. To that effect, if p-refinement reference space is exploited, simply removing all the contribution of the coarse space to the QoI suffices. This leads to a similar indicator to the indicators based on the energy norm, but including the dual weight of the goal-oriented residual.

Results show that the presented algorithm minimises the computational efforts in the spatial discretisation, in the construction of the surrogate and in the MC sampling to characterise the stochastic process. Moreover, an optimal mesh also reduces the computational cost of the model evaluations needed to build the surrogate model or to perform MC sampling if no surrogate model is employed.

This chapter presented the field of Young's moduli as the only parametrised quantity. However, all the algorithmic propositions can be applied to parametrised boundary data and mass densities. Excitation frequency ω may also be treated as an adjustable or unknown parameter.

Chapter 6

Conclusion

The main purpose of the work presented in this thesis is the optimisation of the resolution of discretised boundary value problems with parametric uncertainties. The premise for this optimisation is to identify all sources of error involved in the resolution and to enforce that all of them are of the same order. Due to the different nature of discretisation and stochastic errors, adequate measures to compare them are required. Furthermore, the approach of having a single problem independent criterion controlling the different measures is sought. This criterion is fundamental to automatically control the chain of numerical approximations. To be useful for all types of problems, it must be easily set and it must take into consideration any Quantity of Interest (QoI) plus its variance.

Prior to exploring the relation between all identified errors, each of them has been investigated separately. With this objective, residual error estimators based on Dirichlet BC are selected as the methods to control the discretisation error in chapter 1. Chapter 4 analyses the alternatives within this choice and proposes improved discretisation error estimators. The summarised findings are that patch size exerts the higher impact upon both effectivity and computational cost of residual error estimators. The increase of computational cost can be mostly overcome by using p-refinement in the extended patches. Moreover, the instability introduced by the extension can be addressed through a new family of estimators based on the Saint-Venant principle.

Regarding the parametric error, chapter 2 determines that for the posed problem, the probabilistic approach and polynomial chaos expansion are the most suitable methods to characterise and adaptively reduce the cost of the parametric uncertainty and the stochastic errors.

To conclude the research about self-contained optimisation of errors, chapter 3 attempts to reduce the computational cost at an algebraic level. An analogy between error estimators and preconditioners was successfully tested for a diffusion problem with only Dirichlet boundary conditions. The iterative reduction of the error stagnates after some iterations if Neumann boundary conditions are considered in the initial problem.

Finally, the relation between the described errors is studied and an algorithm driving its adaptive reduction is devised in chapter 5. The local adaptivity residual estimation is extended to goal-oriented quantities of interest. The problem posed to assess the final task is an undamped, steady-state vibration of a structure occupying a bounded domain with a known parametric Young's modulus variation influencing the assumed isotropic linear elasticity behaviour under the assumption of small perturbations. The algorithm presented is completely problem independent and beats uniform refinement in the reduction of the error in a QoI.

6.1 Summary of contributions made

This section consists of a summary of the principal contributions of this dissertation falling into the categories that structure the thesis.

- **Discretisation error control**

  How to improve error control predictions is investigated by means of residual error estimators applying homogeneous Dirichlet boundary conditions. All existing methods in this category split the residual through a partition of unity on the test functions. This partition invariably determines the shape of the local patches. The present work introduces the novel approach to use Saint-Venant principle to define the patches leading to absolute control on

the patch size and shape, as long as the split residual is equilibrated and Saint-Venant principle's distance assumption is fulfilled. Numerical results are provided manifesting that this new approach stabilises some of the previous attempts to define extended element centred patches. Furthermore, since only the residual is split, an additive estimator is obtained overcoming the need of an averaging rule to assemble the global estimation field.

Several existing a-posteriori residual error estimators are reformulated within a common framework allowing not only their comparison but also their hybridisation. Effectivity and efficiency for all the considered estimators are included for a diffusion problem, proving that the new approach allows an improved accuracy if the size of the patches is extended. Moreover, the increase in cost of extended patches is drastically reduced by using polynomial order refinement. Afterwards, a steady convection-diffusion problem is framed to test the validity of the conclusions and the new estimator applied to a non-symmetric problem.

A second minor contribution to error control is an alternative to build an effective indicator of local refinement. In this case, the framework is a dual-weighted goal-oriented error estimator where the QoI does not involve a gradient. Specifically, the stochastic QoI is the expectation of the average of horizontal displacements in a sub-domain of the vibrating structure problem defined at section 5.2.2. Direct localisations of the influence field under these circumstances fail to point to areas where local refinement speeds the error convergence. Most existing methods overcome this difficulty by including a gradient, either directly within the QoI or as an independent estimator to be combined with the goal-oriented local estimator. Another published alternative is to exploit the same principles as the equilibrated residual method. The new proposed approach is based on exploiting Galerkin orthogonality to remove the coarse FE component of the influence field. Then, the local contributions to the influence field are proportional to the local error growth and not to its magnitude. Numerical results are provided supporting the idea that

for the posed vibration problem, pointing to the larger local variation of the error makes a good indicator of refinement, while pointing to larger local error magnitude does not.

- **Improved approximation of the global rich solution by iterative solving local preconditioned system of equations by means of error estimation**

  Error estimation allows the approximation of the solution of a global system of equations by means of a collection of local ones defined at a patch level. On the other hand, preconditioners serve the same purpose when integrated on an iterative method to solve systems of equations. This analogy is further tested by integrating an error estimator as a preconditioner to solve the global system of equations resulting from applying a rich discretisation to a diffusion problem posed. FGMRES and a node centered error estimator where selected because both are based on the residual.

  The analogy would allow to select a target discrete space considered as truth space and iteratively improve the quality of the error estimation belonging to that space. If enough accuracy is requested the iterative approximation can converge with the truth. Nevertheless, if lesser accuracy is required the iterative solver can stop early saving computational time at the expense of losing Galerkin orthogonality in the solution belonging to the truth space.

  Numerical results show excellent performance if only Dirichlet BC are enforced. On the contrary, if Neumann BC are enforced, the convergence to the exact global solution for the rich discretisation reaches a plateau.

- **Simultaneous stochastic and discretisation error control**

  The final and main novel contribution of the ongoing dissertation is an algorithm to optimise and simultaneously control discretisation error, parametric uncertainty, the error introduced by a surrogate model and Monte Carlo sampling error. The single stopping criterion for the algorithm is a relative user defined tolerance or target value. This tolerance is applied to the normalised

difference between the expectation of the QoI using the coarse and rich solutions for each mesh refinement step, where the rich solution can be estimated. For a problem independent normaliser that aims to adequately characterise the stochastic process, the standard deviation can be employed as normaliser. For a problem dependent normaliser the expectation of the coarse QoI can be used, but then, the QoI must be specially selected to describe the problem to solve and the variation around it must not be important.

To the author's knowledge, the only published studies about the relation between the stochastic and discretisation errors are within a SFEM framework [110, 51, 188]. Since stochastic characterisation is enforced at an elemental level in SFEM, this is a major issue which leads some authors to propose two different meshes. Outside SFEM the issue remains, even tough in an indirect manner, where paired meshes are not necessary. For that matter, the devised algorithm aims to enforce that discretisation error is small enough not to interfere in the stochastic process and at the same time, computational time is not lost due to unnecessary discretisation if the stochastic variation is larger. This balance defines the locally adapted optimal relation.

Regarding stochastic optimisation, polynomial chaos expansion is adopted to reduce the cost of producing samples. Bootstrapping techniques are employed to obtain percentiles providing confidence levels for the normalised difference of expectations. Graphical evidence is provided for the need of a normalised criterion and the suitability of symmetric percentiles to obtain certainty that either local refined is needed or the expected accuracy has been reached. If the measure lies between the percentiles, uncertainty must be reduced by adding samples.

Each ingredient of the algorithm has been tested individually and the subsequent results are included. Finally, numerical results for the convergence of the method are provided improving the performance of uniform refinement, which is designated as benchmark.

6.2 Future research

Some of the directions of research that could extend the work presented in this dissertation are listed in this section.

- The analogy between error estimation and preconditioners is inconclusive for problems considering Neumann boundary conditions. It remains to be determined if the reason of the convergence stagnation is related to the convergence issues of FGMRES or if the analogy is valid only under certain conditions.

- The flexibility of patches introduced by the novel error estimation seems specially suitable for methods with ghost penalties [37]. For instance, in cutFEM elements [38], the elements in the interface are linked to adjacent ones. Otherwise, the resulting small area of integration leads to ill conditioning. It seems that designing patches where both elements are included may be particularly useful under these circumstances.

- The conducted numerical experiments make clear that the combination of the expectation as a measure of the stochastic characterisation and PCE surrogates is not appropriate for angular frequencies close to the natural frequencies. The reason is that samples close to any natural frequency completely modify the expectation, and PCE can not reproduce these peaks. Assessing the algorithm with no surrogate model is of special interest in this situation, but the computational time required to reach convergence made it impossible to include results in this dissertation.

- The present work could be easily extended to stochastic inverse problems where Kalman filters [94, 65] or Bayesian Inversion [46, 168] are the most popular methods. In these methods there is not known PDF of the primary process, which is a strong assumption in this work. Instead, the initial primary PDF is a prior belief that is corrected through Gaussian regression.

Bibliography

[1] Abdulle, A. and Nonnenmacher, A. [2011]. "Adaptive finite element heterogeneous multiscale method for homogenization problems". *Comput. Methods Appl. Mech. Eng.*, vol. 200(37-40):pp. 2710–2726. ISSN 00457825. doi: 10.1016/j.cma.2010.06.012.

[2] Abramowitz, M.; Stegun, I.A.; and Romer, R.H. [1972]. *Handbook of Mathematical Functions with Formulas, Graphs, and Mathematical Tables*. National bureau of standards applied mathematics, Washington, 10 edn. ISBN 0486612724, 1046 pp.

[3] Ainsworth, M. [1996]. "The influence and selection of subspaces for a posteriori error estimators". *Numer. Math.*, vol. 73(4):pp. 399–418. ISSN 0029-599X. doi: 10.1007/s002110050198.

[4] Ainsworth, M. and Oden, J.T. [1993]. "A unified approach to a posteriori error estimation using element residual methods". *Numer. Math.*, vol. 65(1):pp. 23–50. ISSN 0029-599X. doi: 10.1007/BF01385738.

[5] Ainsworth, M. and Oden, J.T. [1997]. "A posteriori error estimation in finite element analysis". *Comput. Methods Appl. Mech. Eng.*, vol. 142(1-2):pp. 1–88. ISSN 00457825. doi: 10.1016/S0045-7825(96)01107-3.

[6] Ainsworth, M. and Oden, J.T. [2000]. *A Posteriori Error Estimation in Finite Element Analysis*. John Wiley & Sons, Inc., Hoboken, NJ, USA. ISBN 9780471294115, 240 pp. doi: 10.1002/9781118032824.

[7] Argyris, J.; Papadrakakis, M.; and Stefanou, G. [2002]. "Stochastic finite element analysis of shells". *Comput. Methods Appl. Mech. Eng.*, vol. 191(41-42):pp. 4781–4804. ISSN 00457825. doi: 10.1016/S0045-7825(02)00404-8.

[8] Arnoldi, W.E. [1951]. "The principle of minimized iterations in the solution of the matrix eigenvalue problem". *Q. Appl. Math.*, vol. 9(1):pp. 17–29. ISSN 0033-569X. doi: 10.1090/qam/42792.

[9] Askes, H. and Sluys, L.J. [2000]. "Remeshing strategies for adaptive ALE analysis of strain localization". *Eur. J. Mech. A/Solids*, vol. 19(3):pp. 447–467. ISSN 09977538. doi: 10.1016/S0997-7538(00)00176-5.

[10] Auzinger, W. and Melenk, J.M. [2011]. *Iterative Solution of Large Linear Systems*. Elsevier, Wien, 174 pp.

[11] Axelsson, O. [1994]. *Iterative Solution Methods*. Cambridge University Press. doi: 10.1017/CBO9780511624100.

[12] Axelsson, O. and Vassilevski, P.S. [1991]. "A Black Box Generalized Conjugate Gradient Solver with Inner Iterations and Variable-Step Preconditioning". *SIAM J. Matrix Anal. Appl.*, vol. 12(4):pp. 625–644. ISSN 0895-4798. doi: 10.1137/0612048.

[13] Babuška, I.; Griebel, M.; and Pitkäranta, J. [1989]. "The problem of selecting the shape functions for ap-type finite element". *Int. J. Numer. Methods Eng.*, vol. 28(8):pp. 1891–1908. ISSN 0029-5981. doi: 10.1002/nme.1620280813.

[14] Babuška, I. and Miller, A. [1984]. "The post-processing approach in the finite element method—part 1: Calculation of displacements, stresses and other higher derivatives of the displacements". *Int. J. Numer. Methods Eng.*, vol. 20(6):pp. 1085–1109. ISSN 0029-5981. doi: 10.1002/nme.1620200610.

[15] Babuška, I. and Miller, A. [1987]. "A feedback finite element method with a posteriori error estimation: Part I. The finite element method and some basic properties of the a posteriori error estimator". *Comput. Methods Appl. Mech. Eng.*, vol. 61(1):pp. 1–40. ISSN 00457825. doi: 10.1016/0045-7825(87)90114-9.

[16] Babuška, I.; Nobile, F.; and Tempone, R. [2005]. "Worst case scenario analysis for elliptic problems with uncertainty". *Numer. Math.*, vol. 101(2):pp. 185–219. ISSN 0029-599X. doi: 10.1007/s00211-005-0601-x.

[17] Babuška, I.; Nobile, F.; and Tempone, R. [2010]. "A Stochastic Collocation Method for Elliptic Partial Differential Equations with Random Input Data". *SIAM Rev.*, vol. 52(2):pp. 317–355. ISSN 0036-1445. doi: 10.1137/100786356.

[18] Babuška, I. and Rheinboldt, W.C. [1978]. "A-posteriori error estimates for the finite element method". *Int. J. Numer. Methods Eng.*, vol. 12(10):pp. 1597–1615. ISSN 0029-5981. doi: 10.1002/nme.1620121010.

[19] Babuška, I. and Strouboulis, T. [2001]. *The Finite Element Method and Its Reliability*. Oxford University Press, Oxford. ISBN 9780198502760, 814 pp.

[20] Babuvška, I. and Rheinboldt, W.C. [1978]. "Error Estimates for Adaptive Finite Element Computations". *SIAM J. Numer. Anal.*, vol. 15(4):pp. 736–754. ISSN 0036-1429. doi: 10.1137/0715049.

[21] Baier, C.; D'Argenio, P.; and Groesser, M. [2006]. "Partial Order Reduction for Probabilistic Branching Time". *Electron. Notes Theor. Comput. Sci.*, vol. 153(2):pp. 97–116. ISSN 15710661. doi: 10.1016/j.entcs.2005.10.034.

[22] Bangerth, W. and Rannacher, R. [2001]. "Adaptive Finite Element techniques for the acoustic wave equation". *J. Comput. Acoust.*, vol. 09(02):pp. 575–591. ISSN 0218-396X. doi: 10.1142/S0218396X01000668.

[23] Barthelmann, V.; Novak, E.; and Ritter, K. [2000]. "High dimensional polynomial interpolation on sparse grids". *Adv. Comput. Math.*, vol. 12(4):pp. 273–288. doi: 10.1023/A:1018977404843.

[24] Basu, N.K. [1970]. "Error estimates for a Chebyshev quadrature method". *Math. Comput.*, vol. 24(112):pp. 863–863. ISSN 0025-5718. doi: 10.1090/S0025-5718-1970-0277111-6.

[25] Becker, R. and Rannacher, R. [1996]. "A feed-back approach to error control in finite element methods: Basic Analysis and Examples". *East-West J. Numer.*, vol. 4:pp. 237–264.

[26] Becker, R.; Rannacher, R.; and Suttmeier, F.T. [1997]. "A feed-back approach to error control in finite element methods: application to linear elasticity". *Comput. Mech.*, vol. 19:pp. 434–446. ISSN 0178-7675. doi: 10.1007/s004660050191.

[27] Ben-Haim, Y. [1994]. "A non-probabilistic concept of reliability". *Struct. Saf.*, vol. 14(4):pp. 227–245. ISSN 01674730. doi: 10.1016/0167-4730(94)90013-2.

[28] Bender, C.M. and Orszag, S.A. [1999]. *Advanced Mathematical Methods for Scientists and Engineers I.* Springer New York, New York, NY. ISBN 978-1-4419-3187-0. doi: 10.1007/978-1-4757-3069-2.

[29] Berger, M.J. [1982]. *Adaptive Mesh Refinement for hyperbolic differential equations.* Ph.D. thesis, Stanford University.

[30] Binev, P.; Dahmen, W.; and DeVore, R. [2004]. "Adaptive Finite Element Methods with convergence rates". *Numer. Math.*, vol. 97(2):pp. 219–268. ISSN 0029-599X. doi: 10.1007/s00211-003-0492-7.

[31] Blatman, G. [2009]. *Adaptive sparse polynomial chaos expansions for uncertainty propagation and sensitivity analysis.* Ph.D. thesis, Université Blaise Pascal - Clermont II.

[32] Blatman, G. and Sudret, B. [2008]. "Sparse polynomial chaos expansions and adaptive stochastic finite elements using a regression approach". *Comptes Rendus Mécanique*, vol. 336(6):pp. 518–523. ISSN 16310721. doi: 10.1016/j.crme.2008.02.013.

[33] Brenan, K.E.; Campbell, S.L.; and Petzold, L.R. [1995]. *Numerical Solution of Initial-Value Problems in Differential-Algebraic Equations*. Society for Industrial and Applied Mathematics, Philadelphia. ISBN 978-0-89871-353-4, 256 pp. doi: 10.1137/1.9781611971224.

[34] Brenner, S.C. and Scott, L.R. [2008]. *The Mathematical Theory of Finite Element Methods*, vol. 15 of *Texts in Applied Mathematics*. Springer New York, New York, NY. ISBN 978-0-387-75933-3, 391 pp. doi: 10.1007/978-0-387-75934-0.

[35] Brezinski, C. [1997]. "Projection methods for linear systems". *J. Comput. Appl. Math.*, vol. 77(1-2):pp. 35–51. ISSN 03770427. doi: 10.1016/S0377-0427(96)00121-5.

[36] Bucher, C.G. [1988]. "Adaptive sampling — an iterative fast Monte Carlo procedure". *Struct. Saf.*, vol. 5(2):pp. 119–126. ISSN 01674730. doi: 10.1016/0167-4730(88)90020-3.

[37] Burman, E. [2010]. "Ghost penalty". *Comptes Rendus Math.*, vol. 348(21-22):pp. 1217–1220. ISSN 1631073X. doi: 10.1016/j.crma.2010.10.006.

[38] Burman, E.; et al. [2015]. "CutFEM: Discretizing geometry and partial differential equations". *Int. J. Numer. Methods Eng.*, vol. 104(7):pp. 472–501. ISSN 00295981. doi: 10.1002/nme.4823.

[39] Çalik-Karaköse, Ü.H. and Askes, H. [2015]. "A recovery-type a posteriori error estimator for gradient elasticity". *Comput. Struct.*, vol. 154:pp. 204–209. ISSN 00457949. doi: 10.1016/j.compstruc.2015.04.003.

[40] Carstensen, C.; et al. [2014]. "Axioms of adaptivity". *Comput. Math. with Appl.*, vol. 67(6):pp. 1195–1253. ISSN 08981221. doi: 10.1016/j.camwa.2013.12.003.

[41] Chamoin, L.; et al. [2016]. *Verifying Calculations - Forty Years On*. SpringerBriefs in Applied Sciences and Technology. Springer International Publishing, Cham, 1st edn. ISBN 978-3-319-20552-6. doi: 10.1007/978-3-319-20553-3.

[42] Chen, L. and Rao, S. [1997]. "Fuzzy finite-element approach for the vibration analysis of imprecisely-defined systems". *Finite Elem. Anal. Des.*, vol. 27(1):pp. 69–83. ISSN 0168874X. doi: 10.1016/S0168-874X(97)00005-X.

[43] Chen, Q.; et al. [2018]. "A stochastic micromechanical model for fiber-reinforced concrete using maximum entropy principle". *Acta Mech.*, vol. 229(7):pp. 2719–2735. ISSN 0001-5970. doi: 10.1007/s00707-018-2135-1.

[44] Cirak, F. and Ramm, E. [1998]. "A posteriori error estimation and adaptivity for linear elasticity using the reciprocal theorem". *Comput. Methods Appl. Mech. Eng.*, vol. 156(1-4):pp. 351–362. ISSN 00457825. doi: 10.1016/S0045-7825(97)00220-X.

[45] Clenshaw, C.W. and Curtis, A.R. [1960]. "A method for numerical integration on an automatic computer". *Numer. Math.*, vol. 2(1):pp. 197–205. ISSN 0029-599X. doi: 10.1007/BF01386223.

[46] Cotter, S.L.; Dashti, M.; and Stuart, A.M. [2010]. "Approximation of Bayesian Inverse Problems for PDEs". *SIAM J. Numer. Anal.*, vol. 48(1):pp. 322–345. ISSN 0036-1429. doi: 10.1137/090770734.

[47] Courant, R. [1943]. "Variational methods for the solution of problems of equilibrium and vibrations". *Bull. Am. Math. Soc.*, vol. 49(1):pp. 1–24. ISSN 0002-9904. doi: 10.1090/S0002-9904-1943-07818-4.

[48] de Almeida, J.P.M. and Maunder, E.A. [2017]. *Equilibrium Finite Element Formulations*. John Wiley & Sons, Ltd, Chichester, UK. ISBN 9781118925782, 73–110 pp. doi: 10.1002/9781118925782.

[49] de. Saint-Venant, M. [1855]. *Memoire sur la torsion des prismes*. [S.l.], Harvard University, Digitalised by Google, 332 pp.

[50] Deckelnick, K. and Hinze, M. [2003]. "Error Estimates in Space and Time for Tracking-type Control of the Instationary Stokes System". *In* W. Desch; F. Kappel; and K. Kunisch, eds., "Control Estim. Distrib. Param. Syst.", pp. 87–103. Birkhäuser Basel, Basel. ISBN 978-3-0348-8001-5. doi: 10/bf7xvt.

[51] Der Kiureghian, A. and Ke, J.B. [1988]. "The stochastic finite element method in structural reliability". *Probabilistic Eng. Mech.*, vol. 3(2):pp. 83–91. ISSN 02668920. doi: 10.1016/0266-8920(88)90019-7.

[52] Devroye, L. [1986]. *Non-Uniform Random Variate Generation*. Springer New York, New York, NY. ISBN 978-1-4613-8645-2, 843 pp. doi: 10.1007/978-1-4613-8643-8.

[53] Di Stolfo, P.; et al. [2016]. "An easy treatment of hanging nodes in hp-finite elements". *Finite Elem. Anal. Des.*, vol. 121:pp. 101–117. ISSN 0168874X. doi: 10.1016/j.finel.2016.07.001.

[54] Díez, P.; Parés, N.; and Huerta, A. [2003]. "Recovering lower bounds of the error by postprocessing implicit residual a posteriori error estimates". *Int. J. Numer. Methods Eng.*, vol. 56(10):pp. 1465–1488. ISSN 00295981. doi: 10.1002/nme.620.

[55] Donea, J.; et al. [2004]. "Arbitrary Lagrangian-Eulerian Methods". *In* "Encycl. Comput. Mech.", pp. 1–25. John Wiley & Sons, Ltd, Chichester, UK. ISBN 0470846992. doi: 10.1002/0470091355.ecm009.

[56] Dörfler, W. [1996]. "A Convergent Adaptive Algorithm for Poisson's Equation". *SIAM J. Numer. Anal.*, vol. 33(3):pp. 1106–1124. ISSN 0036-1429. doi: 10.1137/0733054.

[57] Douglas, J. and Dupont, T. [1975]. "A Galerkin Method for a Nonlinear Dirichlet Problem". *Math. Comput.*, vol. 29(131):p. 689. ISSN 00255718. doi: 10.2307/2005280.

[58] Dubois, D. and Prade, H., eds. [2000]. *Fundamentals of Fuzzy Sets*, vol. 7 of *The Handbooks of Fuzzy Sets Series*. Springer US, Boston, MA. ISBN 978-1-4613-6994-3. doi: 10.1007/978-1-4615-4429-6.

[59] Efron, B. [1979]. "Bootstrap Methods: Another Look at the Jackknife". *Ann. Stat.*, vol. 7(1):pp. 1–26. ISSN 0090-5364. doi: 10.1214/aos/1176344552.

[60] Eliáš, J.; et al. [2015]. "Stochastic discrete meso-scale simulations of concrete fracture: Comparison to experimental data". *Eng. Fract. Mech.*, vol. 135:pp. 1–16. ISSN 00137944. doi: 10.1016/j.engfracmech.2015.01.004.

[61] Estep, D. and French, D. [1994]. "Global error control for the continuous Galerkin finite element method for ordinary differential equations". *ESAIM Math. Model. Numer. Anal.*, vol. 28(7):pp. 815–852. ISSN 0764-583X. doi: 10.1051/m2an/1994280708151.

[62] Estep, D.J.; Larson, M.G.; and Williams, R.D. [2000]. "Estimating the error of numerical solutions of systems of reaction-diffusion equations". *Mem. Am. Math. Soc.*, vol. 146(696):pp. 0–0. ISSN 0065-9266. doi: 10.1090/memo/0696.

[63] Evans, D.H. [1971]. "An Application of Numerical Integration Techniques to Statistical Tolerancing, II: A Note on the Error". *Technometrics*, vol. 13(2):p. 315. ISSN 00401706. doi: 10.2307/1266793.

[64] Evans, D.H. [1972]. "An Application of Numerical Integration Techniques to Statistical Tolerancing, III—General Distributions". *Technometrics*, vol. 14(1):pp. 23–35. ISSN 0040-1706. doi: 10.1080/00401706.1972.10488880.

[65] Evensen, G. [2003]. "The Ensemble Kalman Filter: theoretical formulation and practical implementation". *Ocean Dyn.*, vol. 53(4):pp. 343–367. ISSN 1616-7341. doi: 10.1007/s10236-003-0036-9.

[66] Falk, R.S. [1973]. "Approximation of a class of optimal control problems with order of convergence estimates". *J. Math. Anal. Appl.*, vol. 44(1):pp. 28–47. ISSN 10960813. doi: 10.1016/0022-247X(73)90022-X.

[67] Falk, R.S. [1983]. "Error Estimates for the Numerical Identification of a Variable Coefficient". *Math. Comput.*, vol. 40(162):p. 537. ISSN 00255718. doi: 10.2307/2007529.

[68] Falsone, G. and Lombardo, M. [2007]. "Stochastic representation of the mechanical properties of irregular masonry structures". *Int. J. Solids Struct.*, vol. 44(25-26):pp. 8600–8612. ISSN 00207683. doi: 10.1016/j.ijsolstr.2007.06.030.

[69] Ferenc, J. [2013]. "The random variability analysis of the mechanical properties of the selected aluminum alloys". *Tech. Trans.*, vol. 9:pp. 3–18.

[70] Ferrante, F.J.; et al. [2008]. "An Overview of Micromechanics-Based Techniques for the Analysis of Microstructural Randomness in Functionally Graded Materials". *In* "AIP Conf. Proc.", vol. 973, pp. 190–195. AIP. ISSN 0094243X. doi: 10.1063/1.2896775.

[71] Filippi, S. [1964]. "Angenäherte Tschebyscheff-Approximation einer Stammfunktion - eine Modifikation des Verfahrens von Clenshaw und Curtis". *Numer. Math.*, vol. 6(1):pp. 320–328. ISSN 0029-599X. doi: 10.1007/BF01386080.

[72] Gentle, J. [2003]. *Random Number Generation and Monte Carlo Methods*. Statistics and Computing. Springer-Verlag, New York, 2 edn., 382 pp. doi: 10.1007/b97336.

[73] Ghanem, R.G. and Spanos, P.D. [1991]. *Stochastic Finite Elements: A Spectral Approach*. Springer New York, New York, NY, 1 edn. ISBN 978-1-4612-7795-8, 214 pp. doi: 10.1007/978-1-4612-3094-6.

[74] Gilks, W.R.; Richardson, S.; and Spiegelhalter, D.J. [1995]. *Markov Chain Monte Carlo in Practise*. Chapman and Hall/CRC. ISBN 9780412055515, 504 pp.

[75] González-Estrada, O.A.; et al. [2014]. "Mesh adaptivity driven by goal-oriented locally equilibrated superconvergent patch recovery". *Comput. Mech.*, vol. 53(5):pp. 957–976. ISSN 01787675. doi: 10.1007/s00466-013-0942-8.

[76] Graham, L. and Deodatis, G. [2001]. "Response and eigenvalue analysis of stochastic finite element systems with multiple correlated material and geometric properties". *Probabilistic Eng. Mech.*, vol. 16(1):pp. 11–29. ISSN 02668920. doi: 10.1016/S0266-8920(00)00003-5.

[77] Grätsch, T. and Bathe, K.J.J. [2005]. "A posteriori error estimation techniques in practical finite element analysis". *Comput. Struct.*, vol. 83(4-5):pp. 235–265. ISSN 00457949. doi: 10.1016/j.compstruc.2004.08.011.

[78] Greenbaum, A. [1997]. *Iterative Methods for Solving Linear Systems*. Society for Industrial and Applied Mathematics. ISBN 978-0-89871-396-1. doi: 10.1137/1.9781611970937.

[79] Grigoriu, M. [1993]. "On the spectral representation method in simulation". *Probabilistic Eng. Mech.*, vol. 8(2):pp. 75–90. ISSN 02668920. doi: 10.1016/0266-8920(93)90002-D.

[80] Guan, X.; et al. [2015]. "A stochastic multiscale model for predicting mechanical properties of fiber reinforced concrete". *Int. J. Solids Struct.*, vol. 56-57:pp. 280–289. ISSN 00207683. doi: 10.1016/j.ijsolstr.2014.10.008.

[81] Gunzburger, M.D. and Hou, L.S. [1996]. "Finite-Dimensional Approximation of a Class of Constrained Nonlinear Optimal Control Problems". *SIAM J. Control Optim.*, vol. 34(3):pp. 1001–1043. ISSN 0363-0129. doi: 10.1137/S0363012994262361.

[82] Hasofer, A.M. and Lind, N. [1974]. "Exact and Invariant Second Moment Code Format". *J. Eng. Mech.*, vol. 100:pp. 111–121.

[83] He, J. and Fu, Z.F. [2001]. *Modal Analysis*. Butterworth-heinemann, Oxford, 304 pp. doi: 10.1016/B978-0-7506-5079-3.X5000-1.

[84] Helton, J. and Davis, F. [2003]. "Latin hypercube sampling and the propagation of uncertainty in analyses of complex systems". *Reliab. Eng. Syst. Saf.*, vol. 81(1):pp. 23–69. ISSN 09518320. doi: 10.1016/S0951-8320(03)00058-9.

[85] Hoffman, J. [2004]. "On Duality-Based A Posteriori Error Estimation in Various Norms and Linear Functionals for Large Eddy Simulation". *SIAM J. Sci. Comput.*, vol. 26(1):pp. 178–195. ISSN 1064-8275. doi: 10.1137/S1064827503417198.

[86] Hrennikoff, A. [1941]. "Solution of problems of elasticity by the framework method". *J. Appl. Mech.*, vol. 8(4):pp. 165–175.

[87] Hu, X.; et al. [2016]. "Review of improved Monte Carlo methods in uncertainty-based design optimization for aerospace vehicles". *Prog. Aerosp. Sci.*, vol. 86:pp. 20–27. ISSN 03760421. doi: 10.1016/j.paerosci.2016.07.004.

[88] Huerta, A.; Rodriguez-Ferran, A.; and Díez, P. [2002]. "Error estimation and adaptivity for nonlinear FE analysis". *Int. J. Appl. Math. Comput. Sci.*, vol. 12(1):pp. 59–70.

[89] Hughes, T.J.R. [2000]. *The Finite Element Method: Linear Static and Dynamic Finite Element Analysis: Thomas J. R. Hughes*. Dover, Mineola, New York. ISBN 0-486-41181-8, 682 pp.

[90] Huhtala, A.; Bossuyt, S.; and Hannukainen, A. [2014]. "A priori error estimate of the finite element solution to a Poisson inverse source problem". *Inverse Probl.*, vol. 30(8):p. 085007. ISSN 0266-5611. doi: 10.1088/0266-5611/30/8/085007.

[91] Husslage, B.G.M.; et al. [2011]. "Space-filling Latin hypercube designs for computer experiments". *Optim. Eng.*, vol. 12(4):pp. 611–630. ISSN 1389-4420. doi: 10.1007/s11081-010-9129-8.

[92] Johnson, N.L.; Kotz, S.; and Balakrishnan, N. [1994]. *Continuous Univariate Distributions, vol. 1*. Wiley \& Sons, New York, NY, USA. ISBN 9780471584940, 784 pp.

[93] Kahn, H. and Marshall, A.W. [1953]. "Methods of Reducing Sample Size in Monte Carlo Computations". *J. Oper. Res. Soc. Am.*, vol. 1(5):pp. 263–278. ISSN 0030-364X.

[94] Kalman, R.E. [1960]. "A New Approach to Linear Filtering and Prediction Problems". *J. Basic Eng.*, vol. 82(1):p. 35. ISSN 00219223. doi: 10.1115/1.3662552.

[95] Karkkainen, T. [1996]. "Error Estimates for Distributed Parameter Identification in Linear Elliptic Equations". *J. Math. Syst. Estim. Control*, vol. 6(1):pp. 1–20.

[96] Keese, A. [2003]. "A Review of Recent Developments in the Numerical Solution of Stochastic Partial Differential Equations (Stochastic Finite Elements)". *Intern. Rep.*

[97] Kelley, C.T. [1995]. *Iterative Methods for Linear and Nonlinear Equations*. Society for Industrial and Applied Mathematics. ISBN 978-0-89871-352-7, 166 pp. doi: 10.1137/1.9781611970944.

[98] Kelly, D.W. [1984]. "The self-equilibration of residuals and complementary a posteriori error estimates in the finite element method". *Int. J. Numer. Methods Eng.*, vol. 20(8):pp. 1491–1506.

[99] Kelly, D.W.; et al. [1983]. "A posteriori error analysis and adaptive processes in the finite element method: Part I—Error analysis". *Int. J. Numer. Methods Eng.*, vol. 19(11):pp. 1593–1619.

[100] Kerfriden, P.; Ródenas, J.J.; and Bordas, S.P.A. [2014]. "Certification of projection-based reduced order modelling in computational homogenisation by the constitutive relation error". *Int. J. Numer. Methods Eng.*, vol. 97(6):pp. 395–422. ISSN 00295981. doi: 10.1002/nme.4588.

[101] Kleiber, M. and Hien, T. [1992]. *The stochastic finite element method (basic perturbation technique and computer implementation)*. Wiley-Blackwell, Chichester, U.K. ISBN 978-0471936268, 336 pp.

[102] Kleijnen, J.P. [2009]. "Kriging metamodeling in simulation: A review". *Eur. J. Oper. Res.*, vol. 192(3):pp. 707–716. ISSN 03772217. doi: 10.1016/j.ejor.2007.10.013.

[103] Korotov, S. [2008]. "Global a posteriori error estimates for convection-reaction-diffusion problems". *Appl. Math. Model.*, vol. 32(8):pp. 1579–1586. ISSN 0307904X. doi: 10.1016/j.apm.2007.04.013.

[104] Kundu, A.; Matthies, H.; and Friswell, M. [2018]. "Probabilistic optimization of engineering system with prescribed target design in a reduced parameter space". *Comput. Methods Appl. Mech. Eng.*, vol. 337:pp. 281–304. ISSN 00457825. doi: 10.1016/j.cma.2018.03.041.

[105] Kus, P.; Solin, P.; and Andrs, D. [2014]. "Arbitrary-level hanging nodes for adaptive hp-FEM approximations in 3D". *J. Comput. Appl. Math.*, vol. 270:pp. 121–133. ISSN 03770427. doi: 10.1016/j.cam.2014.02.010.

[106] Ladeveze, P. and Leguillon, D. [1983]. "Error Estimate Procedure in the Finite Element Method and Applications". *SIAM J. Numer. Anal.*, vol. 20(3):pp. 485–509.

[107] Ladevèze, P.; Puel, G.; and Romeuf, T. [2006]. "Lack of knowledge in structural model validation". *Comput. Methods Appl. Mech. Eng.*, vol. 195(37-40):pp. 4697–4710. ISSN 00457825. doi: 10.1016/j.cma.2005.10.017.

[108] Larson, M.G. and Barth, T.J. [2000]. *Discontinuous Galerkin Methods*, vol. 11 of *Lecture Notes in Computational Science and Engineering*. Springer Berlin Heidelberg, Berlin, Heidelberg. ISBN 978-3-642-64098-8, 363–368 pp. doi: 10.1007/978-3-642-59721-3.

[109] Larsson, F.; Hansbo, P.; and Runesson, K. [2002]. "Strategies for computing goal-oriented a posteriori error measures in non-linear elasticity". *Int. J. Numer. Methods Eng.*, vol. 55(8):pp. 879–894. ISSN 1097-0207. doi: 10.1002/nme.513.

[110] Li, C. and Der Kiureghian, A. [1993]. "Optimal discretization of random fields". *J. Eng. Mech.*, vol. 119(6):pp. 1136–1154. ISSN 0733-9399. doi: 10.1061/(ASCE)0733-9399(1993)119:6(1136).

[111] Li, J. and Chen, J.B. [2004]. "Probability density evolution method for dynamic response analysis of structures with uncertain parameters". *Comput. Mech.*, vol. 34(5):pp. 400–409. ISSN 0178-7675. doi: 10.1007/s00466-004-0583-8.

[112] Li, J.; Masia, M.J.; and Stewart, M.G. [2017]. "Stochastic spatial modelling of material properties and structural strength of unreinforced masonry in two-way bending". *Struct. Infrastruct. Eng.*, vol. 13(6):pp. 683–695. ISSN 1573-2479. doi: 10.1080/15732479.2016.1188125.

[113] Li, Y. and Cui, J. [2005]. "The multi-scale computational method for the mechanics parameters of the materials with random distribution of multi-scale grains". *Compos. Sci. Technol.*, vol. 65(9):pp. 1447–1458. ISSN 02663538. doi: 10.1016/j.compscitech.2004.12.016.

[114] Lin, J.; Zhang, Y.; and Zhao, Y. [2011]. "Pseudo Excitation Method and Some Recent Developments". *Procedia Eng.*, vol. 14:pp. 2453–2458. ISSN 18777058. doi: 10.1016/j.proeng.2011.07.308.

[115] Liu, W.K.; Belytschko, T.; and Mani, A. [1986]. "Probabilistic finite elements for nonlinear structural dynamics". *Comput. Methods Appl. Mech. Eng.*, vol. 56(1):pp. 61–81. ISSN 00457825. doi: 10.1016/0045-7825(86)90136-2.

[116] Liu, W.K.; Belytschko, T.; and Mani, A. [1986]. "Random field finite elements". *Int. J. Numer. Methods Eng.*, vol. 23(10):pp. 1831–1845. ISSN 0029-5981. doi: 10.1002/nme.1620231004.

[117] Loeve, M. [1978]. *Probability theory.* Springer-Verlag, New York, 4th edn. ISBN 978-0-387-90262-3, 416 pp.

[118] Madsen, H.; Krenk, S.; and Lind, N. [2006]. *Methods of Structural Safety.* Dover, Mineola, N.Y. ISBN 0486445976, 416 pp.

[119] Mattis, S.A. and Wohlmuth, B. [2018]. "Goal-oriented adaptive surrogate construction for stochastic inversion". *Comput. Methods Appl. Mech. Eng.*, vol. 339:pp. 36–60. ISSN 00457825. doi: 10.1016/j.cma.2018.04.045.

[120] McKay, M.D.; Beckman, R.J.; and Conover, W.J. [1979]. "A Comparison of Three Methods for Selecting Values of Input Variables in the Analysis of Output from a Computer Code". *Technometrics*, vol. 21(2):p. 239. ISSN 00401706. doi: 10.2307/1268522.

[121] Melchers, R.E. [1989]. "Importance sampling in structural systems". *Struct. Saf.*, vol. 6(1):pp. 3–10. ISSN 0167-4730. doi: https://doi.org/10.1016/0167-4730(89)90003-9.

[122] Mirza, S.A.; MacGregor, J.G.; and Hatzinikolas, M. [1979]. "Statistical descriptions of strength of concrete". *J. Struct. Div.*, vol. 105(6):pp. 1021–1037. ISSN 1098-6596.

[123] Morin, P.; Nochetto, R.H.; and Siebert, K.G. [2000]. "Data Oscillation and Convergence of Adaptive FEM". *SIAM J. Numer. Anal.*, vol. 38(2):pp. 466–488. ISSN 0036-1429. doi: 10.1137/S0036142999360044.

[124] Moshtaghin, A.F.; et al. [2016]. "Experimental characterization of longitudinal mechanical properties of clear timber: Random spatial variability and size effects". *Constr. Build. Mater.*, vol. 120:pp. 432–441. ISSN 09500618. doi: 10.1016/j.conbuildmat.2016.05.109.

[125] Neyman, J. [1937]. "Outline of a Theory of Statistical Estimation Based on the Classical Theory of Probability". *Philos. Trans. R. Soc. A Math. Phys. Eng. Sci.*, vol. 236(767):pp. 333–380. ISSN 1364-503X. doi: 10.1098/rsta.1937.0005.

[126] Nobile, F.; Tempone, R.; and Webster, C.G. [2008]. "A Sparse Grid Stochastic Collocation Method for Partial Differential Equations with Random Input Data". *SIAM J. Numer. Anal.*, vol. 46(5):pp. 2309–2345. ISSN 0036-1429. doi: 10.1137/060663660.

[127] Nouy, A. [2009]. "Recent Developments in Spectral Stochastic Methods for the Numerical Solution of Stochastic Partial Differential Equations". *Arch. Comput. Methods Eng.*, vol. 16(3):pp. 251–285. ISSN 1134-3060. doi: 10.1007/s11831-009-9034-5.

[128] Nowak, A.S. and Szerszen, M.M. [2003]. "Calibration of design code for buildings (ACI 318): Part 1 - Statistical models for resistance". *ACI Struct. J.*, vol. 100(3):pp. 377–382. ISSN 08893241.

[129] Oden, J.T. and Prudhomme, S. [2001]. "Goal-oriented error estimation and adaptivity for the finite element method". *Comput. Math. with Appl.*, vol. 41(5-6):pp. 735–756. ISSN 08981221. doi: 10.1016/S0898-1221(00)00317-5.

[130] Paladim, D.A.; et al. [2016]. "Guaranteed error bounds in homogenisation: an optimum stochastic approach to preserve the numerical separation of scales". *Int. J. Numer. Methods Eng.*, vol. 110(2):pp. 103–132. doi: 10.1002/nme.5348.

[131] Pannachet, T.; Askes, H.; and Sluys, L.J. [2009]. "p-Version error estimation for linear elasticity". *Comput. Mech.*, vol. 43(5):pp. 603–615. ISSN 0178-7675. doi: 10.1007/s00466-008-0333-8.

[132] Papadrakakis, M. and Papadopoulos, V. [1996]. "Robust and efficient methods for stochastic finite element analysis using Monte Carlo simulation". *Comput. Methods Appl. Mech. Eng.*, vol. 134(3-4):pp. 325–340. ISSN 00457825. doi: 10.1016/0045-7825(95)00978-7.

[133] Paraschivoiu, M.; Peraire, J.; and Patera, A.T. [1997]. "A posteriori finite element bounds for linear-functional outputs of elliptic partial differential equations". *Comput. Methods Appl. Mech. Eng.*, vol. 150(1-4):pp. 289–312. ISSN 00457825. doi: 10.1016/S0045-7825(97)00086-8.

[134] Parés, N. and Diez, P. [2017]. "A new equilibrated residual method improving accuracy and efficiency of flux-free error estimates". *Comput. Methods Appl. Mech. Eng.*, vol. 313:pp. 785–816. ISSN 00457825. doi: 10.1016/j.cma.2016.10.010.

[135] Parés, N.; et al. [2006]. "The computation of bounds for linear-functional outputs of weak solutions to the two-dimensional elasticity equations". *Comput. Methods Appl. Mech. Eng.*, vol. 195(4-6):pp. 406–429. ISSN 00457825. doi: 10.1016/j.cma.2004.10.013.

[136] Patera, A.T. [1984]. "A spectral element method for fluid dynamics: Laminar flow in a channel expansion". *J. Comput. Phys.*, vol. 54(3):pp. 468–488. ISSN 00219991. doi: 10.1016/0021-9991(84)90128-1.

[137] Pled, F.; Chamoin, L.; and Ladevèze, P. [2011]. "On the techniques for constructing admissible stress fields in model verification: Performances on

engineering examples". *Int. J. Numer. Methods Eng.*, vol. 88(5):pp. 409–441. ISSN 00295981. doi: 10.1002/nme.3180.

[138] Prager, W. and Synge, J.L. [1947]. "Approximations in elasticity based on the concept of function space". *Quart. Appl. Math*, vol. 5(3):pp. 241–269.

[139] Prudhomme, S. and Oden, J.T. [1999]. "On goal-oriented error estimation for elliptic problems: application to the control of pointwise errors". *Comput. Methods Appl. Mech. Eng.*, vol. 176(1):pp. 313–331.

[140] Prudhomme, S.; et al. [2000]. "Review of A Priori Error Estimation for Discontinuous Galerkin Methods". Tech. rep., Texas Institute for Computational and Applied Mathematics.

[141] Pryse, S.; Adhikari, S.; and Kundu, A. [2018]. "Sample-based and sample-aggregated based Galerkin projection schemes for structural dynamics". *Probabilistic Eng. Mech.*, vol. 54:pp. 118–130. ISSN 02668920. doi: 10.1016/j.probengmech.2017.09.002.

[142] Quiñonero-candela, J.; Rasmussen, C.E.; and Herbrich, R. [2005]. "A unifying view of sparse approximate Gaussian process regression". *J. Mach. Learn. Res.*, vol. 6:pp. 1935–1959. ISSN 1533-7928. doi: 10.1163/016918609X12529286896877.

[143] Rafiee, R. and Eskandariyun, A. [2017]. "Comparative study on predicting Young's modulus of graphene sheets using nano-scale continuum mechanics approach". *Phys. E Low-dimensional Syst. Nanostructures*, vol. 90(December 2016):pp. 42–48. ISSN 13869477. doi: 10.1016/j.physe.2017.03.006.

[144] Ramuhalli, P.; Udpa, L.; and Udpa, S. [2005]. "Finite-Element Neural Networks for Solving Differential Equations". *IEEE Trans. Neural Networks*, vol. 16(6):pp. 1381–1392. ISSN 1045-9227. doi: 10.1109/TNN.2005.857945.

[145] Rannacher, R. and Suttmeier, F.T. [1998]. "A posteriori error control in finite element methods via duality techniques: Application to perfect

plasticity". *Comput. Mech.*, vol. 21(2):pp. 123–133. ISSN 0178-7675. doi: 10.1007/s004660050288.

[146] Rannacher, R. and Vexler, B. [2005]. "A Priori Error Estimates for the Finite Element Discretization of Elliptic Parameter Identification Problems with Pointwise Measurements". *SIAM J. Control Optim.*, vol. 44(5):pp. 1844–1863. ISSN 0363-0129. doi: 10.1137/040611100.

[147] Robert, C.P. and Casella, G. [2004]. *Monte Carlo Statistical Methods*. Springer New York. ISBN 978-0-387-21239-5.

[148] Robert, C.P. and Casella, G. [2004]. *Monte Carlo Statistical Methods*. Springer Texts in Statistics. Springer New York, New York, NY. ISBN 978-1-4419-1939-7. doi: 10.1007/978-1-4757-4145-2.

[149] Ródenas, J.J.; et al. [2007]. "Improvement of the superconvergent patch recovery technique by the use of constraint equations: the SPR-C technique". *Int. J. Numer. Methods Eng.*, vol. 70(6):pp. 705–727.

[150] Rognes, M.E. and Logg, A. [2013]. "Automated Goal-Oriented Error Control I: Stationary Variational Problems". *SIAM J. Sci. Comput.*, vol. 35(3):pp. C173–C193. ISSN 1064-8275. doi: 10.1137/10081962X.

[151] Rubinstein, R.Y. and Kroese, D.P. [2007]. *Simulation and the Monte Carlo Method*. Wiley Series in Probability and Statistics. John Wiley & Sons, Inc., Hoboken, NJ, USA, 2 edn. ISBN 9780470230381, 345 pp. doi: 10.1002/9780470230381.

[152] Saad, Y. [1993]. "A Flexible Inner-Outer Preconditioned GMRES Algorithm". *SIAM J. Sci. Comput.*, vol. 14(2):pp. 461–469. ISSN 1064-8275. doi: 10.1137/0914028.

[153] Saad, Y. [2003]. *Iterative Methods for Sparse Linear Systems*. Society for Industrial and Applied Mathematics. ISBN 978-0-89871-534-7, 547 pp. doi: 10.1137/1.9780898718003.

[154] Saad, Y. and Schultz, M.H. [1986]. "GMRES: A Generalized Minimal Residual Algorithm for Solving Nonsymmetric Linear Systems". *SIAM J. Sci. Stat. Comput.*, vol. 7(3):pp. 856–869. ISSN 0196-5204. doi: 10.1137/0907058.

[155] Saad, Y. and Van Der Vost, H.A. [2000]. "Iterative solution of linear systems in the 20th century". *J. Comput. Appl. Math.*, vol. 123(1):pp. 1–33.

[156] Sachdeva, S.K.; Nair, P.B.; and Keane, A.J. [2006]. "Comparative study of projection schemes for stochastic finite element analysis". *Comput. Methods Appl. Mech. Eng.*, vol. 195(19-22):pp. 2371–2392. ISSN 00457825. doi: 10.1016/j.cma.2005.05.010.

[157] Sandboge, R. [1999]. "Adaptive Finite Element methods for reactive compressible flow". *Math. Model. Methods Appl. Sci.*, vol. 09(02):pp. 211–241. ISSN 0218-2025. doi: 10.1142/S0218202599000129.

[158] Sankaran, S. [2009]. "Stochastic optimization using a sparse grid collocation scheme". *Probabilistic Eng. Mech.*, vol. 24(3):pp. 382–396. ISSN 02668920. doi: 10.1016/j.probengmech.2008.11.002.

[159] Sauer-Buge, A. and Peraire, J. [2004]. "Computing Bounds for Linear Functionals of Exact Weak Solutions To the Advection-Diffusion-Reaction". *SIAM J. Sci. Comput.*, vol. 02139(26):pp. 636–652.

[160] Seo, H.S. and Kwak, B.M. [2002]. "Efficient statistical tolerance analysis for general distributions using three-point information". *Int. J. Prod. Res.*, vol. 40(4):pp. 931–944. ISSN 00207543. doi: 10.1080/00207540110095709.

[161] Sharifi, H. and Larouche, D. [2014]. "Numerical Study of Variation of Mechanical Properties of a Binary Aluminum Alloy with Respect to Its Grain Shapes". *Materials (Basel).*, vol. 7(4):pp. 3065–3083. ISSN 1996-1944. doi: 10.3390/ma7043065.

[162] Shinozuka, M. and Deodatis, G. [1991]. "Simulation of Stochastic Processes by Spectral Representation". *Appl. Mech. Rev.*, vol. 44(4):p. 191. ISSN 00036900. doi: 10.1115/1.3119501.

[163] Smolyak, S. [1963]. "Quadrature and interpolation formulas for tensor products of certain classes of functions". *Sov. Math. Dokl.*, vol. 4:pp. 240–243.

[164] Soize, C. and Ghanem, R. [2004]. "Physical systems with random uncertainties: chaos representations with arbitrary probability". *SIAM J. Sci. Comput.*, vol. 26(2):pp. 395–410.

[165] Šolín, P.; Červený, J.; and Doležel, I. [2008]. "Arbitrary-level hanging nodes and automatic adaptivity in the hp-FEM". *Math. Comput. Simul.*, vol. 77(1):pp. 117–132. ISSN 03784754. doi: 10.1016/j.matcom.2007.02.011.

[166] Stefanou, G. [2009]. "The stochastic finite element method: Past, present and future". *Comput. Methods Appl. Mech. Eng.*, vol. 198(9-12):pp. 1031–1051. ISSN 00457825. doi: 10.1016/j.cma.2008.11.007.

[167] Stein, E.; Rüter, M.; and Ohnimus, S. [2007]. "Error-controlled adaptive goal-oriented modeling and finite element approximations in elasticity". *Comput. Methods Appl. Mech. Eng.*, vol. 196(37-40):pp. 3598–3613. ISSN 00457825. doi: 10.1016/j.cma.2006.10.032.

[168] Stuart, A.M. [2010]. "Inverse problems: A Bayesian perspective". *Acta Numer.*, vol. 19(5):pp. 451–559. ISSN 0962-4929. doi: 10.1017/S0962492910000061.

[169] Sudret, B. and der Kiureghian, A. [2000]. "Stochastic Finite Element Methods and Reliability: A State-of-the-Art Report". *Univ. Calif. Berkeley*, vol. November:p. 189.

[170] Tai, X.C. and Neittaanki, P. [1992]. "Error Estimates for Numerical Identification of Distributed Parameters". *J. Comp. Math., Suppl. issue*, vol. 10:pp. 66–78.

[171] Takeuchi, J. and Kosugi, Y. [1994]. "Neural network representation of finite element method". *Neural Networks*, vol. 7(2):pp. 389–395. ISSN 08936080. doi: 10.1016/0893-6080(94)90031-0.

[172] Tatang, M.A. [1995]. *Direct Incorporation of Uncertainty in Chemical and Environmental Engineering Systems.pdf*. Ph.D. thesis, Massachusetts institute of technology.

[173] Taylor, S. and Bender, D. [1991]. "Stochastic model for localized tensile strength and modulus of elasticity in lumber". *Wood fiber Sci.*, vol. 23(4):pp. 501–519.

[174] Thoft-Christensen, P. and Baker, M.J. [1982]. *Structural Reliability Theory and Its Applications*. Springer Berlin Heidelberg, Berlin, Heidelberg. ISBN 978-3-642-68699-3, 267 pp. doi: 10.1007/978-3-642-68697-9.

[175] Timoshenko, S. and N Goodier, J. [1951]. *The Theory of Elasticity*. McGraw-hill, New York.

[176] Van Beers, W.C. and Kleijnen, J.P. [2003]. "Kriging for interpolation in random simulation". *J. Oper. Res. Soc.*, vol. 54(3):pp. 255–262. ISSN 01605682. doi: 10.1057/palgrave.jors.2601492.

[177] van der Vaart, A.W. [1998]. *Bootstrap*, pp. 326–340. Cambridge Series in Statistical and Probabilistic Mathematics. Cambridge University Press. doi: 10.1017/CBO9780511802256.024.

[178] Van der Vorst, H.A. and Vuik, C. [1994]. "GMRESR: a family of nested GMRES methods". *Numer. Linear Algebr. with Appl.*, vol. 1(4):pp. 369–386. ISSN 1070-5325. doi: 10.1002/nla.1680010404.

[179] Verdugo, F.; Parés, N.; and Díez, P. [2014]. "Error Assessment in Structural Transient Dynamics". *Arch. Comput. Methods Eng.*, vol. 21(1):pp. 59–90. ISSN 11343060. doi: 10.1007/s11831-014-9096-x.

[180] Vuik, C. [1993]. "Further Experiences with GMRESR". *Supercomputer*, vol. 10(3):pp. 13–27.

[181] Vuik, C. [2017]. *Iterative Solution Methods*. Delf Institute of Applied Mathematics, Delft, 118 pp.

[182] Wang, X.; Cen, S.; and Li, C. [2013]. "Generalized Neumann Expansion and Its Application in Stochastic Finite Element Methods". *Math. Probl. Eng.*, vol. 2013(1):pp. 1–13. ISSN 1024-123X. doi: 10.1155/2013/325025.

[183] Webster, C.G. [2007]. *Sparse grid stochastic collocation techniques for the numerical solution of partial differential equations with random data*. Ph.D. thesis, Florida State University.

[184] Wiberg, N.E.; Abdulwahab, F.; and Li, X.D. [1997]. "Error estimation and adaptive procedures based on superconvergent patch recovery (SPR) techniques". *Arch. Comput. Methods Eng.*, vol. 4(3):pp. 203–242. ISSN 1134-3060. doi: 10.1007/BF02913818.

[185] Wu, F. and Zhong, W. [2013]. "A hybrid approach for the time domain analysis of linear stochastic structures". *Comput. Methods Appl. Mech. Eng.*, vol. 265:pp. 71–82. ISSN 00457825. doi: 10.1016/j.cma.2013.06.006.

[186] Xiu, D. and Karniadakis, G. [2002]. "The Wiener-Askey polynomial chaos for stochastic differential equations". *SIAM J. Sci. Comput.*, vol. 24(2):pp. 619–644.

[187] Yamazaki, F.; et al. [1988]. "Neumann Expansion for Stochastic Finite Element Analysis". *J. Eng. Mech.*, vol. 114(8):pp. 1335–1354. ISSN 0733-9399. doi: 10.1061/(ASCE)0733-9399(1988)114:8(1335).

[188] Zeldin, B.A. and Spanos, P.D. [1998]. "On random field discretization in stochastic finite elements". *J. Appl. Mech.*, vol. 65(2):p. 320. ISSN 00218936. doi: 10.1115/1.2789057.

[189] Zhang, J. and Ellingwood, B. [1994]. "Orthogonal series expansions of random fields in reliability analysis". *J. Eng. Mech.*, vol. 120(12):pp. 2660–2677. ISSN 0733-9399. doi: 10.1061/(ASCE)0733-9399(1994)120:12(2660).

[190] Zienkiewicz, O.C. and Zhu, J.Z. [1987]. "A simple error estimator and adaptive procedure for practical engineerng analysis". *Int. J. Numer. Methods Eng.*, vol. 24(2):pp. 337–357.

[191] Zienkiewicz, O.C. and Zhu, J.Z. [1992]. "The superconvergent patch recovery and a posteriori error estimates. Part 1: The recovery technique". *Int. J. Numer. Methods Eng.*, vol. 33(7):pp. 1331–1364.

[192] Zienkiewicz, O.C. and Zhu, J.Z. [1992]. "The superconvergent patch recovery and a posteriori error estimates. Part 2: Error estimates and adaptivity". *Int. J. Numer. Methods Eng.*, vol. 33(7):pp. 1365–1382.